PROTON AND NEUTRON INTERACTIONS IN SOME LIGHT NUCLEI

by

JOHN G. JENKIN

A thesis submitted to The Australian National University
for the degree of Doctor of Philosophy.

January 1964

To my parents

PREFACE

This thesis deals with two somewhat different topics, although the difficulty of neutron detection underlies much of the work.

The first section is concerned primarily with a study of the nucleus C^{11} in energy states above 10 MeV excitation, and was made by investigating the $B^{10}(p,n)C^{10}$, $B^{10}(p,\alpha)Be^{7}$ and $B^{10}(p,He^{3})Be^{8}$ reactions in the tandem Van de Graaff accelerator energy range. In the first experiment an activation technique was used, and the development of the apparatus is discussed. The equipment was also used in a study of the $F^{19}(p,n)Ne^{19}$ excitation function. Both of the activation experiments required a knowledge of the half-lives of the respective final nuclei, and their measurement with high precision was undertaken.

The second section describes the performance and interpretation of an experiment to measure angular distributions of neutrons scattered by alpha particles, for neutron energies from 16 to 26 MeV. The principal purpose of the experiment was to provide data necessary for determining the n-He^4 phase-shifts in this energy range. However, the resonance at 22.15 MeV neutron energy, corresponding to the 16.70 MeV state of He^5, and the yield curve of the $He^4(n,d)T$ reaction have also been studied in detail.

A number of appendices have been used in the arrangement of the thesis. The material in them is subsidiary to the main argument, but it should not be thought that they are unimportant.

The main theme of Section One was suggested by Professor E.W. Titterton, and the detailed work of designing the apparatus, taking the data and analysing the results was done, in equal part, by Mr. L.G. Earwaker and myself, under Professor Titterton's supervision.

The experiment of section two was planned by Dr. R.E. Shamu, who designed the apparatus. The work reported was done jointly with Dr. Shamu.

Almost all of the work described has been published as follows :

"Half-lives of Carbon-10 and Neon-19",
Nature 195 (1962) 271.

"The $B^{10}(p,n)C^{10}$ Excitation Function from Threshold to 10.6 MeV",
Nuclear Physics 42 (1963) 521

"The $B^{10}(p,\alpha)Be^{7}$ Reaction between 2 and 11 MeV",
Nuclear Physics (to be published)

"The $B^{10}(p,He^{3})Be^{8}$ Reaction",
Physics Letters 4 (1963) 142

"The $F^{19}(p,n)Ne^{19}$ Reaction between 5 and 11 MeV",

Nuclear Physics 44 (1963) 453

"Neutron-Alpha Scattering in the 20-MeV Range",

Bull. Am. Phys. Soc. 8 (1963) 477, and Phys. Rev. (to be published).

Mr. Earwaker, Professor Titterton and I also investigated "Energy Levels of B^9", Nuclear Physics (to be published), the substance of which has not been included in this thesis.

No part of this thesis has been submitted for a degree in any other university.

John G. Jenkin.

ACKNOWLEDGEMENTS

Research in experimental nuclear physics today is a highly co-operative venture, and this thesis could not have been written without the help of many people.

I am indebted to Professor Titterton for the opportunity of working in the Department of Nuclear Physics, and I am grateful to him for his encouragement and active supervision of much of the work. Lyndsay Earwaker's placidness and enthusiasm always aided our endeavours.

My warm thanks are also due to Dr. R.E. Shamu for his patient and efficient instruction in the large number of techniques necessary for, and often peculiar to, fast neutron work.

Many members of the Departments of Nuclear and Theoretical Physics have given aid from time to time. In particular Dr. T.R. Ophel and Dr. F.C. Barker have contributed substantially to my understanding of various topics.

Mr. F.A. Howe and his associates at Aldermaston in England supplied a large number of excellent boron targets which were used for the work reported in Section One. Their generosity is appreciated.

The A.N.U. Research Scholarship which I held for three years, during which time the work reported here was done, was a generous one.

Miss S. Eley has typed the thesis capably.

The work could not have been done without the help and understanding of my wife.

CONTENTS

CHAPTER THREE

THE $B^{10}(p,n)C^{10}$ EXCITATION FUNCTION

CHAPTER FOUR

THE $B^{10}(p,\alpha)Be^{7}$ REACTION BETWEEN 2 AND 11 MeV

CHAPTER FIVE

THE $F^{19}(p,n)Ne^{19}$ REACTION BETWEEN 5 AND 11 MeV

SECTION TWO

CHAPTER SIX

NEUTRON-ALPHA SCATTERING FROM 16 TO 24 MeV

SECTION ONE

CHAPTER ONE INTRODUCTION

A distinguishing feature of low energy nuclear reactions is the existence of strong, well defined resonances in the various cross sections. The accumulation of data on the position and properties of such energy levels in light nuclei represents one of the major fields of nuclear research. The primary purpose of the investigations reported in Section One of this thesis was to determine the position and properties of some such levels which have become accessible with the high resolution, high stability tandem Van de Graaff accelerator.

Such information is best obtained through reactions where the nucleus of interest becomes the intermediate, or compound, nucleus. It was Neils Bohr (1936) who first stated how the observed resonances in cross sections could be understood in terms of virtual states of nuclei. The fact that the resonances were not single particle levels implied that the interaction between the incoming nucleon and the individual nucleons of the target nucleus was strong. As a consequence, the incoming particle and the nucleus it struck coalesced, forming a compound system in which the energy of the incident particle was shared rapidly with many of the target nucleons. Therefore the compound state lasted a long time; until one or more nucleons obtained enough energy, by some statistical process, to escape from the nucleus, or the nucleus de-excited by γ-ray emission. Bohr's picture described a nuclear reaction as a two-stage process : the formation of a compound nucleus by the bombardment of a target nucleus with some projectile, and its eventual decay by the emission of a particle or γ-ray, in a manner independent of the mode of formation. This theory was successful in explaining nuclear resonance reactions in which the resonance energies were clearly related to levels of the compound nucleus. So began a long line of theoretical work that resulted in the R-matrix theory of nuclear reactions. This theory, pioneered primarily by Wigner and co-workers, is very general, and contains very few assumptions. Since the early experimental studies of Fermi (1934), a tremendous amount of work has also been accomplished in this field. This experimental work has been analysed successfully using the theoretical findings referred to above, and has prompted further endeavours.

When the theory is extended to higher energies, where the compound system is excited in the region of <u>many</u> overlapping levels, the statistical approximation is applied (see, for example, Weisskopf, 1937). The assumption is made that sufficient time is available for thermodynamic equilibrium to be established. Under these conditions the mode of decay should be independent of the method of formation, so that the cross section for an (a,b) reaction is written

$$\sigma(a,b) = \sigma_c(a)P_c(b),$$

where $\sigma_c(a)$ is the cross section for formation of the compound nucleus by capture of a particle a, and $P_c(b)$ is the independent probability that the compound nucleus decays by emission of a particle b. The result is an averaging of the interference terms between different angular-momentum transitions; that is, the phase relations between the matrix elements of the transitions to and from the compound state are random.

The B^{10} + p work reported in this thesis has been analysed successfully in terms of the first of these two theories, namely the formal theory of resonances. However, the nuclear excitation energy region reached by the tandem accelerator is often somewhere between the energy regions where the above theories are expected to apply. This is therefore a difficult energy region to deal with theoretically, and very little work has been done which has direct relevance to data taken there. This problem arises in connection with the remainder of the work discussed in Section One, and some attention is given to the matter.

Not all collisions result in the formation of a compound nucleus, of course. There is always a finite probability that the incident particle will transfer its energy directly to a single nucleon in a target nucleus as it grazes its surface, or to a few nucleons in the nuclear surface, resulting in the emission of particles of higher energy than that expected from the compound-nucleus picture. The several types of so-called direct interactions fall into this category. In the work reported here some fraction of the reactions proceed through such mechanisms, but no attempt has been made to study these in any detail. The compound nucleus events were of primary interest.

1.1 The Choice of the Work

Several factors contributed to the choice of the work described in the first section of this thesis.

Firstly, the purchase by the Nuclear Physics Department of a tandem Van de Graaff, electrostatic, positive ion accelerator greatly extended the energy range available for experiments in this laboratory. The machine, a model EN tandem made by the High Voltage Engineering Corporation (HVEC) of the USA, is capable of accelerating protons (and other positive ions) to energies in excess of 11 MeV, while still retaining all of the desirable Van de Graaff accelerator characteristics. These include energy, current and positional stability of the beam, high homogeneity and continuous control of beam energy, and simplicity of operation and maintenance. Although two charge-exchange processes are necessary in the acceleration, beam intensities can be obtained which proved to be more than adequate for the experiments described here. The beam is, of course, subjected to magnetic analysis, and during our work the tandem and magnet were calibrated for energy every four months or so using the following accurately known reaction thresholds, $Al^{27}(p,n)$, $C^{13}(p,n)$, $B^{11}(p,n)$ and $Ni^{58,60}(p,n)$.

With this machine a new and higher range of excitation energies in nuclei became available for accurate investigation. However, the choice of such nuclei was somewhat restricted by the necessity of obtaining suitable targets. While the type of target chosen depended on a large number of factors, including the experiment and techniques to be used, targets were required which were thin and isotopically "pure", so that the large backgrounds arising from 10 MeV particle bombardment were kept to a minimum and the resolution obtained with machine and detector was used effectively. The self-supporting foil target had become even more desirable than before.

A good example of the development in target-making techniques which followed as a result of this need is the element boron. Self-supporting boron targets were particularly difficult to make due to the element's high melting point (2000-2080)^{o}C. In 1961 Muggleton and Howe developed a method for preparing thin, self-supporting boron foils in vacuum, which involved the use of a tightly focussed electron beam to provide intense but local heating. Later Erskine and Gemmel (1963) reported an improved version of the same type of apparatus incorporating a water-cooled anode to reduce contamination of the target with crucible material, and an improved method of removing the evaporated foil from the temporary backing. Following negotiations by Professor Titterton, Mr. Howe and his associates at Aldermaston graciously supplied a range of boron targets, enriched to 89% B^{10} and varying in thickness from 50 to 250 $\mu gm/cm^2$.

A third factor which influenced the choice of the work was the fact that little was known about the nucleus C^{11} in energy states above 10 MeV excitation, that is, in the tandem energy range (see, for example, Ajzenberg-Selove and Lauritsen, A-S and L, 1959). A state at 10.08 MeV excitation was well established, and there seemed good evidence for others at 10.68 and 10.89 MeV.

Work by Cerino (1956) on the $B^{10}(d,n)C^{11}$ reaction using nuclear emulsions had suggested levels at 11.26 and 11.52 MeV, and states at 12.3, 13.8 and 15.7 had been proposed by Kalinin et al. as a result of a poor resolution, stacked foil experiment. However, a great deal of information clearly remained to be found. Several B^{10} + p experiments at once suggested themselves as possible modes for investigating this energy region, particularly in view of the elegant B^{10} self-supporting targets which were available.

An attempt by Gibbons and Macklin (1959) to investigate the $B^{10}(p,n)C^{10}$ reaction with an array of BF_3 counters had been largely unsuccessful; they were only able to put an upper limit on the cross section at about 5.4 MeV proton energy. The only other reported $B^{10}(p,n)C^{10}$ work was carried out by Ajzenberg and Franzen (1954) when they detected, in nuclear emulsions, the neutrons produced by 17 MeV proton bombardment of an enriched boron target. However, the inherent difficulty of detecting neutrons with high precision can be overcome in the $B^{10}(p,n)C^{10}$ case, since this reaction is extremely well suited to investigation by an activation technique, 100% of the positron decays of C^{10} proceeding via the 0.717 MeV level of B^{10}. The detection of coincidences between the 0.717 MeV γ-ray and one of the 0.511 MeV annihilation radiation quanta allowed a unique identification of the $B^{10}(p,n)C^{10}$ reaction, even in the presence of other positron activities.

The decision to carry out this experiment also fulfilled another desirable if not necessary condition applying to the choice of the thesis work, namely the building up of the range of experimental apparatus available with the Canberra tandem. A good piece of activation apparatus was a useful addition to the magnetic spectrometers and scattering chambers. Chapter 3 describes the development of the activation apparatus, and its use in a study of the $B^{10}(p,n)C^{10}$ reaction.

Several new C^{11} states were discovered in this and other investigations (Ophel et al., 1962), and it was evident that further work to try and determine some of the properties (such as spin, parity and reduced widths) of these levels, and other levels below the $B^{10}(p,n)C^{10}$ threshold, would be useful. The availability of the solid state detector in a highly developed form made the choice of a charged-particle experiment most attractive. Physicists at the California Institute of Technology were known to be investigating the elastic scattering of protons from B^{10}; so it was decided to study the $B^{10}(p,\alpha)Be^7$ reaction in the hope that, together with other work, it would complete a quite extensive survey of the excitation energy region in C^{11} from 10 to 19 MeV. This $B^{10}(p,\alpha)Be^7$ work is described in chapter 4. During the course of the experiment it became clear from the charged particle spectra being collected that data on the $B^{10}(p,He^3)Be^8$ reaction could be obtained simultaneously. This was done, and the material is discussed in conjunction with the $B^{10}(p,\alpha)$ considerations of chapter 4.

During the $B^{10}(p,n)C^{10}$ work the activation apparatus was developed to a stage where it was performing very reliably and producing data at a fast rate. $F^{19}(p,n)Ne^{19}$ is another neutron-producing reaction well suited to investigation by an activation method, and so the B^{10} + p experiments were followed by a study of this reaction. The work is reported in chapter 5. Excitation energies in Ne^{20} up to 23.3 MeV were attained, and the interpretation of the excitation function data in terms of Ne^{20} structure was not clear. The analysis of the data is discussed.

The two activation experiments reported in chapters 3 and 5 were based on measurements of the positron activities of the final nuclei of the respective reactions. The analysis of the experiments required the values of the half-lives of these nuclei, and the uncertainty of their magnitude was reflected in a corresponding uncertainty in the activation results. Indeed, the performance of the experiments depended on an accurate knowledge of the half-lives. The C^{10} decay constant was known to only 5%; that for Ne^{19} had been measured many times with various degrees of accuracy, but even the better values did not agree. Hence, before any of the activation work was begun, the half-lives of C^{10} and Ne^{19} were measured with high precision. The high degree of accuracy achieved was made possible by a number of factors, among them being the availability of one of the "new generation" multi-channel pulse height analysers. These determinations are described in chapter 2.

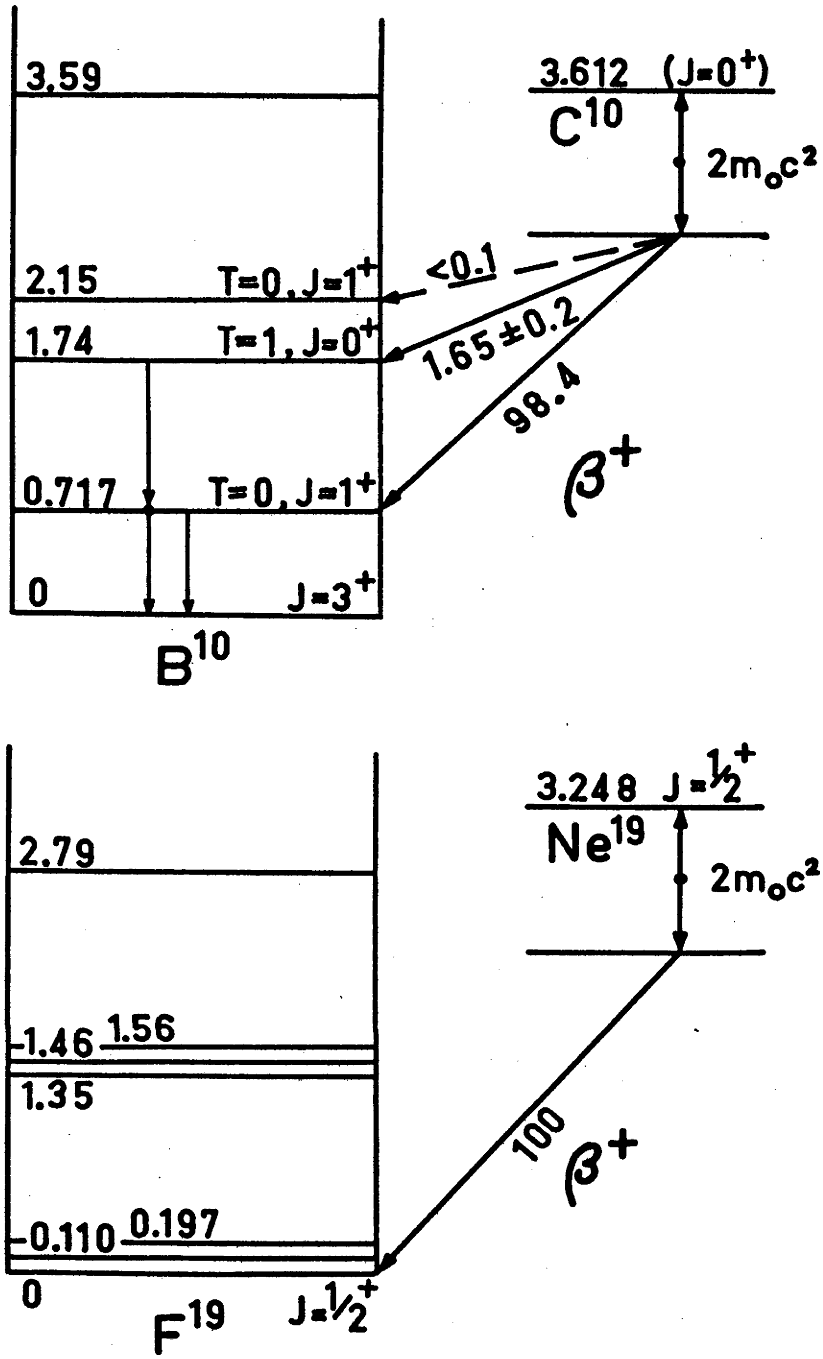

Fig. 1 The positron decay schemes for C^{10} and Ne^{19}.

CHAPTER TWO

THE HALF-LIVES OF C^{10} AND Ne^{19}

2.1 Introduction

Both C^{10} and Ne^{19} decay by positron emission, and both transitions are allowed and favoured (or superallowed). Their respective decay schemes are shown in figure 1. When this work began only two measurements of the C^{10} half-life had been reported; the first of 8.8 sec. (Delsasso et al., 1940) was thought to be in error due to an impurity in the boron powder used, the second, due to Sherr et al. (1949) was 19.1 ± 0.8 sec. The latter measurement was made by collecting on ascarite (NaOH on asbestos) the radioactive gases produced by 17 MeV proton bombardment of B^{10} enriched $CaF_2.B^{10}F_3$. In the case of Ne^{19}, about seven values ranging from 17.4 ± 0.2 sec. to 20.3 ± 0.5 sec. had been reported (A-S and L, 1959), and even the ones with least error did not agree.

As mentioned in chapter 1, the main purpose in measuring these two half-lives was to obtain improved values for use in the $B^{10}(p,n)C^{10}$ and $F^{19}(p,n)Ne^{19}$ activation studies. It is appropriate to outline here the simple theory pertinent to the activation measurements to show how the experimental results depended on the values of the decay constants of the beta-decaying final nuclei. However, there were other reasons why accurate values of these half-lives were valuable, and these reasons are outlined after the activation theory. This is followed by details of the experiment and the subsequent analysis of the results.

2.2 Activation Theory

The first requirement in the analysis of the activation measurements was a knowledge of the incident beam energy. This has been discussed in chapter 1. In addition, it was necessary to know the number of transmutations per incident proton. A formula connecting this yield with the experimentally measured quantities can be derived as follows :

Let n_1 = number of reactions per proton

n_2 = number of protons incident per second on the target

C_1 = number of decays recorded

C_2 = number of decays recorded corrected for previous bombardments C_3 and for backgrounds

i.e. $C_2 = C_1 - C_3 -$ backgrounds

f = efficiency of experimental apparatus for detecting decays

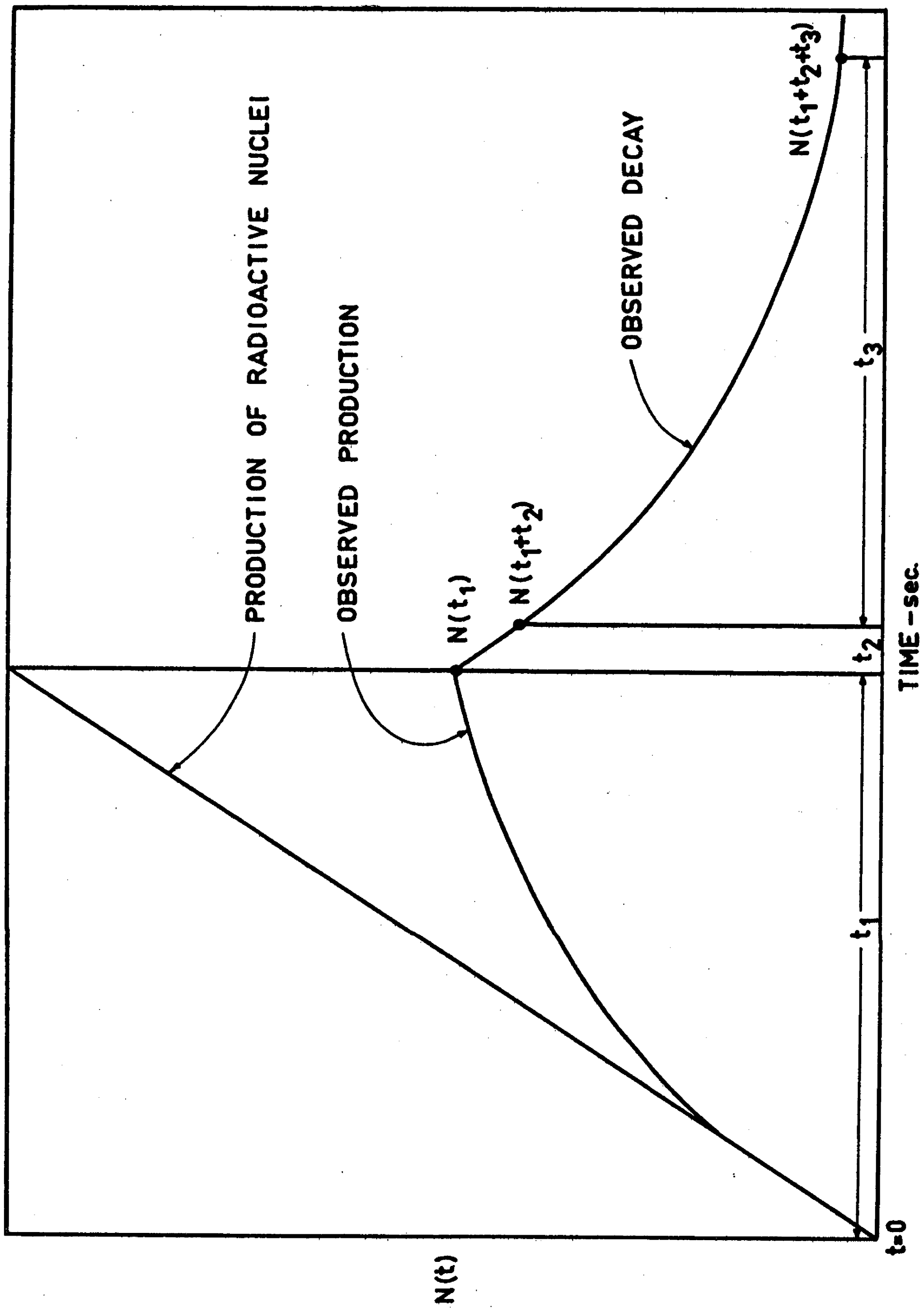

Fig. 2 A representation of the production and decay of activity, induced in a target by an accelerator beam.

t_1 = bombardment time

t_2 = time between end of bombardment and commencement of counting

t_3 = counting time

$N(t)$ = number of radioactive nuclei present at time t ($t = 0$, commencement of bombardment)

λ = decay constant of radioactive nuclei

$= \frac{0.693}{\tau}$, τ = half-life.

The situation is depicted in figure 2.

The total number of radioactive atoms produced during the bombardment time t_1 was

$$n_1 n_2 t_1$$

In practice the number of such atoms present at time $t = t_1$ was

$$N(t_1) = N(1 - e^{-\lambda t_1})$$

where N = equilibrium number of atoms

$= n_1 n_2/\lambda$ (Kaplan, 1956)

At time $t = t_1 + t_2$, t_2 seconds after the bombardment,

$$N(t_1 + t_2) = N(t_1)e^{-\lambda t_2}$$

$$= N_o(e^{-\lambda t_2})(1 - e^{-\lambda t_1}) .$$

At the end of the counting period

$$N(t_1 + t_2 + t_3) = N(t_1)\, e^{-\lambda(t_2 + t_3)}$$

$$= N_o(e^{-\lambda t_2})(e^{-\lambda t_3})(1 - e^{-\lambda t_1}).$$

Therefore, the number of positrons produced in the counting time was

$$n_\beta = N(t_1 + t_2) - N(t_1 + t_2 + t_3)$$

$$= (n_1 n_2/\lambda)(e^{-\lambda t_2})(1 - e^{-\lambda t_1}) \times (1 - e^{-\lambda t_3}).$$

The number recorded (corrected for previous bombardments and backgrounds) was

$$C_2 = f\, n_\beta ,$$

and so the final expression for the yield n_1, in transmutations per proton, is

$$n_1 = C_2\lambda / n_2 f(e^{-\lambda t_2})(1 - e^{-\lambda t_1})(1 - e^{-\lambda t_3}).$$

Experimentally, the quantities to be measured were C_2, n_2, f, t_1, t_2, t_3 and λ.

The measurement of the first six of these is discussed in conjunction with the activation measurements; the determination of λ is the subject of the present chapter. It is to be noted that the choice of the lengths of time t_1, t_2 and t_3 depended largely on the value of the half-life of the radioactive atoms.

If the target thickness T cm. is known, it is possible to make a direct measurement of the cross section σ for the reaction. The yield from a nuclear reaction (the number of reactions per proton, n_1) produced by protons of energy E is given by

$$n_1 = \int_{E_1}^{E_2} n_1(E).dE$$

where $E_2 - E_1$ is the energy spread of the proton beam and

$$n_1(E) = \int_{x=0}^{T} \sigma(E_x).d.dx$$

d = target density (number of nuclei/cm^3)

x = distance proton penetrates target (cm.)

E_x = energy of proton at x.

In the special case, which is satisfied in all the experiments reported in Section One, where the variation in σ over the energy ranges corresponding to the target thickness and the spread of energy in the proton beam can be neglected, this expression simplifies to

$$n_1 = \sigma.d.T$$

or, the number of reactions per proton,

$$n_1 = \sigma.n$$

n = target thickness in number of target nuclei/cm^2

2.3 Other reasons for measuring $\tau(C^{10})$ and $\tau(Ne^{19})$

In 1934 Fermi devised a successful theory of beta-decay based on Pauli's neutrino hypothesis. He drew an analogy between the emission of electrons and neutrinos from nuclei and the emission of photons from excited atoms. The forces involved are weak, so the problem was treated using perturbation theory. A basic result of the theory was the expression for the disintegration constant for the transition of a system from an initial state i to a final state f

$$\lambda = (2\pi/\hbar) \left| H_{if} \right|^2 \ dn/dE$$

where dn/dE is the number of accessible final states per unit of total energy released

and H_{if} is the relevant matrix element

$$H_{if} = \int \psi_f^* H \psi_i \, dv ,$$

in which ψ_i and ψ_f are the initial and final state wave functions and H is the Hamiltonian operator describing the weak interaction between the electron-neutrino field and the nucleus.

Unfortunately neither the wave functions nor the interaction operator was, or now is, known. Fermi attacked the problem by writing down quite arbitrarily for H the simplest form that was consistent with the demands of relativity theory - both the election and neutrino move at high speed. There were only five possible forms that met all requirements, each having a form

$$H_{if} = g \int \left[U_f^* \phi_e (\underline{r}) \phi_\nu (\underline{r}) \right] O_x U_i \, dv.$$

Where $\phi_e(\underline{r})$ and $\phi_\nu(\underline{r})$ were the wave functions for the electron and neutrino, U_i and U_f described the nucleus before and after the emission process, g was the Fermi constant, and O_x was an operator that could have one of five forms, corresponding to a scaler, polar-vector, tensor, axial-vector or pseudo-scaler interaction. Fermi himself postulated that the interaction responsible for beta-decay was essentially a vector interaction, often called the Universal Fermi Interaction. Gamow and Teller (1936), on the other hand, suggested that axial coupling between the transforming nucleon and the electron-neutrino field was of primary importance. At present, the Gamow-Teller picture appears to describe most cases of beta-decay, but there are a few instances where the Fermi interaction is required to describe the observations. The $C^{10} \rightarrow B^{10}$, allowed and favoured, $J^{\pi} = 0^{+} \rightarrow 0^{+}$, beta transition to the second excited state of B^{10} is one such case. So, from time to time, the decay of C^{10} has been under close scrutiny (for example, Sherr and Gerhart, 1953, Bartis et al., 1962). The measurement of $f\tau$ values†, and hence of half-lives, for 0^{+} to 0^{+} positron transitions was known to be of use in calculating the vector coupling constant for beta-decay; for this can be compared

---

† The $f\tau$ product or comparative half-life provides a useful criterion for the classification of radioactive transitions as allowed or forbidden to various degrees (Konopinski, 1941). Here f is a theoretical factor which corrects the observed half-life τ for the effects of the nuclear charge and the energy of the transition, thus reducing all half-lives to a comparable basis.

with the coupling constant for muon decay, and so is of interest in establishing the validity of the Universal Fermi Interaction (Freeman et al., 1962). Hence there were inducements other than the immediate one for measuring the half-lives with the maximum possible accuracy.

2.4 Experimental Details and Results

The experimental apparatus used for the half-life work was that developed for the activation measurements. This equipment is discussed in full in chapter 3, where the relevance of its many features is clear. Here, only that amount of detail necessary for the understanding of the half-life work is given.

C^{10} was produced by the $B^{10}(p,n)C^{10}$, ($Q = -4.40$ MeV) reaction. A 200-250 μgm/cm^2 self-supporting boron target, enriched to 89% B^{10} (by weight), was bombarded for 60 seconds with 0.1 μA of 7.5 MeV protons from the tandem accelerator.

The branching ratios for the β^+-decay of C^{10} are 98.4% to the first excited state of B^{10}(0.717 MeV excitation) and 1.65 ± 0.2% to the second excited state, which then γ cascades through the first excited state to the ground state (Sherr and Gerhart, 1953). Hence the decay of C^{10} was uniquely identified by the 0.717 MeV γ-ray which followed the emission of all of the

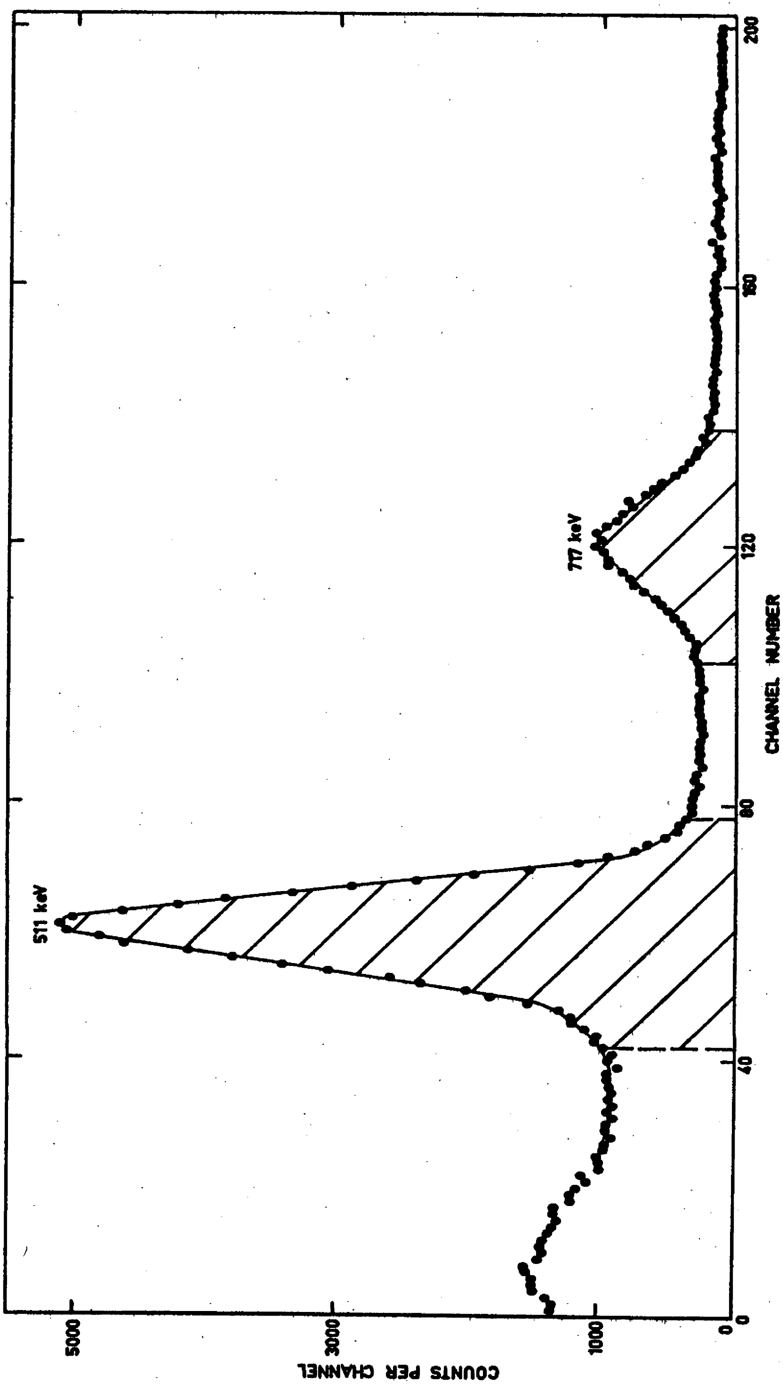

Fig. 3(a) A gamma-ray spectrum taken with one of the crystal spectrometers after a bombardment of B^{10} with 8 MeV protons. The hatched areas indicate the energy intervals selected for the coincidence measurements.

positrons (see figure 1). It was decided, therefore, to use this γ-ray to measure the half-life, particularly as the target contained 8% C^{11}, which gave rise to a strong 20 min. positron activity. A 7.6 cm. x 7.6 cm. NaI(Tl) crystal spectrometer was set up with its front face 1.3 cm. from the target, and a γ-ray spectrum taken with the crystal is shown in figure 3a. A Franklin non-overload, double-delay-line, preamplifier-amplifier system followed the photomultiplier, and pulses in the 0.717 MeV γ-ray photopeak were selected with a single channel analyser and fed to an RIDL model 34-12 400-channel analyser, operating in its Time (multichannel scaler) Mode. In this mode the pulses of constant amplitude from the single channel analyser were stored in channel x until an external timing signal advanced the storage address to channel (x + 1). With a series of equally spaced timing pulses the number of counts per channel as a function of channel number was proportional to the number of decays as a function of time. A 100 kc/sec. crystal oscillator, having a stability better than one part in 10^5, was scaled down to provide a pulse which, after differentiation and amplification, was used to advance the analyser address every two seconds (figure 3b). The decay of the count rate in the single channel window was followed for 290 seconds, about fifteen C^{10} half-lives.

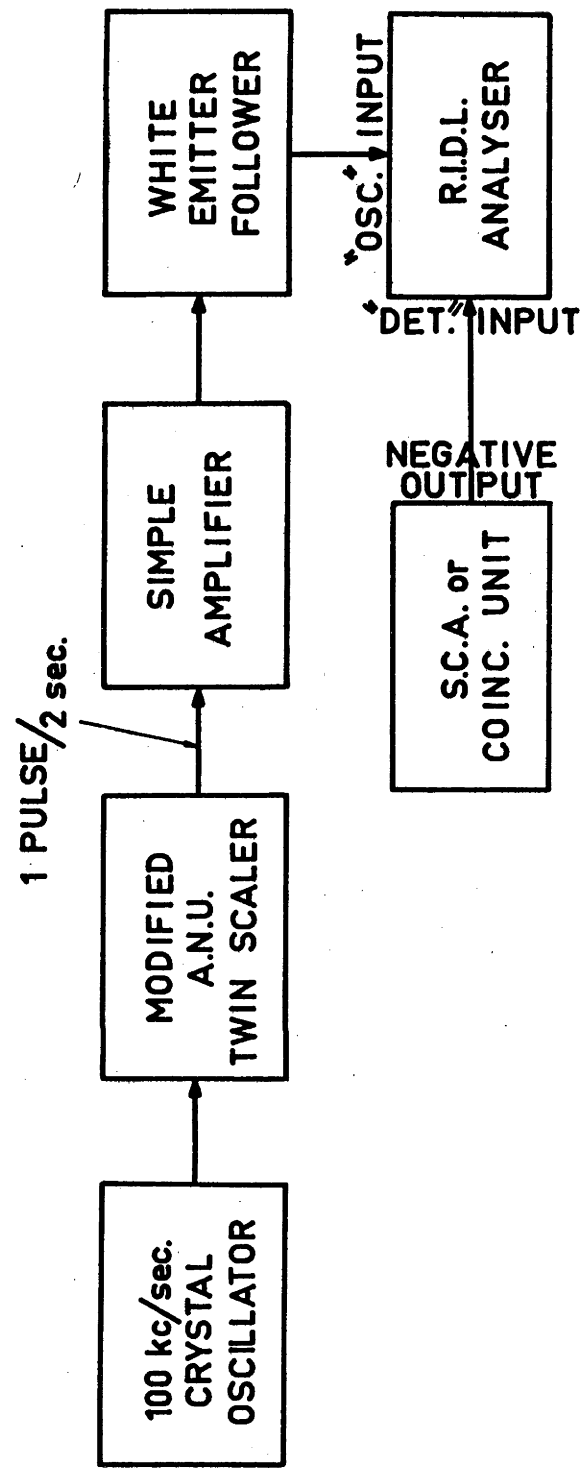

Fig. 3(b) A block diagram of the circuitry used to advance the multichannel analyser address every two seconds.

It is worth noting here that at the beginning of this work an RCL model 20618 512-channel analyser was used, operating in its Scaler Time (multichannel scaler) Mode. This analyser had its own clock, capable of providing address advance pulses over a wide range of frequencies. However, the basic frequency of this mechanical clock was found to be very temperature sensitive, and to vary by as much as $\pm$ 2 percent over time intervals as short as 2 hours, despite the manufacturer's claim of better than 0.2 percent stability. Also, the clock pulses occupied memory time, and so contributed to the analyser dead-time. The RIDL plus external clock system was clearly preferable.

The total counting rate detected had a maximum value of about 9×10^3 counts per second, and the counting rate in the single channel analyser window had a maximum value of 1.5×10^3 counts per second. Under these conditions the opposing effects of pile up and counting loss combined so as to alter even the highest counting rate by a negligible amount. The effective dead time of the analyser was also negligible, since the probability of two or more pulses occurring in the 10 μsec. memory-cycle time was extremely small.

Throughout the measurements the gain of the counter system was monitored by observing the pulse height of the 0.511 MeV photopeak with another RIDL multichannel pulse height

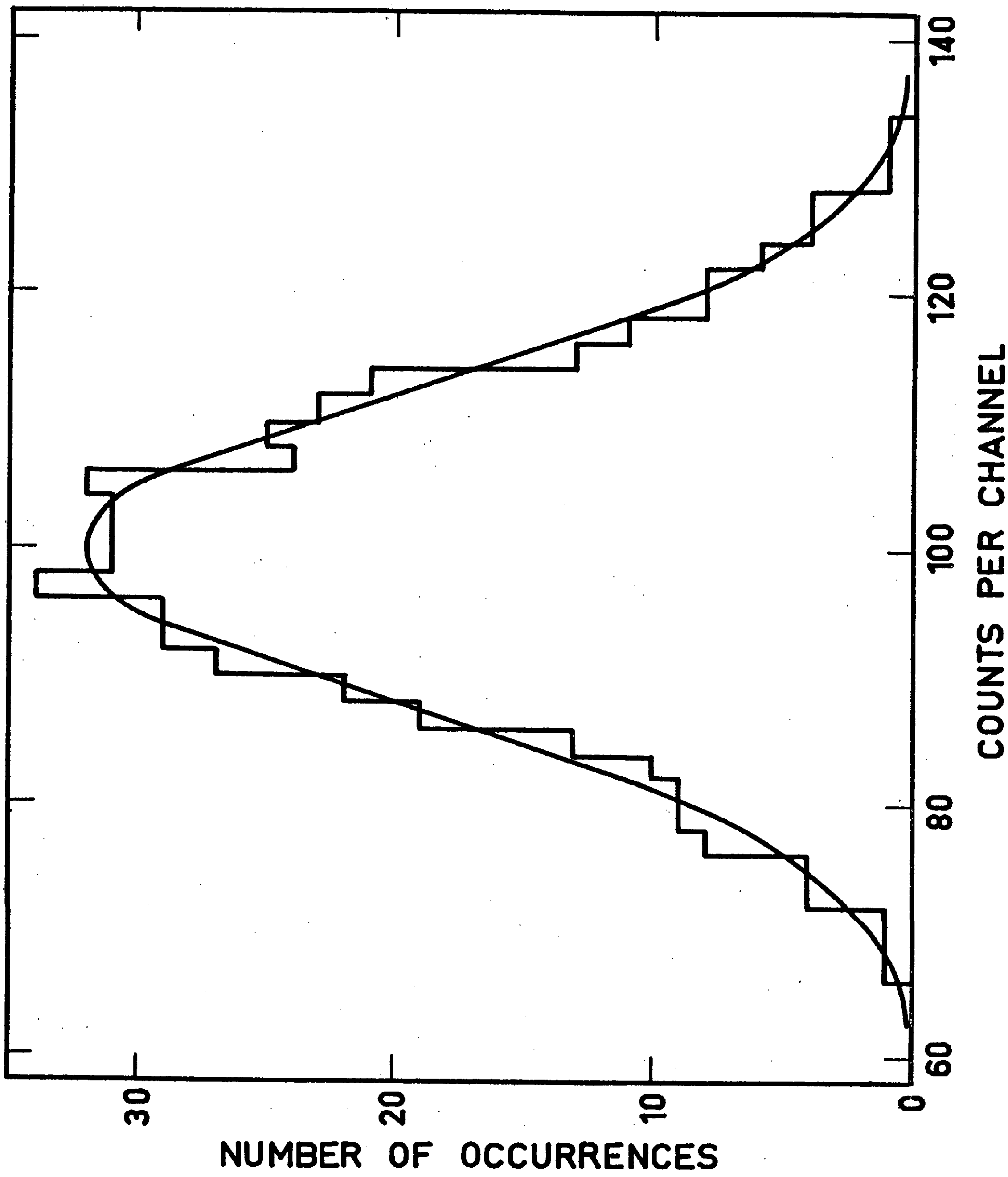

Fig. 4 A plot of background counts per channel versus their frequency of occurrence. The smooth curve is a Gaussian Distribution function.

analyser. No significant gain changes were observed. The beam currents used in the bombardment of the target were, indeed, chosen to make all these possible corrections negligible.

There was a background counting rate of about 30 counts per second beneath the decay curve, as can be seen from figure 5. It was important to verify accurately that this background was constant during the counting period. Data was accumulated for approximately 15 half-lives during each run, so the last 30 channels each contained less than 0.02 percent of the C^{10} activity present at the beginning of the counting period. A large number of runs were collected, and the counts in the last 30 channels normalised so that their mean value was 100 counts. The resultant counts per channel were plotted as a function of their frequency of occurrence. As figure 4 shows, the resulting histogram was fitted very well with a Gaussian Distribution function, proving that no long-lived activities were interfering with the data, that is, that the background was constant. The possibility of the presence of short-lived activities was negated by the linearity of the logarithmic plot of the data, discussed in the next section dealing with the analysis of the results.

As a further check that no other activities were affecting the data, a number of half-life measurements were made by following the decay of the coincidence count rate from a

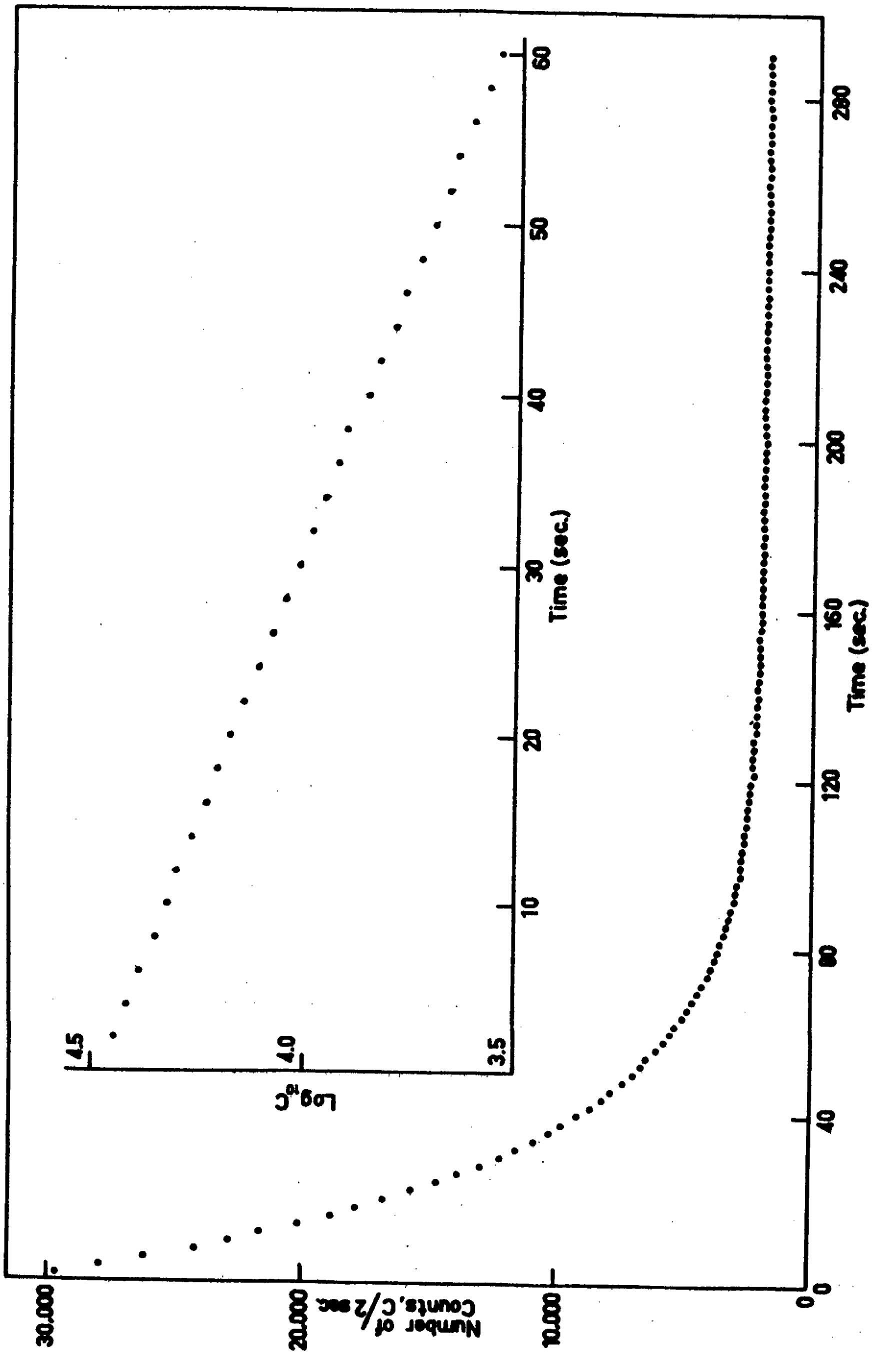

Fig. 5 A typical decay curve for C^{10}, together with a logarithmic plot of the data after subtraction of the background.

Dynatron type 1036C coincidence unit of 0.2 μsec. resolving time. Here, two 7.6 cm. x 7.6 cm. NaI(Tl) crystals, placed on opposite sides of, and 1.3 cm. from, the target were used, one feeding a single channel analyser with a window over the 0.717 MeV photopeak, and the other a similar analyser with a window over the 0.511 MeV photopeak.

About 90 separate experimental runs were made by one or other of the two methods described above, and these were combined into six independent groups of 15 for the analysis described in the next section. This allowed each determination of the C^{10} half-life to have a high degree of statistical accuracy. The data used for one calculation is shown in figure 5.

Apart from the differences now to be mentioned, the data for determining the half-life of Ne^{19} was collected and processed in the same manner as that described for C^{10}. The $F^{19}(p,n)Ne^{19}$, $Q = -4.04$ MeV, reaction was used. A F^{19} target was obtained by vacuum evaporation of manganous fluoride (MnF_2) on to a 300 μgm/cm^2 gold foil, as neither the manganese nor gold gave rise to positron activities when bombarded with protons. This target was subjected to 0.1 μA, 4.8 MeV proton bombardment. Because the decay of Ne^{19} proceeds 100 percent to the ground state of F^{19} (A-S and L, 1959), the decay of the Ne^{19} nuclei produced was followed by observing the decay in the counting rate of pulses passing through a single

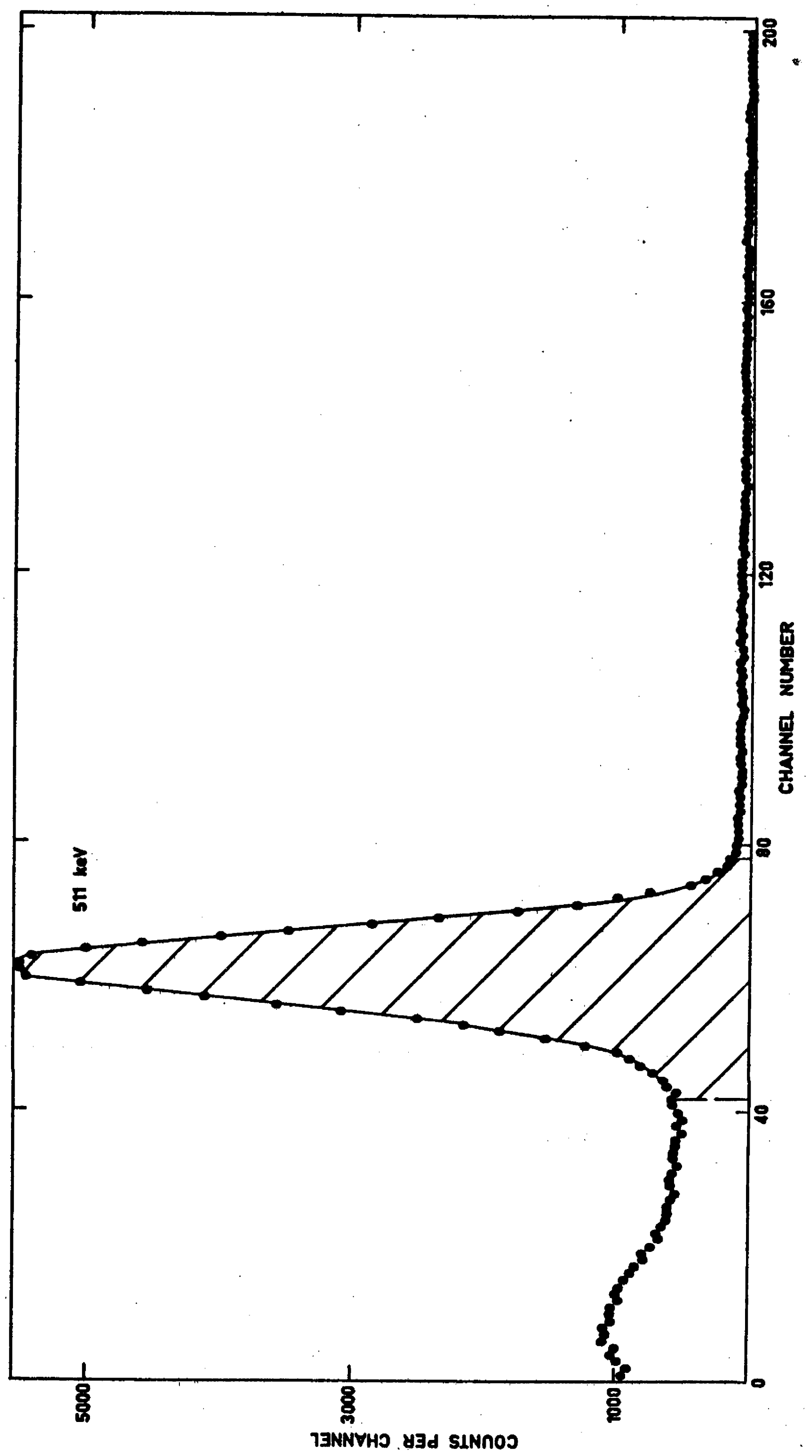

Fig. 6 A gamma-ray spectrum taken with one of the crystal spectrometers after a bombardment of F^{19} with 8.3 MeV protons. The hatched area indicates the energy interval selected for the coincidence measurements.

channel analyser window set over the 0.511 MeV annihilation γ-ray photopeak. Figure 6 shows a γ-ray spectrum obtained with the 7.6 cm x 7.6 cm crystal spectrometer used.

As a check on the presence of other activities, the decay of coincidences between the two annihilation quanta was also followed. This did not exclude from the measurement other positron activities on the target, but, because of the relation in space between the directions of the $\frac{1}{2}$-MeV quanta resulting from a positron annihilation, it did exclude the detection of other positron activities <u>not</u> emanating from the target. For example, the activity induced in the quartz viewer used to observe the position and focus of the beam was not detected. The linearity of the logarithmic plots indicated that the effect of any impurity in the target was negligible.

2.5 Analysis of the Results

The fact that only one decay was measured in each experimental run meant that about 15 of them could be added together to provide data with from 30,000 to 40,000 counts in the first channel. The last 25 channels of each such set of data were averaged, and the mean value subtracted from all channels as the constant background. As noted earlier, no other corrections had to be applied. The logarithm to the base 10 of the net counts per channel was tabulated.

For the decay of radioactive nuclei

$$N(t) = N(0)e^{-\lambda t}$$

where time t = 0 is the commencement of the counting period

$N(t)$ is the number of radioactive nuclei present at time t

and λ is the relevant decay constant.

Hence $\log_{10} N(t)/N(0) = -0.4343\lambda t$.

However, the number of nuclei $N(t)$ is proportional to the measured activity $A(t)$ (Kaplan, 1956), so that

$$N(t)/N(0) = A(t)/A(0)$$

or $\log_{10} A(t) = \log_{10} A(0) - 0.4343\lambda t$.

Hence, if the $\log_{10}$ of the measured activity is plotted against time, a straight line should result whose slope is equal to -0.4343λ. The half-life is then very easily found from the relation

$$\tau = 0.693/\lambda .$$

A plot of the logarithm of the net counting rate versus time for one set of half-life data is shown in figure 5.

Each point was then weighted by the reciprocal of the square of its statistical uncertainty (its variance σ^2), and a straight line fitted to the first 30 of the points by the linear least squares method of Rose (1953). That is, a functional fit was made to the logarithm of the net number of counts per two seconds, μ_i, via

$$\mu_i = \sum_{\lambda} \alpha_{\lambda} A_{i\lambda}$$

where, in our case,

$$\mu_i = \log N_i(t_i)$$

$$\alpha_1 = \log N_o$$

$$\alpha_2 = -0.4343\,\lambda$$

$$\alpha_3 = \alpha_4 = \ldots. = 0$$

$$A_{i1} = 1, A_{i2} = t_i$$

$$A_{i3} = A_{i4} = \ldots. = 0.$$

The coefficients α_{λ} were determined from

$$\sum_i w_i(\mu_i - \sum_{\lambda}\alpha_{\lambda} A_{i\lambda})^2 = \text{minimum},$$

where the weights $w_i = 1/\sigma^2 = N_i$,

since $d(\log N_i) = (1/N_i)\, dN_i = N_i^{-\frac{1}{2}}$, $d(N_i) = N_i^{\frac{1}{2}}$,

or $\sigma^2(\log N_i) = 1/N_i$.

Rose also derived an expression for the RMS error in α_{λ}. As no computer was available, these calculations, which were not difficult, were made by hand, yielding the slope of the fitted straight line ($\alpha_2 = -0.4343\,\lambda$), and hence the half-life, and its RMS error. It is to be remembered that, although only C^{10}

decays via the first excited state of B^{10} were counted, the decay constant obtained was that for the total C^{10} activity.

This analysis was performed on the six independent sets of C^{10} half-life data, and the five independent Ne^{19} measurements. The results are given in Table 1.

TABLE 1.

Half-life of C^{10} (sec.)			Half-life of Ne^{19} (sec.)		
Method	Value	Error	Method	Value	Error
0.717	19.46	0.05	0.511	17.40	0.10
0.717	19.55	0.12	COINC	17.48	0.10
0.717	19.45	0.05	0.511	17.29	0.15
COINC	19.42	0.05	0.511	17.32	0.14
COINC	19.40	0.07	COINC	17.64	0.15
0.717	19.40	0.08			

The standard deviation about their average of the respective half-life values was also calculated, giving $\pm$ 0.05 and $\pm$ 0.13 sec. for C^{10} and Ne^{19} respectively. The good agreement between these values and the RMS errors obtained from the least squares fitting was strong evidence against statistically significant, long-term variations in the apparatus. The standard deviation of each of the averages of the half-life values, sometimes called the standard error (Evans, 1955), is given with the averages, which were the final results of this work

$$\tau(C^{10}) = 19.45 \pm 0.03 \text{ sec.}$$
$$\tau(Ne^{19}) = 17.43 \pm 0.06 \text{ sec.}$$

The C^{10} value differs markedly from that reported by Sherr et al. (19.1 $\pm$ 0.8 sec.), and it is not in close agreement with a measurement reported subsequently, namely 19.27 $\pm$ 0.08 sec. by Bartis et al. (1962). The Ne^{19} half-life is in good agreement with one of the better values previously reported, namely 17.4 $\pm$ 0.2 sec. due to Herrmannsfeldt et al. (1959), but not with others.

Combining the C^{10} half-life with the branching ratio for decay to the second excited state of B^{10} gave the partial half-life for the interesting $0^+ \rightarrow 0^+$ transition as 19.80 sec.

2.6 Discussion

The C^{10} and Ne^{19} half-life values obtained are very accurate; the errors are less than 0.15% and 0.35% respectively. Until recently very few half-lives have been reported with such a degree of certainty. If a computer had been available, this could have been improved further if so desired, since it would have been possible to test for slight curvatures in the logarithmic plots, that is, for the presence of very weak activities, and to check the results obtained by minimizing $\sum_{i} w_i(\mu_i - \sum_{\lambda} A_{i\lambda}\alpha_{\lambda})^2$ with respect to λ rather than α_{λ} in a non-linear least-squares straight-line fit. It is emphasized that the agreement between the RMS errors obtained from the fitting and the standard deviations about their average of the half-life values means that such calculations were not important in the work described above. However, in general, the ease, speed and accuracy of a computer are clearly preferable, allowing exhaustive tests of the data to be made.

The equipment now available, such as the new generation of multi-channel analysers and computers, when used in conjunction with careful and thoughtful experimental work, makes possible the measurement of half-lives to almost any required degree of accuracy. The method described in this chapter, where a unique γ-ray or other means of isolating the activity of interest is available, is a particularly powerful one.

CHAPTER THREE

THE $B^{10}(p,n)C^{10}$ EXCITATION FUNCTION

3.1 Introduction

The major reasons for this study, and its part in the investigation of C^{11} energy states, have been discussed in Chapter 1. Neutron detection, even to a degree of accuracy an order of magnitude worse than can be obtained in charged particle work, remains one of the most difficult experimental problems in nuclear physics; and as the high resolution machines attain higher and higher energies this problem becomes more and more acute, because the energy and the rate of production of background neutrons rise alarmingly. As shall be illustrated here, and again in chapter 6, many of the best methods for measuring neutron events are indirect, in that the neutrons themselves are not detected. The activation technique is one such method.

Transitions to the ground state of C^{10} in the reaction $B^{10}(p,n)C^{10}$ are inhibited by the large spin change, $\Delta J = 3$, involved. As a result the cross section below the first excited state threshold is small, and no excitation function for the reaction had been measured. Information on high lying levels of

C^{11} was scarce, particularly above the $B^{10}(p,n)C^{10}$ threshold. Kalinin et al. (1957) had carried out a poor resolution stacked foil experiment which suggested the presence of broad resonances in the $B^{10}(p,\alpha)Be^{7}$ excitation function at E_p = 5.6 and 7.8 MeV, corresponding to broad levels in C^{11} at 13.8 $\pm$ 0.2 and 15.7 $\pm$ 0.2 MeV excitation energy, and subsequently Ophel et al. (1962) had established the level in C^{11} at 13.90 $\pm$ 0.02 MeV using the $B^{10}(p,p'\gamma)$ reaction; but this was all that was known.

The work recorded here was undertaken to measure the $B^{10}(p,n)C^{10}$ excitation function from threshold (E_p = 4.835 MeV, Takayanagi et al., 1961) to 10.6 MeV, and to search for levels of C^{11} between 13.1 and 18.3 MeV excitation. As has been mentioned, the reaction was investigated most readily using an activation technique, since coincidences between the 0.717 MeV γ-ray and one of the 0.511 MeV annihilation radiation quanta (figs. 1 and 3a, chapter 2) allowed unique identification of the C^{10} activity even in the presence of other positron activities; for example, the $B^{11}(p,n)C^{11}(\beta^{+})B^{11}(\tau = 20$ min.) reaction, produced in the B^{11} content of the targets used, had a cross section approximately 50 times that of $B^{10}(p,n)C^{10}$, and contributed largely to the failure of previous attempts to study the $B^{10}(p,n)C^{10}$ reaction.

The development of the activation apparatus used is discussed before consideration of the performance and interpretation of the experiment itself.

3.2 Aparatus

The measurement of an excitation function by an activation technique over an energy range as large as that of this experiment involves the activation and subsequent decay of the target a very large number of times. If the $B^{10}(p,n)C^{10}$ experiment was to be done in a reasonable time it was clear that the processes involved had to be automated to the maximum extent. Care was then needed to see that accuracy was maintained.

Apart from the necessity of automation, other design considerations included

(a) the use of two 7.6 cm. x 7.6 cm. NaI(Tl) γ-ray spectrometers to detect the γ-rays from the decay of C^{10},

(b) maximum counting efficiency, particularly as the $B^{10}(p,n)C^{10}$ cross section was expected to be small,

(c) maximum shielding of the two crystals, particularly during the bombardment periods, to minimize gain shifts due to high count rates and activation of the NaI crystals,

(d) mounting positions for several targets and facilities for positioning them accurately and automatically in the beam (this facility, designed to allow relatively long-lived activities to die away, was not used

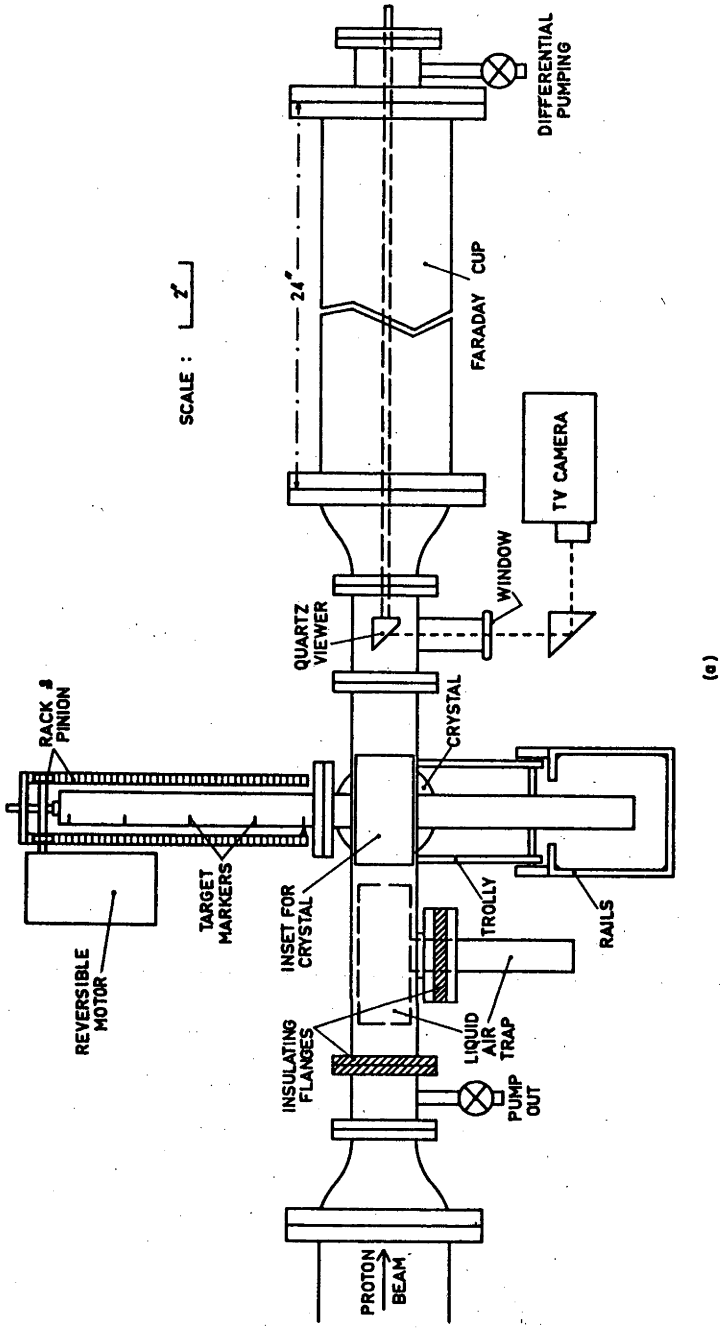

Fig. 7(a) A side elevation of the target chamber and associated equipment.

extensively in this work because such activities did not affect the results),

(e) a cold trap to minimize contamination of the targets by mercury and carbon, and

(f) the provision of a quartz disc, viewed by a television camera, to align the beam onto the target.

The target chamber and counter arrangement are shown in figure 7. The chamber body was made of brass, and had to be completely lined with 0.02 cm. thick tantalum sheet to prevent activation of the brass walls by the proton beam. Early in the experiment accidental bombardment of the walls when aligning the beam resulted in the production of long lived activities in the copper and zinc components of the brass. These radioisotopes emitted γ-rays with energies from 0.5 to 1.8 MeV, greatly increasing the random coincidence counting rate. Also, all sources of positron activity had to be eliminated for the $F^{19}(p,n)Ne^{19}$ work which was to follow the $B^{10} + p$ investigations, since no unique γ-ray existed in that case.

A tantalum cylinder capable of moving vertically inside two sleeves, one above and one below the chamber, provided mounting positions for five targets. A remotely controlled motor and TV camera were used to drive the target support, and position the chosen target in the line of the beam to better than 0.05 cm.

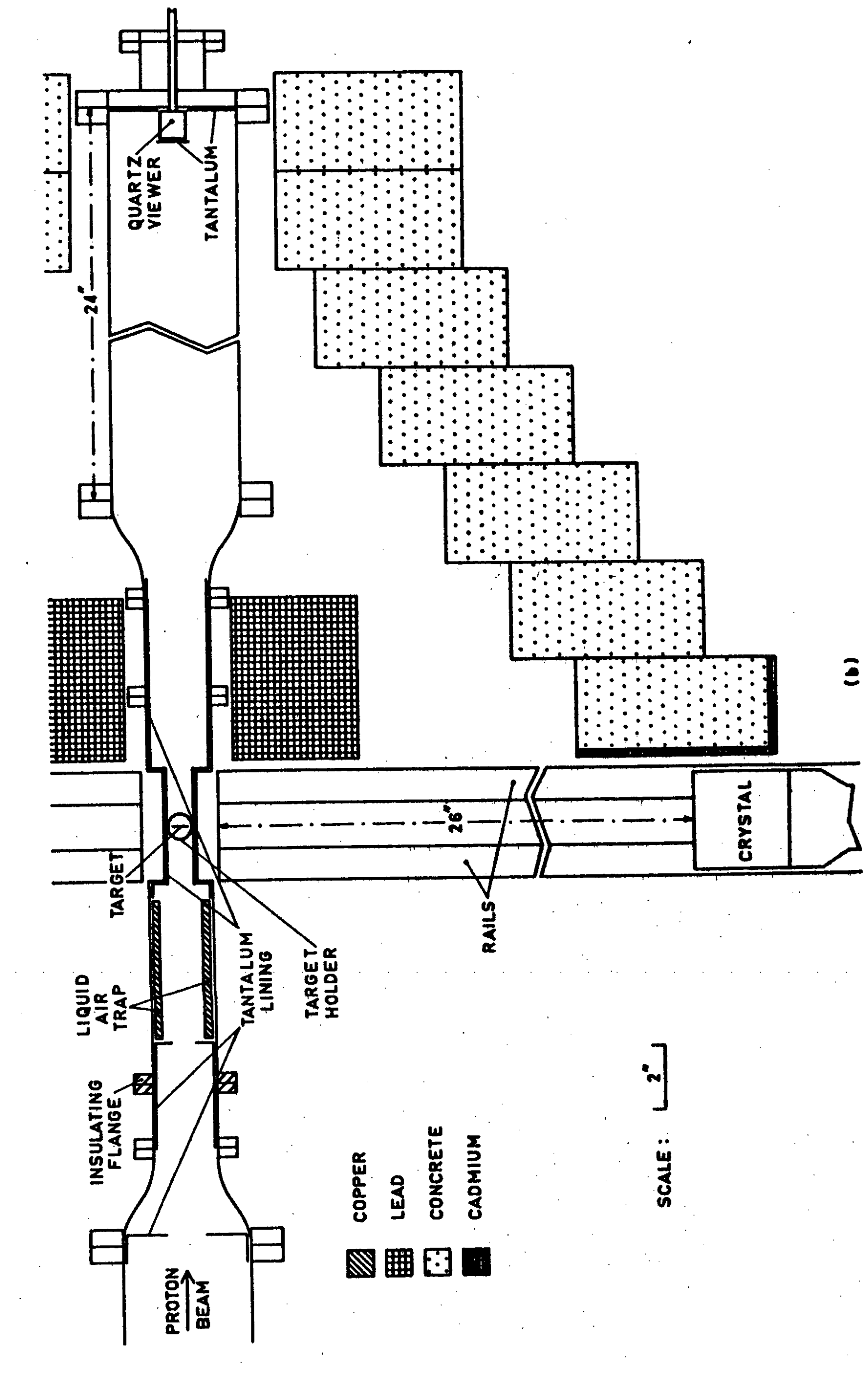

Fig. 7(b) A horizontal section through the target chamber and associated equipment, showing the tantalum lining and the shielding of the NaI crystals.

A liquid air vapour trap of similar design to ones used previously in the laboratory (Bashkin and Ophel, 1962) was placed directly in front of the target. Some difficulty was experienced during the experiment with "jumps" occurring in the excitation function, being one or more points which, by the discontinuous nature of the curve obtained, were clearly in error by as much as 20%. It is believed that this trouble was due to incorrect current integration, caused by conduction through the large amount of water which condensed onto the target chamber near the vapour trap. Certainly after the use of the trap was discontinued no more "jumps" were observed; neither was there any detectable build-up on the target of mercury or carbon.

At the beginning of the work a HVEC, compressed-air-driven,quartz viewer was used in the position shown, but as the quartz became highly positron active, it was arranged to withdraw it to the end of the beam tube during counting operations. Here rotation of the viewer caused a tantalum flap to fall across the quartz disc, shielding it from the beam which passed through the thin targets.

In order to increase the detection efficiency, two flat sections were inset into the side of the chamber to take the front faces of the crystals. To minimize activation of the Na and I (for example, $I^{127}(n,\gamma)I^{128}(\beta^-)$ which gives a strong 0.45 MeV

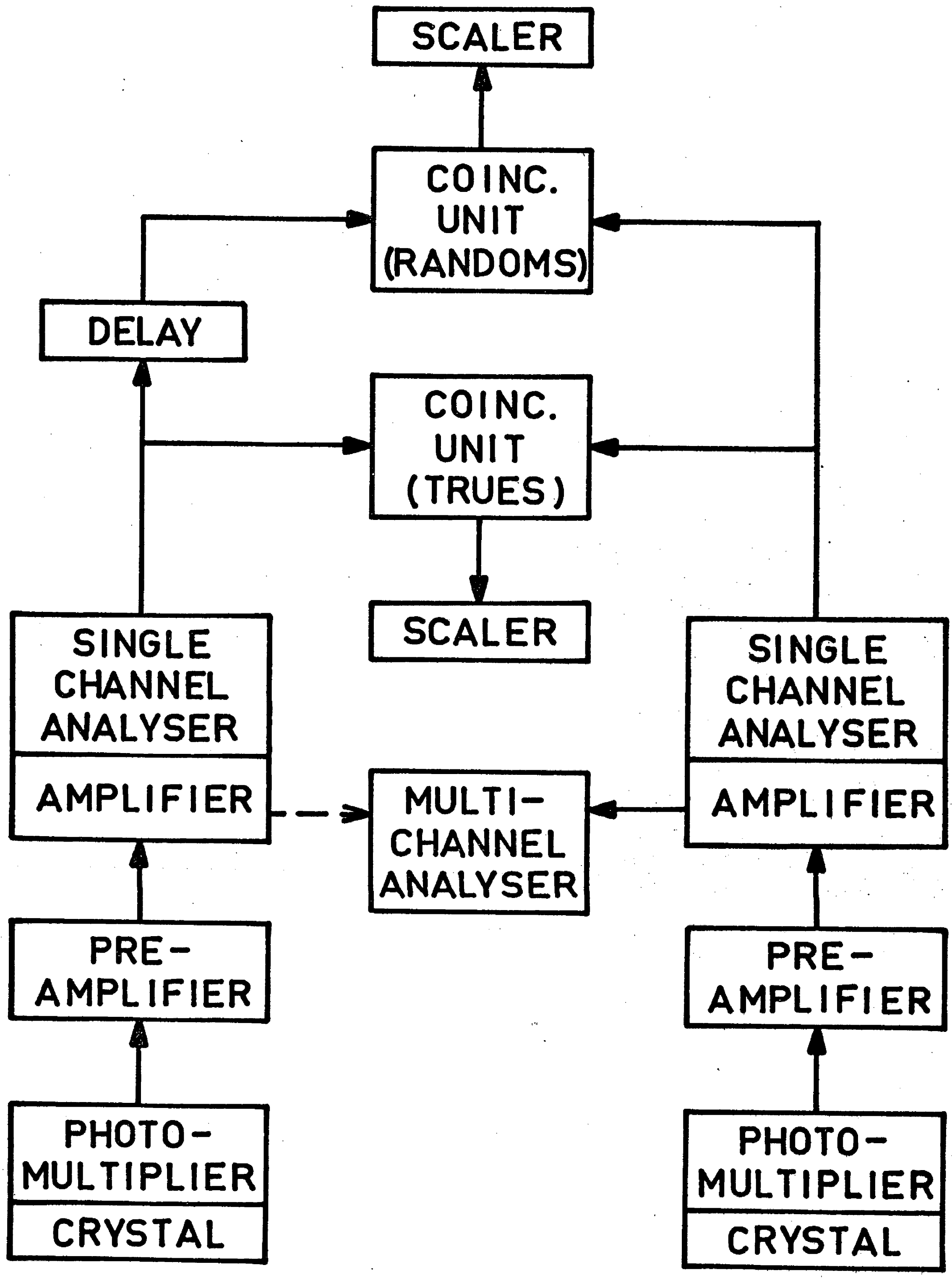

Fig. 8 A block diagram of the detection equipment used in the experiment.

γ-ray), the two counters were mounted on small, remotely controlled and compressed-air-driven trolleys, which were withdrawn 66 cm. from the target during the bombardment period, and then brought to within 1.3 cm. of the target for the counting period.

The shielding used is illustrated in figure 7(b). Concrete lined with cadmium sheet served to shield the crystals from neutrons originating in the Faraday cup. Lead blocks were used to protect the detectors in the counting position from residual positron activity in the quartz, and in the distant position from the high flux of γ-rays produced when aligning the beam with the quartz viewer. Lead sheet 0.32 cm. thick was wrapped around the crystals to reduce the intensity of low energy γ-rays from both the target and the capture of slow neutrons in the cadmium.

3.3 Detectors

The use of two 7.6 cm. x 7.6 cm. NaI spectrometers mounted on trolleys has been mentioned. As figure 8 shows these Harshaw crystal-photomultiplier integral units were followed by Franklin, double-delay-line preamplifier-amplifier systems, and pulses in the 0.717 and 0.511 MeV γ-ray photopeaks were selected with single channel analysers and fed to a slow coincidence unit with a resolving time of 0.2 μsec. Accidental or random coincidences were counted simultaneously with a second coincidence unit having a one second delay in one channel.

To prevent large gain variations in the photomultipliers caused by the high counting rates experienced when the beam was incident on the target, the photomultipliers were shut off during the bombardment by applying a reverse bias of -90 volts between their photocathodes and focus grids (Farinelli and Malvano, 1958). Small, slow gain drifts, made apparent by the position of the 0.511 MeV γ-ray photopeak recorded on a multichannel analyser, were corrected by Helipot adjustment of the high voltage supply of each photomultiplier.

3.4 Targets

For proton energies up to 8.5 MeV a target of separated boron metal ($> 99.9\%$ B^{10}) of nominal thickness 600 $\mu gm/cm^2$ deposited on a thick tantalum backing † was used. The energy loss in this target was about 44 keV at E_p = 5 MeV. Preliminary measurements showed that this target was non-uniform, and hence care had to be taken to bombard the same portion of the target throughout the experiment. The movable quartz viewer mentioned above was used for this purpose, and at each setting the beam

† Obtained from the Harwell Electromagnetic Separator Group.

was focussed to a spot less than 0.5 cm. in diameter located centrally to better than 0.05 cm. This procedure allowed reproduceable results to be obtained.

Above 8.5 MeV, neutrons from the tantalum backing (Hansen et al., 1962) of the target produced prohibitively high activities in the NaI detectors, even at the distant position they occupied during the bombardment time. For the remainder of the experiment a self-supporting boron film containing 105 $\mu gm/cm^2$ of B^{10} was used. This target contained 89% B^{10}, 8% B^{11}, some carbon and traces of tantalum. At first, reproduceable results could not be obtained with the foil target. Calculations showed that it was probable that the C^{10} nuclei formed in the reaction were recoiling out of the target and being lost from the counting region. A 3 mgm/cm^2 gold foil was placed directly behind the target to stop these recoiling nuclei, and the consistent results then obtained were experimental proof of the diagnosis.

3.5 Experimental Procedure

The experimental procedure was as follows. The target was irradiated for 60 seconds (slightly greater than three half lives) by which time 90% of the equilibrium activity was established, thus making small timing errors insignificant. The beam current was measured by an Elcor model A309A current integrator and was

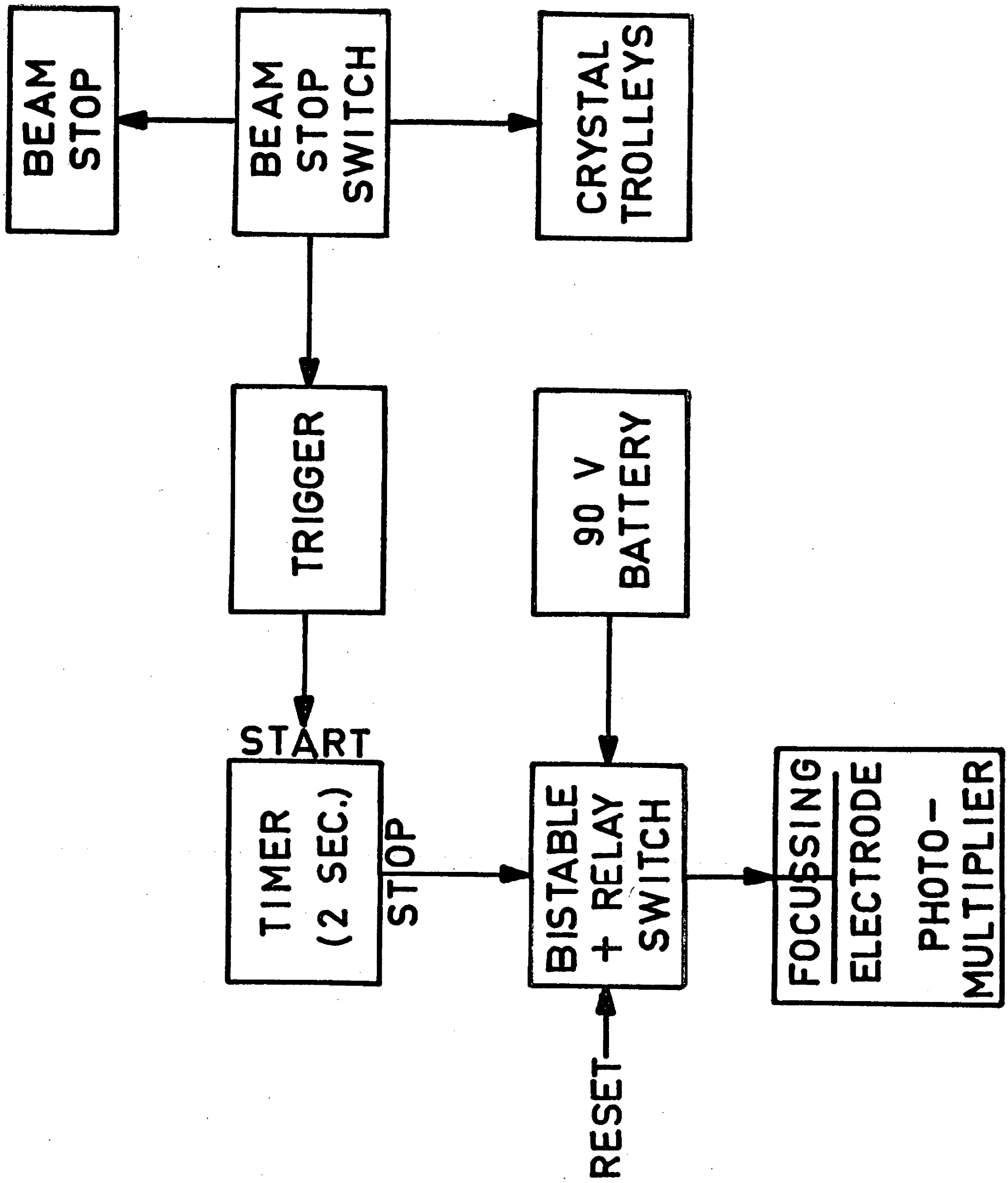

Fig. 9 A block diagram of the circuitry used for remotely controlling the activation experiments.

held as constant as possible during bombardment. Pen records of the beam current were kept during a number of days of data collection, and the beam current fluctuations observed contributed an error of less than 0.1% to the activity calculated assuming a constant current. This error calculation is discussed in detail in Appendix A. During the beam-on period the crystals were withdrawn from the target and the photomultipliers were biassed off. At time 60 sec. a switch simultaneously operated a plunger to interrupt the beam 6m from the target, started an electronic timer and activated the compressed-air cylinders to bring the crystals up to the counting position (see figure 9). The crystals took 1.5 sec. to move into position. At time 62 sec. the timer operated a fast acting relay switch which started the counting by removing the 90 volts bias from the photomultipliers. Coincidences in the two detectors were recorded for 60 sec., the count being terminated by reapplying the 90 volts bias with a manual reset pushbutton. Random coincidences were recorded at the same time. At least a further two minutes was allowed before bombarding again, which meant that less than 0.2% of the previous activity remained at the commencement of the following bombardment.

The beam current was chosen to be small enough so that counting losses were less than one percent. Typical values were $0.03\mu A$ and $0.1\mu A$ for the thick and thin targets respectively.

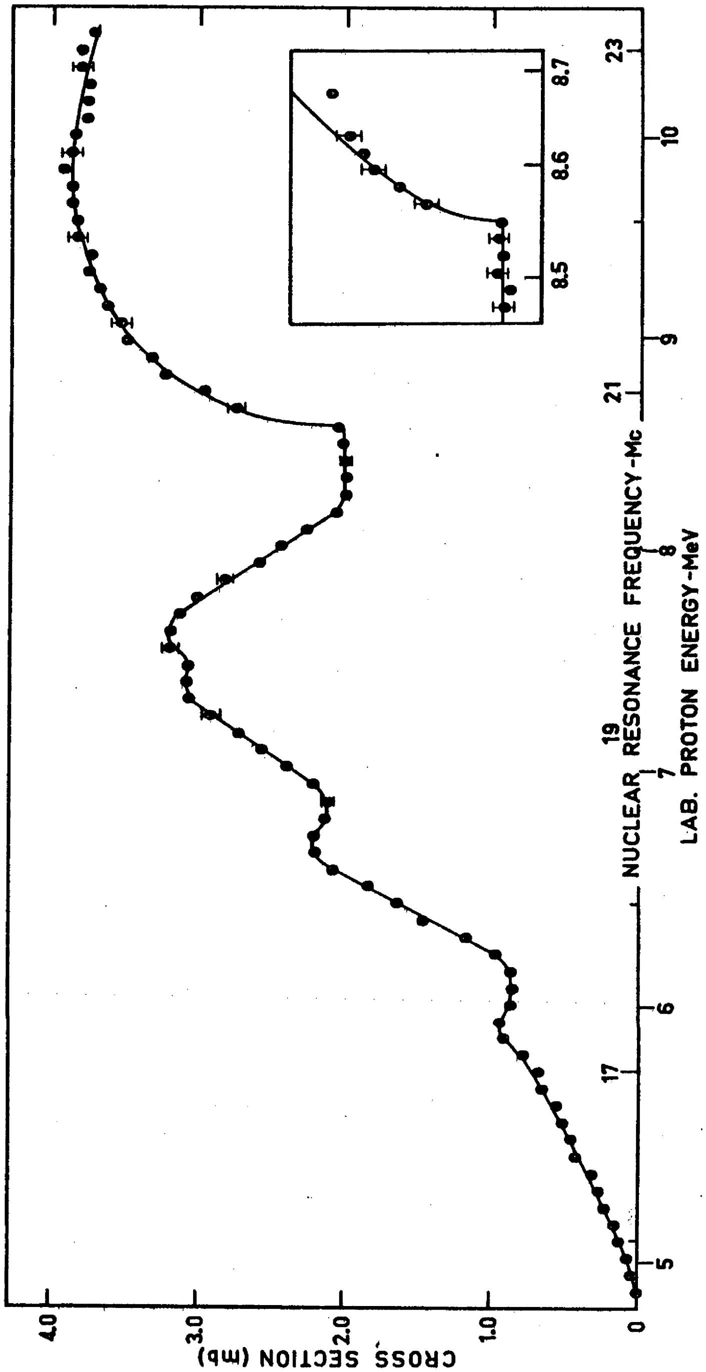

Fig. 10 The total $B^{10}(p,n)C^{10}$ cross section as a function of energy. The inset is a detail of the curve in the region of E_p = 8.5 MeV, the solid line being a $E_n^{\frac{1}{2}}$ fit to the points.

3.6 Results and Discussion

The relative cross section was obtained in the form net true coincidence counts in 60 sec./μ Coulomb, which was proportional to C_2/n_2 in the notation of chapter 2. During a run over a selected energy range, at least three determinations were made at each proton energy and averaged. The statistical error on this average was $\pm 3\%$. Each energy interval was covered between six and nine times and the resulting excitation function shown in figure 10 represents an average of these individual runs weighted equally after normalisation. The r.m.s. error on the average curve, obtained from the deviation of each measurement from the mean, was $\pm 2\%$, a little greater than the statistical error. This meant that the structure of the curve in the region $E_p = 7.5$ MeV was not absolutely certain. However, the fact that the averaging failed to smear the curve into a single broad peak suggested the existence of two resonances in this region.

The excitation curve consisted of resonance structure superimposed on a continuous background. Presumably the background was due to direct interaction mechanisms and to constructive interference between the direct interaction and single particle resonance contributions. The resonance structure was of primary importance.

3.6.1 Levels in C^{11}

The maxima in the excitation function, occurring at proton energies of 5.92 ± 0.02, 6.68 ± 0.04, 7.33 ± 0.05 and 7.60 ± 0.05 MeV, corresponded to broad levels in the compound nucleus C^{11} at excitation energies of 14.08 ± 0.02, 14.78 ± 0.04, 15.36 ± 0.05 and 15.61 ± 0.05 MeV.

Although the $B^{10}(p,n)C^{10}$ reaction had not been studied previously the lower excitation energies reached in this experiment had been attained through the $B^{10}(p,p'\gamma)$ and $B^{10}(p,\alpha)$ reactions. Taking into account the broad nature of the levels and the difference in penetration factors for the respective reactions, it was reasonable to suppose that the level at 14.08 MeV corresponded to the level previously reported at 13.8 ± 0.2 MeV (Kalinin et al., 1957) and 13.90 ± 0.02 MeV (Ophel et al., 1962). The ill-defined level of Kalinin et al. at 15.7 ± 0.2 MeV probably reflected the "double resonance" observed in this experiment near to 15.5 MeV excitation.

3.6.2 Absolute Cross Section

The "thick" target used in the experiment between threshold and $E_p = 8.5$ MeV was non-uniform and unsuitable for an absolute cross section measurement. The self-supporting B^{10} target used to

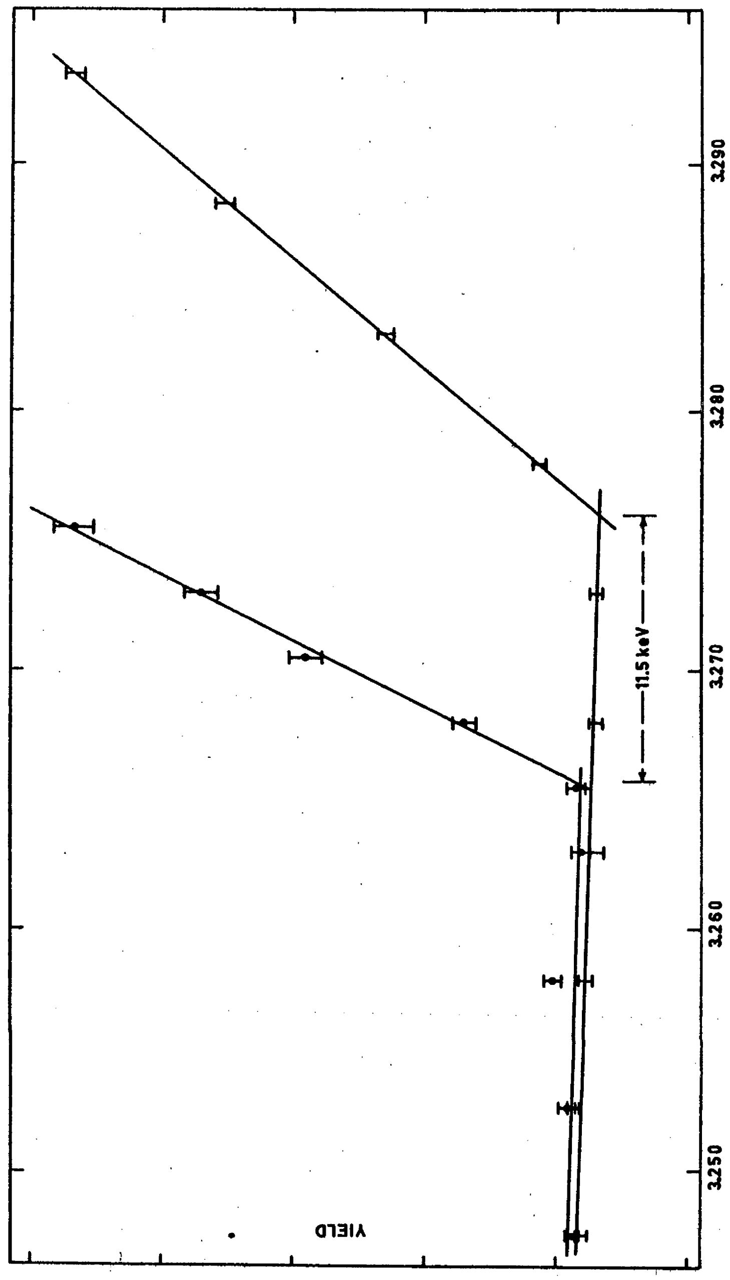

Fig. 11 The measurement of the thickness of the self-supporting B^{10} target. The dots represent the $C^{13}(p,n)$ threshold data taken with the slow neutron detector. The other curve shows the energy shift of the threshold when the B^{10} film was placed in front of the C^{13} target.

obtain data from E_p = 8.5 to 10.6 MeV was much more uniform. Its thickness was measured by observing the energy shift of the $C^{13}(p,n)$ threshold when the proton beam passed through it (figure 11). A Nuclear Enterprises type NE 401 boron loaded plastic scintillator was used to detect the slow neutrons. From the measured energy loss in the target the content of B^{10} was calculated as 105 $\pm$ 10 $\mu gm/cm^2$, or 6.44×10^{18} B^{10} nuclei/cm^2.

The detection efficiency of the coincidence counting system used in the experiment also had to be known. For the decay of one C^{10} atom this was $2\varepsilon_1\varepsilon_2$, where ε_1 and ε_2 were the γ-ray photo-peak total detection efficiencies of the spectrometers for the 0.511 MeV annihilation quantum and 0.717 MeV γ-ray respectively. The calculation and measurements of ε_1 and ε_2 are discussed in detail in Appendix B. It is sufficient to say here that a satisfactory calculation of ε_2 was very difficult because of the high absorption ($\sim$50%) in the 0.32 cm. of lead shielding and in the target chamber. Instead the absorption was measured experimentally for the 0.66 MeV γ-rays from a Cs^{137} source, and used to correct the calculated 0.717 MeV γ-ray detection efficiency without absorption. An experimental determination of ε_1 was made using a Na^{22} source. Apart from the uncertainties in ε_1 and ε_2 other errors were in the current integrator, which was accurate to $\pm$1%, and in the timing of the bombardments and counting periods, which were accurate to $\pm$0.5%. The r.m.s. error on the average number of counts per micro Coulomb was therefore estimated to be $\pm 2\%$. The distribution of errors is shown in Table 2; other sources of uncertainty, for example, in the value of the half-life, were negligible compared with those listed.

Table 2

Distribution of errors in the absolute cross section measurement

Source of error	Percentage
Target thickness	$\pm 10\%$
Counts/μ coulomb	$\pm 2\%$
Total detection efficiency $\mathcal{E}_1$	$\pm 2.5\%$
Total detection efficiency $\mathcal{E}_2$	$\pm 5\%$
Total error	$\pm 12\%$

The reaction cross section, σ, was calculated as follows :
In chapter 2 it was found that, in general, the number of reactions per proton, n_1, was given by

$$n_1 = C_2 \lambda \Big/ n_2 f (e^{-\lambda t_2})(1-e^{-\lambda t_1})(1-e^{-\lambda t_3})$$

where C_2 = number of counts recorded

f = efficiency of counting arrangement

n_2 = number of protons/sec. incident on the target

λ = decay constant

t_1, t_2, t_3 = bombardment, waiting and counting times respectively;

and, under certain conditions which were fulfilled in the $B^{10}(p,n)C^{10}$ experiment, n_1 was also given by

$$n_1 = \sigma . n$$

where n = number of target nuclei/cm^2.

Other factors considered were :

(a) There was no correlation between the directions of the 0.511 and 0.717 MeV γ-rays. There was a correlation between the positron direction and that in which the 0.717 MeV γ-ray was emitted, but the directions of the two 0.511 MeV quanta were independent of the positron path provided the positron did not annihilate in flight; and so both the 0.511 and 0.717 MeV γ-rays were isotropic and non-correlated.

(b) $f = 2\mathcal{E}_1\mathcal{E}_2 = 2\mathcal{E}_1(r_2\mathcal{E}_2^T)$ (see Appendix B) where the 2 arose from the fact that the two annihilation quanta were emitted in opposite directions.

Hence, for this case,

$$n_1 = c_2\lambda \big/ 2n_2\mathcal{E}_1\mathcal{E}_2(e^{-\lambda t_2})(1-e^{-\lambda t_1})(1-e^{-\lambda t_3})$$ where all the quantities on the right-hand side were known, and $\sigma = n_1/n$.

The absolute reaction cross section at a proton energy of 8.50 MeV was found to be 2.0 $\pm$ 0.2 mb. A cross section for the reaction had been reported by only one other group. Gibbons and Macklin (1959) suggested the value $\sigma \leqslant 2$ mb at 5.51 MeV, while our measurements gave 0.50 ± 0.04 mb at 5.51 MeV.

3.6.3 First Excited State of C^{10}

The sharp rise in cross section at $E_p = 8.55$ MeV was interesting. It corresponded closely to the energy at which neutron transitions to the first excited state of C^{10} became energetically possible. Because of the large spin difference, neutron emission to the ground state of C^{10} was restricted, hence the yield was low. At the threshold of the first excited state, however, s-wave neutron emission became possible and, in the absence of resonances in this energy region and for a thin target, the yield above threshold was expected to rise according to the square root of the centre of mass neutron energy E_n (Blatt and Weisskopf, 1952, for example). This region of the excitation function was repeated in greater detail and the data fitted by a curve of the form cross section $\alpha E_n^{\frac{1}{2}}$ (see inset in figure 10). The continuous line represents the fitted $E_n^{\frac{1}{2}}$ curve, and it can be seen that a reasonably good fit to the experimental data was obtained. Assuming that the cross section rise at $E_p = 8.55$ MeV was a threshold corresponding to the first excited state, the level was located at 3.38 ± 0.03 MeV compared to the previous determination of 3.4 ± 0.2 MeV (Ajzenberg and Franzen, 1954).

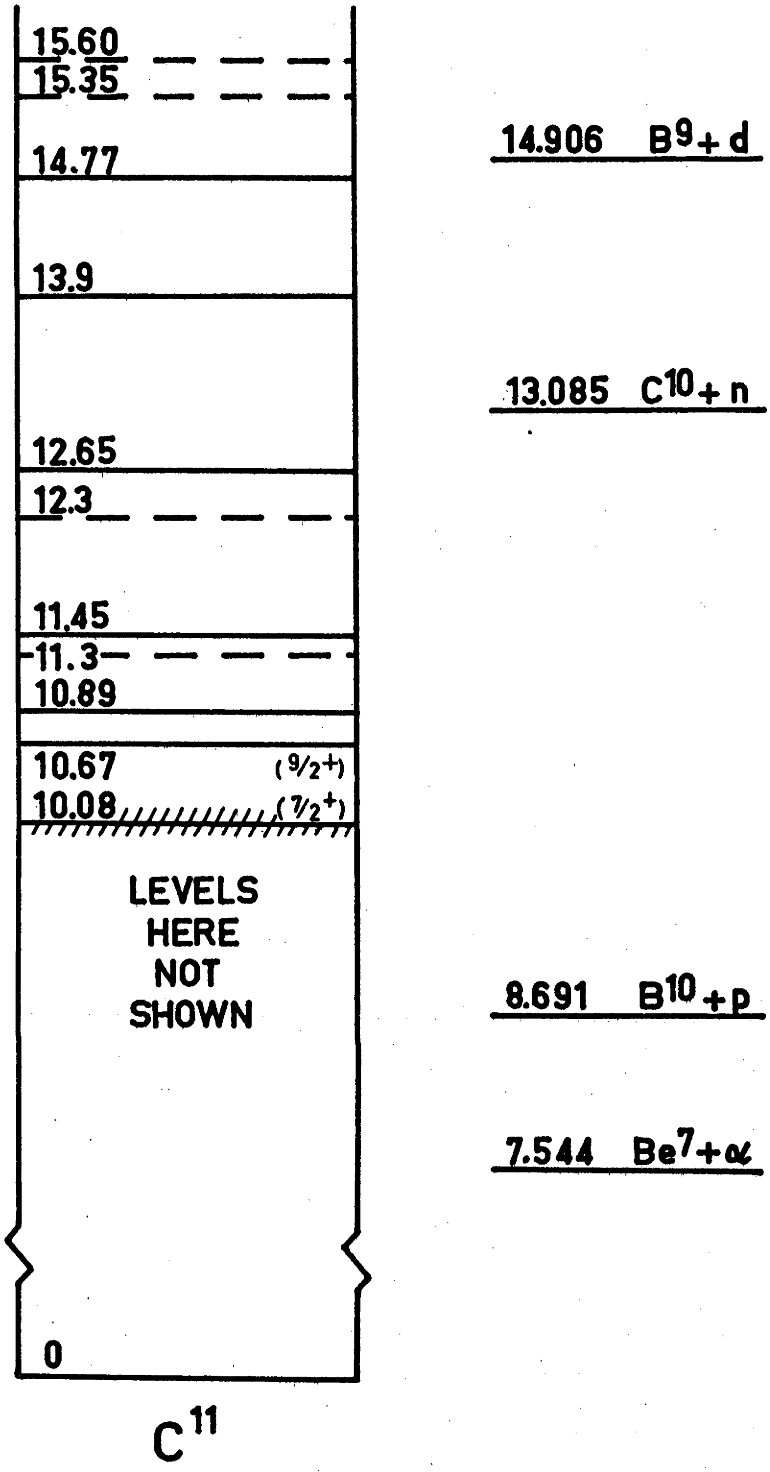

Fig. 12 The energy level scheme for C^{11} at the time when the $B^{10}(p,\alpha)Be^7$ work was begun.

CHAPTER FOUR

THE $B^{10}(p,\alpha)Be^7$ REACTION BETWEEN 2 and 11 MEV

4.1 Introduction

As mentioned in chapter 1, a study of the $B^{10}(p,\alpha)Be^7$ reaction logically followed the $B^{10}(p,n)C^{10}$ investigations. A number of C^{11} energy levels, both below and above the $B^{10}(p,n)C^{10}$ threshold, were known, but few attempts had been made to determine their properties. For reasons that will become clear later, attention was restricted to those levels above 10 MeV excitation in C^{11}. A summary of the C^{11} energy states known at the beginning of this work is given in figure 12.

Approximately 10 groups of workers had observed the 10.08 MeV state using a number of B^{10} + p and B^{10} + d reactions (A-S and L, 1959 and 1962). Cronin (1954) and Overley and Whaling (1962) had assigned a spin of $7/2^+$ to this level, and determined a number of its other properties, such as reduced widths, using the $B^{10}(p,\alpha)Be^7$ and $B^{10}(p,p)B^{10}$ reactions. Overley and Andreev et al. (1962) had confirmed the existence of a state at 10.67 MeV, first seen in the $B^{10}(d,n)C^{11}$ work of Cerino (1956) and Graue and Trumpy (1957). Overley had suggested that the spin and parity were $9/2^+$, and had given values for the α_o and proton reduced widths. Cerino, Graue,and Day and Huus' (1954) investigations of the $B^{10}(p,\gamma)C^{11}$ reaction had placed a state at 10.89 MeV, while Cerino had suggested further possible levels at 11.3 and 11.5 MeV. The latter had been confirmed by the work of Ophel et al. (1962), whose $B^{10}(p,x\gamma)$ studies had also suggested states at 12.65 and 13.90 MeV. The $B^{10}(p,n)C^{10}$ experiment of chapter 3 had earlier confirmed the originally uncertain 13.9 MeV state of Kalinin et al. (1957). The (p,n) work had also suggested further states 14.8, 15.4 and 15.6 MeV. No confirmation had been found for the 12.3 MeV state tentatively suggested by Kalinin and Bain et al. (1955).

The $B^{10}(p,\alpha)Be^{7}$ experiment was begun in the hope of more firmly establishing many of these levels and of determining some of their properties. Because the alpha-particle has spin zero, there was only one channel spin available to the outgoing system, and this increased the possibility of making assignments of spins, parities and reduced widths to states of the intermediate system, C^{11}, by studying the angular distributions of the alpha-particles produced.

Semi-conductor,charge-particle detectors were used. A great deal has justifiably been written about the revolution these counters have wrought in low energy nuclear physics (for example, G.L. Miller et al. (1962)). Their more outstanding characteristics can be appreciated if a comparison is made with other charged-particle detectors. They are superior to scintillators because of their linearity over a very wide range of energies, their speed of response, low background, and the low voltage supply required for their operation. However, they do have slight limitations with respect to size and depth of depletion layer. The variability of the depletion layer of a solid state counter is one of its major assets, and this facility was used in the $B^{10}(p,\alpha)Be^{7}$ experiment. They are highly stable devices, and their resolution is only a little inferior to that obtainable with magnets. Compared to magnetic spectrometers they have the advantages of allowing an entire spectrum to be taken at once, a larger effective solid angle, smallness of size and relative cheapness.

With these detectors excitation functions were taken for alpha-particle groups from the $B^{10}(p,\alpha)Be^{7}$ reaction proceeding to the ground (α_0) and first excited (α_1) states of Be^{7}, for proton bombarding energies from 1.8 to 10.8 MeV. Thirty angular distributions for both α_0 and α_1 were taken between proton energies of 2.8 and 7.0 MeV. The limits on the energy ranges over which these data were taken are explained in section 4.2.

During this study of the $B^{10}(p,\alpha)Be^{7}$ reaction it became clear that information on the $B^{10}(p,He^{3})Be^{8}$ reaction could be obtained simultaneously. Measurements of the excitation functions for the (p,He^{3}) reaction leading to the ground state of Be^{8} were taken at laboratory angles of 50^{o} and 90^{o}, together with a number of angular distributions obtained in the energy range E_p = 4 to 10 MeV.

Existing information about the reaction $B^{10}(p,He^3)Be^8$ was of a preliminary nature only. Craig et al. (1952) had identified the reaction at two proton energies using an electrostatic analyzer to detect the He^3 particles. They had determined an approximate differential cross section at E_p = 3.4 MeV and measured the reaction Q-value. Reynolds (1955) had also observed the reaction, but made no quantitative measurements.

4.2 Experimental Procedure and Results

A 100 μgm/cm^2 self-supporting boron target, containing 89% B^{10} and 8% B^{11} by weight, was mounted on a rotatable support at the centre of an 18 cm diameter scattering chamber, and was bombarded with a 0.02 μA proton beam from the Canberra tandem accelerator. The beam entered the chamber through two 1.6 mm diameter collimating holes in carbon discs, which were followed by two carbon antiscatter discs with 3.2 mm diameter holes. After passing through the target the beam was collected in a Faraday cup, which was insulated from the chamber to allow integration of the beam current.

The alpha-particles were detected by a 4.5 mm x 4.5 mm,

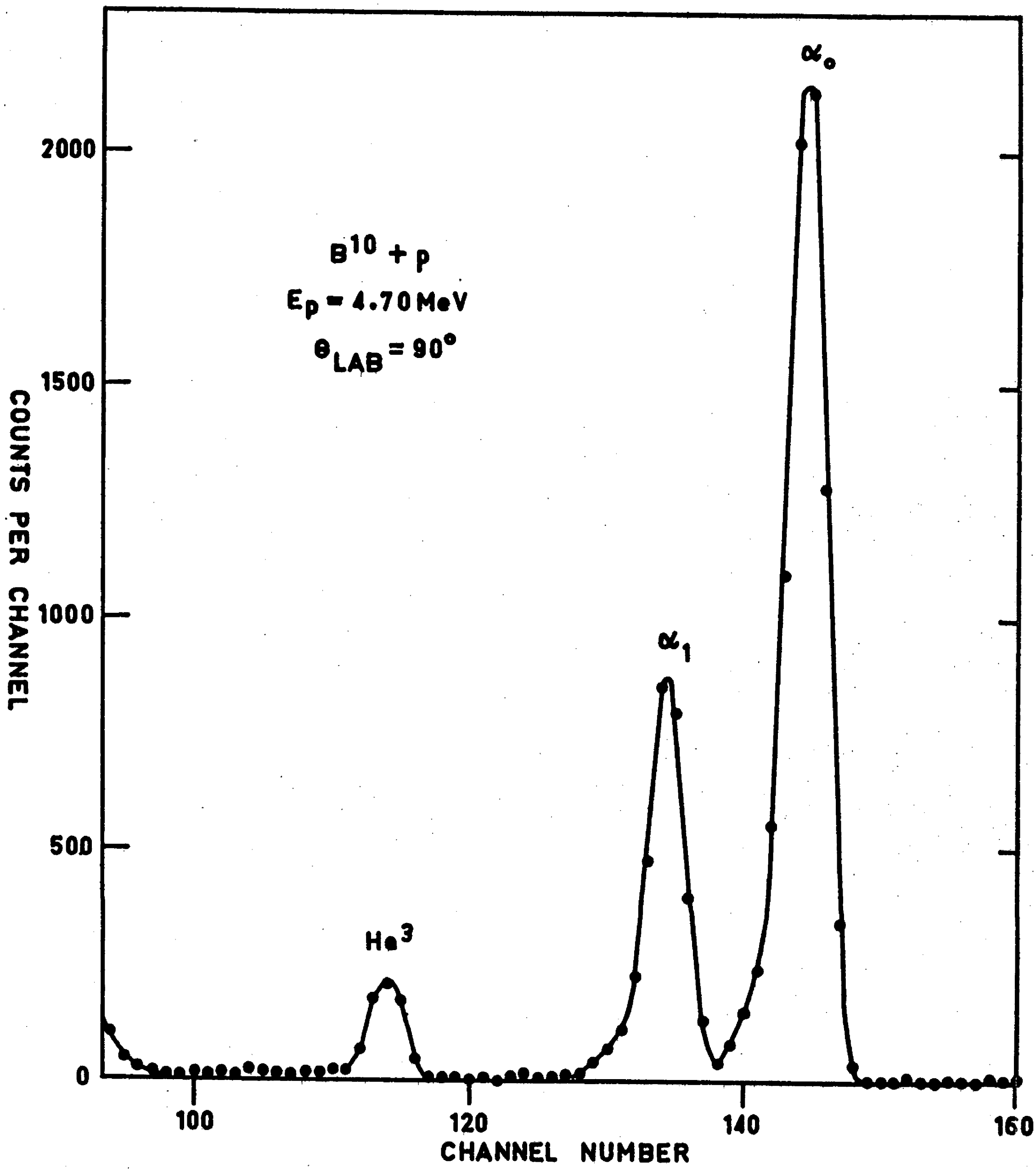

Fig. 13 A spectrum of helium-particles from the bombardment of B^{10} by protons of energy 4.70 MeV, observed at a laboratory angle of 90°.

300 Ω-cm, gold-silicon surface barrier detector, which was mounted inside the vacuum, 6.35 cm. from the target, in such a manner that it could be placed at any angle, with respect to the beam axis, around the target. The angular scale was determined by taking measurements of the energy of the α_o particles at a number of angles to the left and right of the beam direction. The sensitive depth of the counter was adjusted, by varying the reverse bias on it, in such a manner that the maximum energy which protons deposited in the counter was always considerably less than the He^3 and α-particle energies. By this procedure it was possible to separate the helium particles from the high background of elastically scattered protons. The pulses from the detector were amplified by an Ortec charge-sensitive preamplifier-amplifier system, and were collected by a multi-channel pulse-height analyser. It was established experimentally that if the dead-time of the analyser was not allowed to exceed 5%, "pile-up" of pulses in the electronics was negligible. A spectrum, taken at a proton energy of 4.70 MeV, is shown in figure 13.

Spectra were taken at a number of energies and angles to prove that the small peak clearly evident in most of them (see figure 13) was due to He^3 particles from the $B^{10}(p,He^3)Be^8$ reaction, proceeding to the ground state of Be^8. This proof is discussed in Appendix C. A similar method was used to first

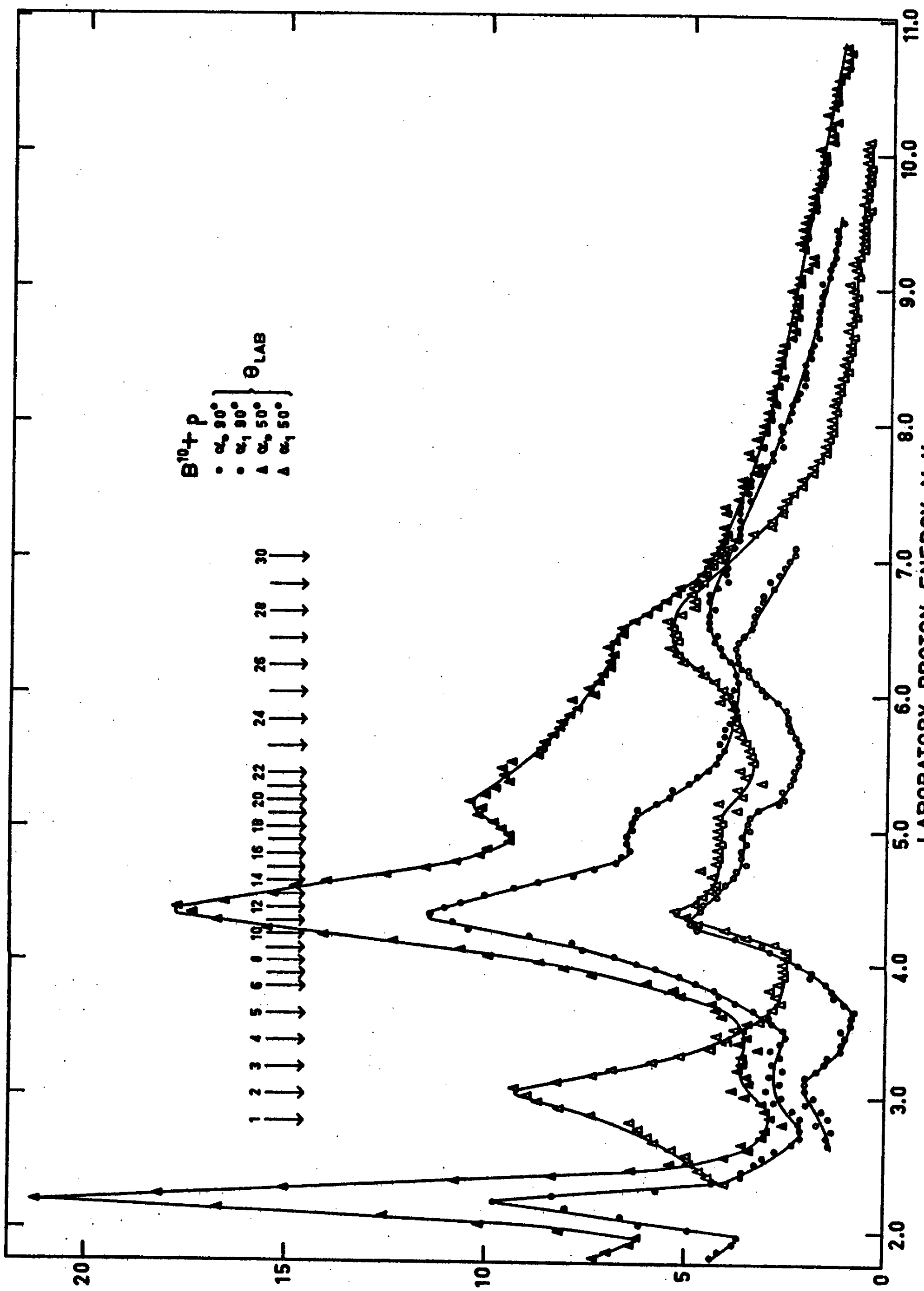

Fig. 14 Excitation functions for the α_0 and α_1 groups from the $B^{10}(p,\alpha)Be^7$ reaction, taken at laboratory angles of 50^o and 90^o. Statistical errors are of the order of the size of the points. The arrows indicate energies where angular distributions were measured.

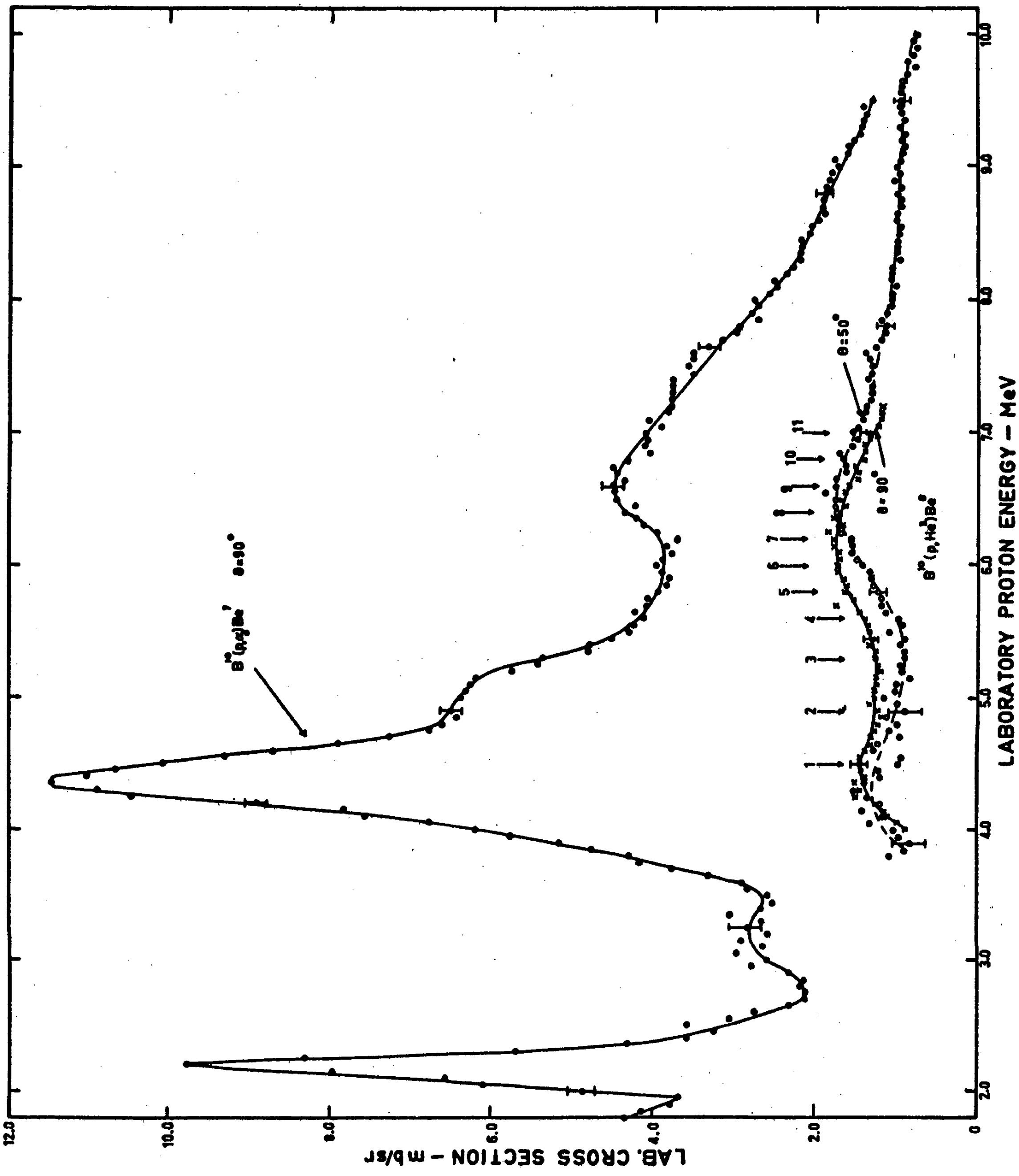

Fig. 15 The ground state transition cross sections as a function of energy for the $B^{10}(p,He^3)Be^8$ and $B^{10}(p,\alpha_0)Be^7$ reactions, the former for laboratory angles of 50° and 90° and the latter for 90°. The arrowed points indicate energies where He^3 angular distributions were measured.

identify the α_o and α_1 groups from the $B^{10}(p,\alpha)Be^7$ reaction.

To obtain absolute cross sections for the reactions it was necessary to measure the thickness of B^{10} in the target. This was done by comparing the yields of $B^{10}(p,\alpha_o)$ alpha-particles from the target used and from a target of the same composition and method of manufacture, whose thickness had been determined previously by measuring the energy lost in the target by 3.3 MeV protons (see chapter 3). This comparison was made at several energies, and the thickness of B^{10} determined as (77 ± 15) μgm/cm^2.

The yields of α_o, α_1 and He^3 were measured, as functions of proton bombarding energy, every 50 keV from 1.8 to a maximum of 10.8 MeV, at laboratory angles of 50^o and 90^o. The excitation functions obtained are shown plotted as differential cross sections in figures 14 and 15. The α_o excitation function at 50^o was taken up to 10.8 MeV bombarding energy, but that at 90^o was measured to only 9.5 MeV because of increased overlapping above this energy of the ground state alpha-particle group and the He^3 group. For a similar reason the α_1 and He^3 excitation functions at 90^o cease well below the corresponding ones at 50^o. The lower limit of the excitation functions, namely $E_p = 1.8$ MeV, was imposed by the minimum energy helium-particles that could be detected by the solid state counter. Below this energy the increased noise and poorer resolution of the detector, caused by the very low bias that had to be applied to suppress all the

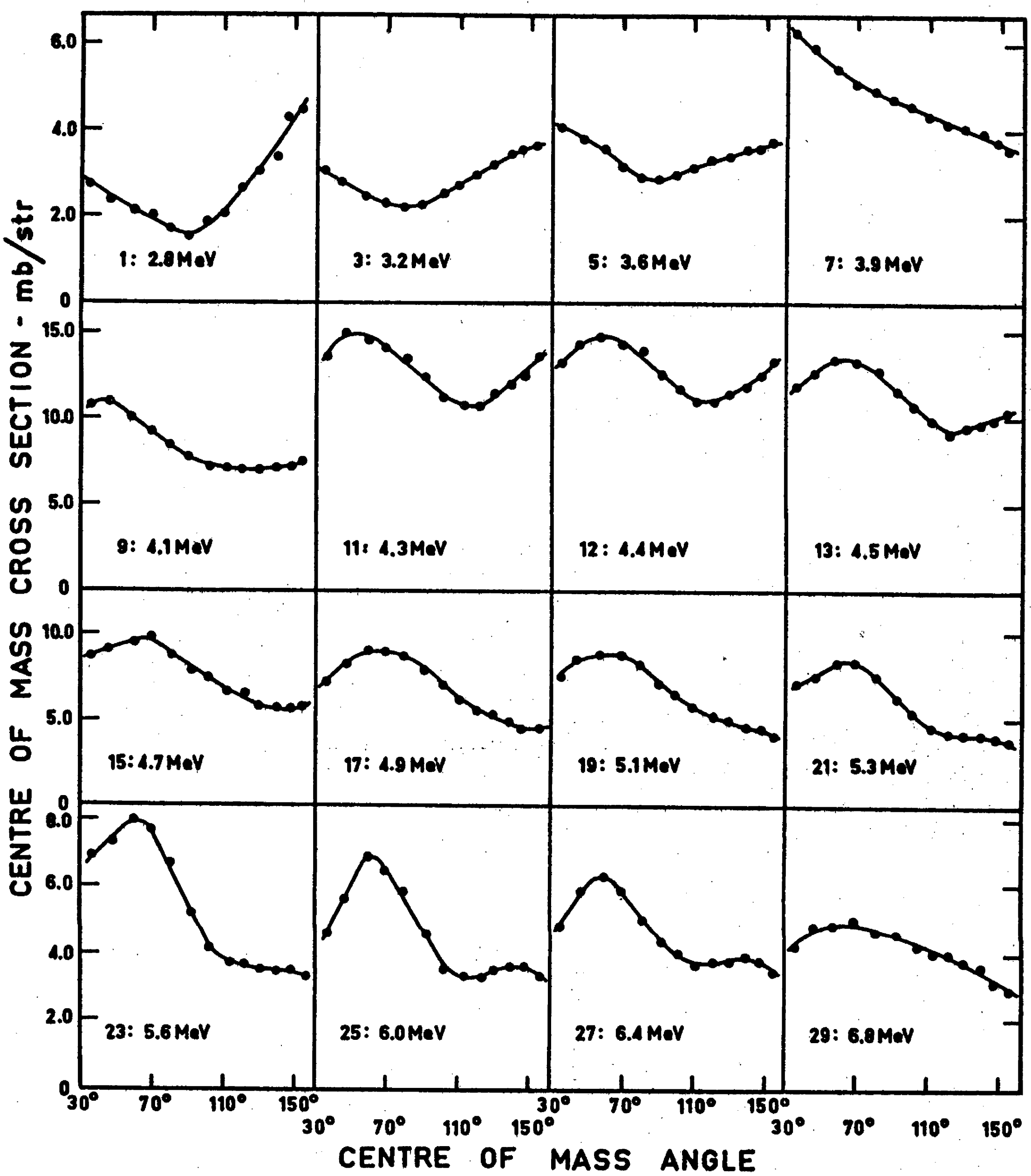

Fig. 16 Selected angular distributions of the α_0 group from the $B^{10}(p,\alpha)Be^7$ reaction. The curves are experimental, and the numbering corresponds to that of fig. 14. Statistical errors are of the order of the size of the points.

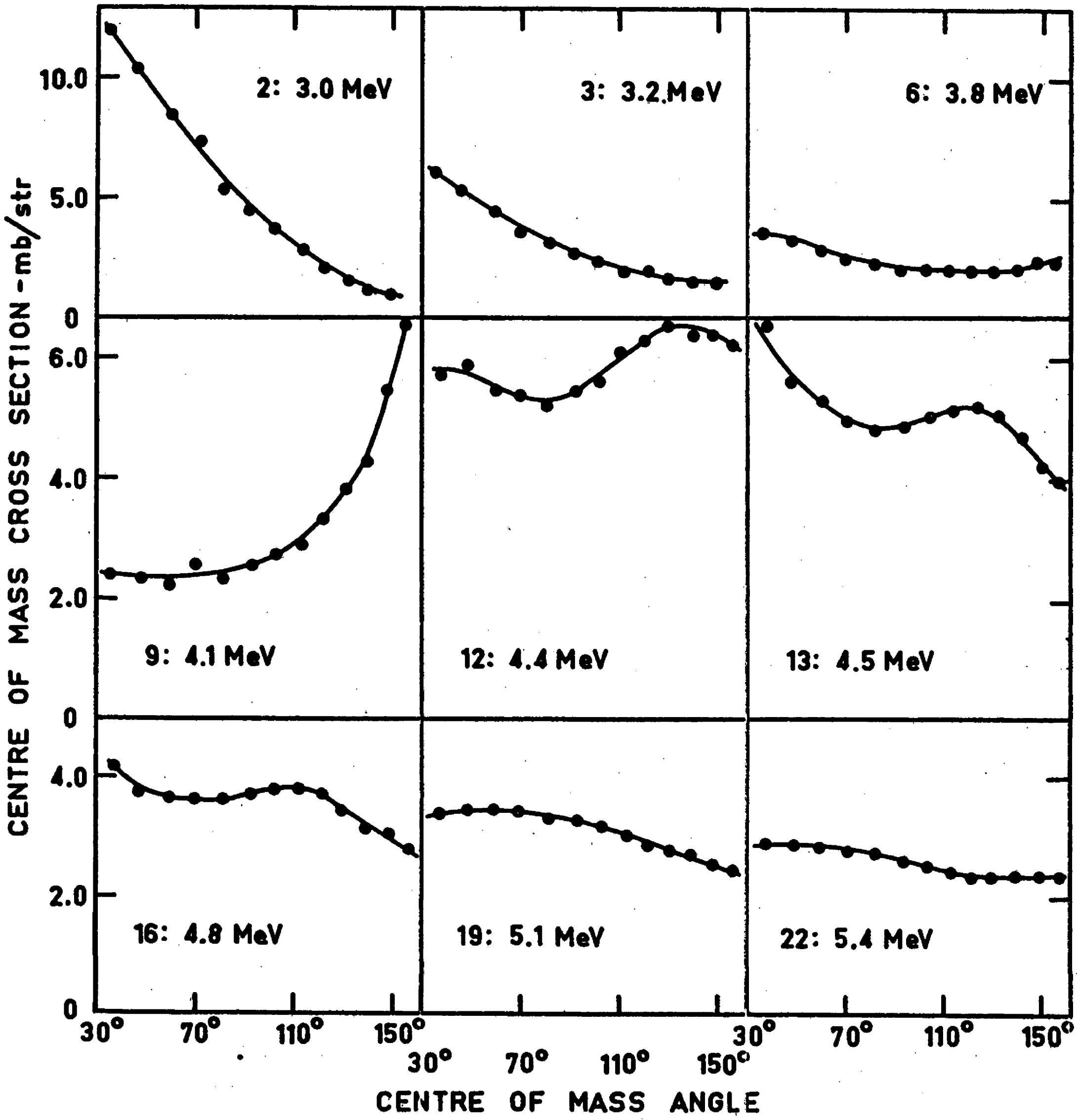

Fig. 17 Selected angular distributions of the α_1 group from the $B^{10}(p,\alpha)Be^7$ reaction. The curves are experimental, and the numbering corresponds to that of fig. 14. Statistical errors are of the order of the size of the points.

scattered proton pulses, made the spectra obtained unusable.

The value of (10 $\pm$ 2) mb/str. for the $B^{10}(p,\alpha_o)$ differential cross section at 90^o at the E_p = 2.2 MeV resonance is not in agreement with the (18 $\pm$ 2) mb/str. reported previously by Overley and Whaling (1962). The solid angle subtended by the sensitive area of the counter at the centre of the target was 4.87×10^{-3} str.

Angular distributions for α_o, α_1 and He^3 particles were measured at the proton energies shown arrowed in figures 14 and 15, and selections of them are shown in figures 16,17 and 18. Angular distributions could not be taken at lower proton energies because the low energy helium particles could not be detected at backward angles. As the proton energy was increased above 6.0 MeV, He^3 measurements at backward angles again became impossible due to increased overlapping of the He^3 group and the first excited state α group. Most of the angular distributions were taken with thirteen angles, from $\theta_{lab} = 30^o$ to 150^o in 10^o steps, enabling an estimate to be made of the magnitude of the contributions of terms of orders 0 to 6 to the polynomial expansion described in section 4.3.1. Measurements were not made at smaller and larger angles because of the possibility of intercepting the beam with the counter assembly.

Data were taken with the target at 45^o to the beam direction. The angular range 30^o to 100^o was covered with the target foil in

4.3 Analysis and Discussion of Results

4.3.1 Least Squares Analysis of Angular Distributions

An expression for the angular distribution of the particles resulting from a reaction in which a single resonance level of the compound nucleus is excited has been given by Blatt and Biedenharn (1952), who simplified the general equations of earlier workers by eliminating all sums over magnetic quantum numbers. Such a reaction is characterized by the quantities $\alpha\ s\ \ell_1\ \ell_2\ J\ \alpha'\ s'\ \ell_1'\ \ell_2'$, where α denotes the particular pair of particles in the ingoing channel, s is the vector sum of the spins of the pair (the channel spin), ℓ_1 and ℓ_2 are two possible values of the relative orbital angular momentum between the pair, and J is the spin of the compound state through which the reaction passes. The primed quantities have identical definitions in the outgoing channel. The differential cross section is then given by

$$d\sigma/d\Omega(\alpha,\alpha') \;=\; \lambda\!\!\!^{-}{}_{\alpha}^{2}/(2i+1)(2I+1)\sum_{L=0}^{L_{max}} B_L(\alpha',\alpha)P_L(\cos\theta),$$

where $B_L(\alpha',\alpha) \;=\; \left\{(-1)^{s'-s}\Big/4\left[(E-E_o)^2+(\Gamma/2)^2\right]\right\}\times$

$$\sum_{\ell_1 \ell_2 \ell_1' \ell_2' s s'} Z(\ell_1\, J\, \ell_2\, J,\, s\, L)\; Z(\ell_1'\, J\, \ell_2'\, J,\, s'\, L)\; g_{\alpha s \ell_1}\, g_{\alpha s \ell_2}\, g_{\alpha' s' \ell_1'}$$

$$g_{\alpha' s' \ell_2'} \times \cos\left[\xi_{\alpha \ell_1} - \xi_{\alpha \ell_2} + \xi_{\alpha' \ell_1'} - \xi_{\alpha' \ell_2'}\right] .$$

Here $\lambdabar_\alpha$ is the de Broglie wave length divided by 2π ,

i and I are the projectile and target nucleus spins,

E_o is the resonance energy,

Γ is the total width of the resonance,

$g_{\alpha s \ell}$ is the square root of the partial width $\Gamma_{\alpha s \ell}$

and $\xi_{\alpha \ell_1} - \xi_{\alpha \ell_2}$ is the phase difference between the two partial waves.

The Z (a b c d, e f) are the Z coefficients defined by Biedenharn, Blatt and Rose (1952), which are closely related to the Racah coefficients. They obey all the selection rules for Racah coefficients * as well as the selection rule Z = 0 unless (a + c + f) is even. The most useful tabulation of the Z coefficients has been given by Sharp et al. (1954). In the $B^{10}(p,\alpha)Be^7$ reaction, B^{10} had spin 3^+ and the proton had spin $\frac{1}{2}^+$, so there were two possible ingoing channel spins 7/2 and 5/2.

---

* The function is defined only for integral or half-integral values of the quantities a b c d e and f, with the limitation that each of the four triads (a b e), (c d e), (a c f) and (b d f) has an integral sum.

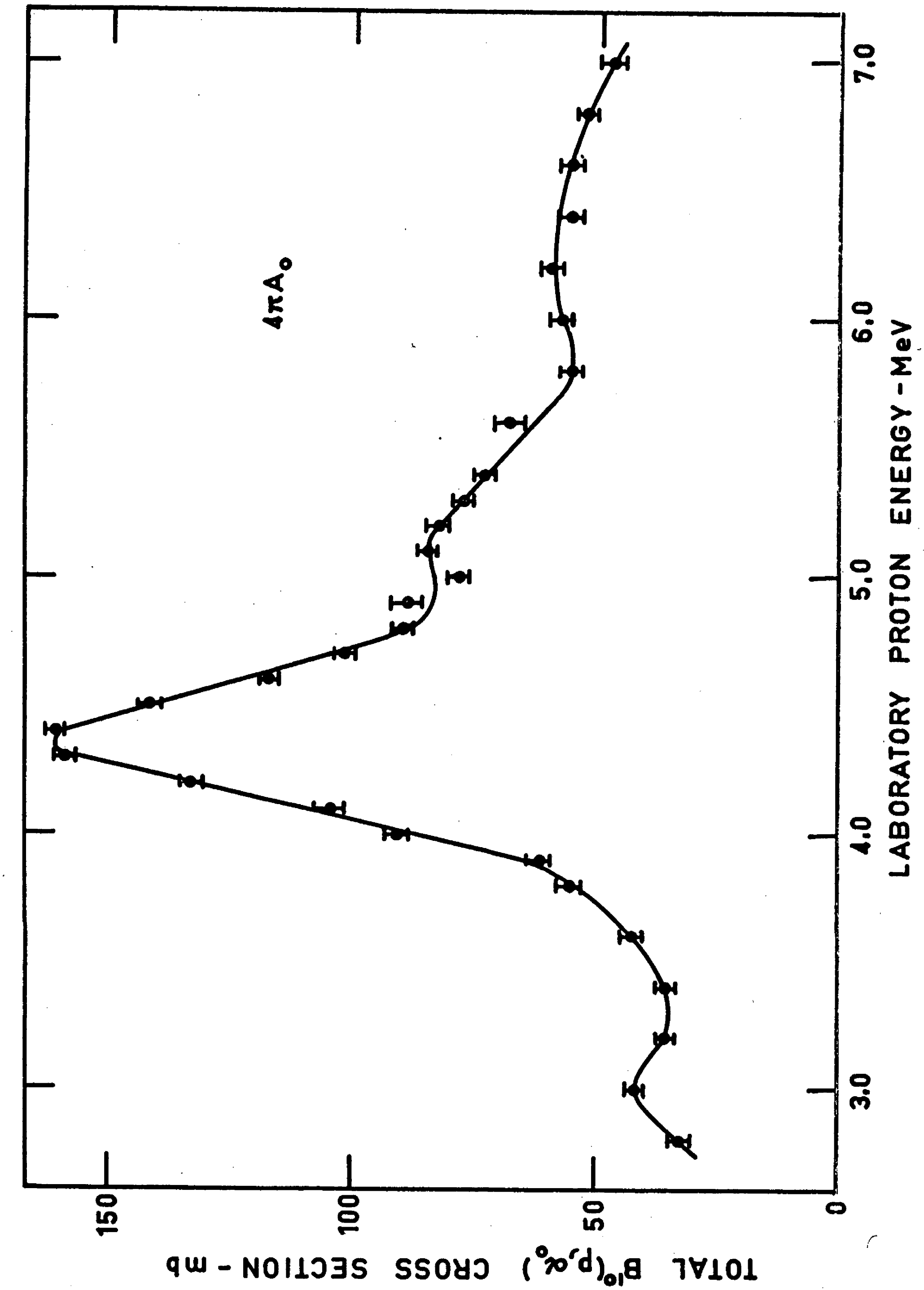

Fig. 19 The energy dependence of the total cross section $4\pi A_0$, for the α_0 group from the $B^{10}(p,\alpha)Be^7$ reaction, derived from a Legendre polynomial analysis of the α_0 angular distributions.

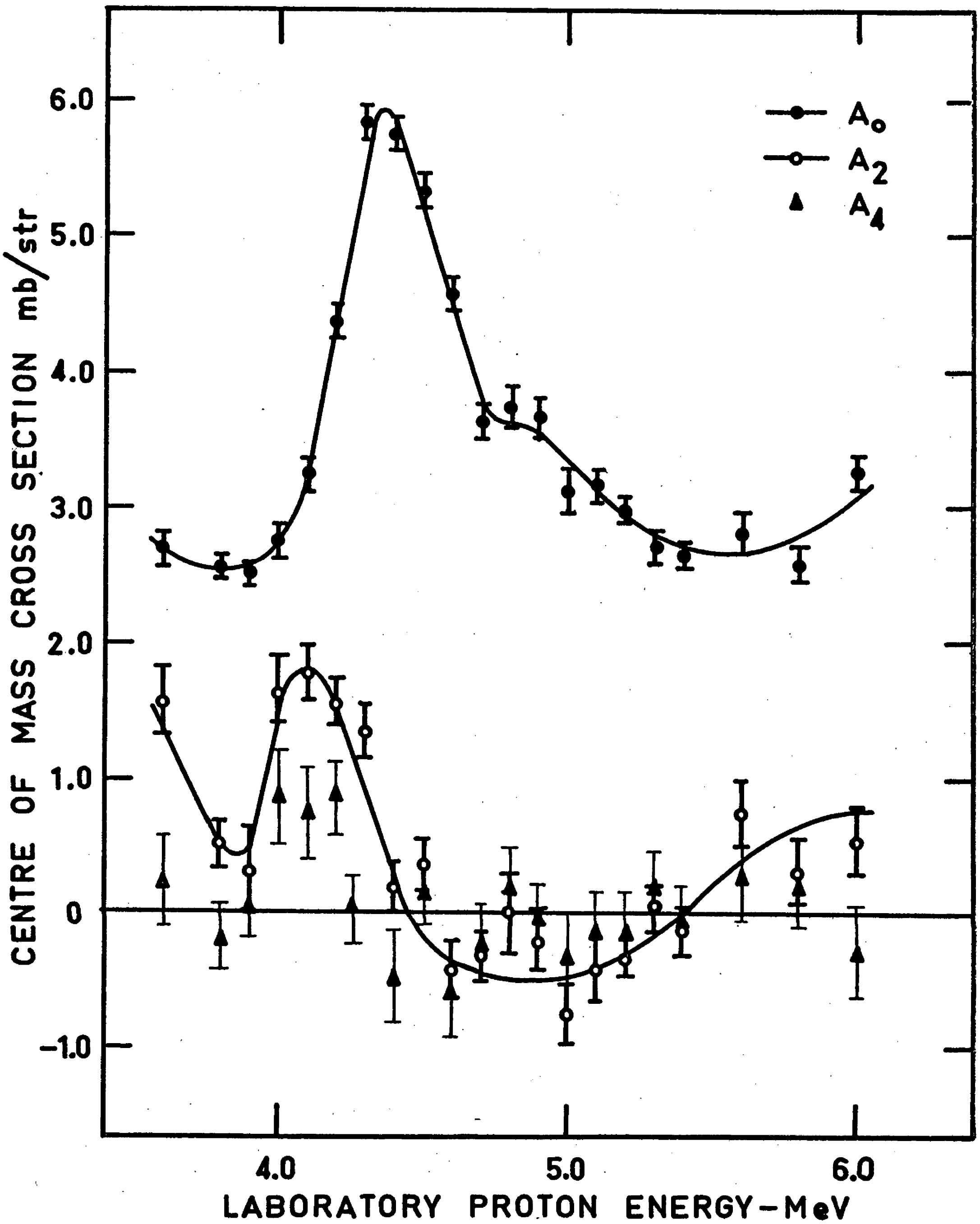

Fig. 21 The energy dependence of the coefficients A_L ($L = 0,2,4$) obtained from the expansion $\sum_L A_L P_L(\cos\theta)$ of the angular distributions of the α_1 group from the $B^{10}(p,\alpha)Be^7$ reaction.

4.3.2 The E_p = 2.2 MeV level

The known resonance at E_p = 2.18 MeV (10.67 MeV excitation in C^{11}) was very evident (figure 14). Overley and Whaling, on the basis of their proton elastic scattering cross section and the non-resonant behaviour of the α_1 group, had suggested that the level was $J^{\pi} = 9/2^+$, with the proton and α_o partial widths contributing equally to a total width of 200 keV. This figure for Γ was confirmed by a measurement of (220 $\pm$ 30) keV. Unfortunately it was not possible in our experiment to take angular distributions over the resonance in an attempt to verify this spin and parity assignment because the low energy alpha-particles could not be detected at backward angles.

4.3.3 The E_p = 4.4 MeV level

The dominant resonance in the remainder of the energy range covered was that at a bombarding energy of 4.4 MeV. This level, at 12.65 MeV excitation in C^{11}, was resonant for both α_o and α_1, and had a total width of approximately 400 keV. These values were in agreement with those of Ophel et al., who reported a level at 4.36 MeV, 400 keV wide. The absolute total cross sections ($4\pi A_o$) for the $B^{10}(p,\alpha_o)$ and $B^{10}(p,\alpha_1)$ reactions at $E_p = 4.4$ MeV were (160 ± 30)mb and (75 ± 15) mb respectively, the errors being imposed by the uncertainty in the target thickness measurement.

It was assumed that there was only a single level in the peak at 4.4 MeV, and that the usual single level formulae applied. Then the argument proceeded as follows :

A lower limit on the spin J of the compound state was imposed by a knowledge of the absolute cross section. The cross section for a resonant reaction at the peak may be written

$$\sigma = \pi \lambda\!\!\!^{-2} \left[(2J+1)/(2i+1)(2I+1)\right] 4\Gamma_p \Gamma_r / \Gamma^2 \qquad \ldots\ldots (1)$$

where Γ_p is the partial width for the incoming channel

Γ_r is the partial width for the outgoing channel

and Γ is the total width.

Here $\Gamma \simeq \Gamma_p + \Gamma_{\alpha_0} + \Gamma_{\alpha_1} + \Gamma_{He^3} + \Gamma_{p_1'}$

$\simeq \Gamma_p + \Gamma_{\alpha_0} + \Gamma_{\alpha_1}$, since $\Gamma_{p_1'}$ was negligible (Ophel) and

since the He^3 data showed no resonance structure in this energy region. Because the ratio of the partial widths at any energy is equal to the ratio of their cross sections at that energy, Γ was expressed as $\Gamma = \Gamma_p + a\Gamma_{\alpha_0}$, where Γ_{α_1} was found in terms of Γ_{α_0} and a was therefore a known constant at the resonance energy. The $B^{10}(p,\alpha_0)Be^7$ cross section then had its maximum value when $\Gamma_p = a\,\Gamma_{\alpha_o}$, and so the following inequality was established :

$$\sigma(p,\alpha_o) \leqslant (\pi \lambda\!\!\!^{-2}/a) \left[(2J+1)/(2i+1)(2I+1)\right]$$

where J was the only unknown quantity.

The lower limit on the spin of the 12.65 MeV state of C^{11}, imposed by the total (p,α_o) and (p,α_1) cross sections after subtraction of an estimated background from other states, was $J^{\pi} \geqslant 11/2^{\pm}$*.

Using equation (1) for $r = \alpha_o$ and $r = \alpha_1$, in turn, and substituting the measured value $\Gamma = 400$ keV and a J value $\geqslant 11/2$, it was possible, by solving these two equations and the total width equation simultaneously, to get predicted values for the partial widths Γ_p, Γ_{α_o} and Γ_{α_1} for each spin value chosen. The penetrabilities $P_{\alpha\ell}$ for the protons and alpha-particles of various orbital angular momenta ℓ were calculated using the graphs of Coulomb Functions compiled by Sharp et al.

---

* If the present data had been normalised to that of Overley and Whaling at $E_p = 2.2$ MeV, then the total (p,α_o) cross section at $E_p = 4.4$ MeV would have been approximately 280 mb. After background subtraction, this would have implied a spin $J^{\pi} \geqslant 19/2$ for the state.

(1955). The channel radius was chosen according to the prescription $R = 1.45(A_1^{1/3} + A_2^{1/3}) \times 10^{-13}$ cm. Then the relationship $\Gamma_{\alpha s \ell} = P_{\alpha \ell} \cdot \gamma^2_{\alpha s \ell}$ was used to calculate predicted reduced widths $\gamma_{\alpha s \ell}$. There is an approximate upper limit to the value any reduced width can have, the so-called Wigner limit (Teichmann and Wigner, 1952) $0 \leqslant \gamma^2 \lesssim 3\hbar^2/2\mu R^2$,

where $\hbar$ is Planck's constant divided by 2π

μ is the reduced mass in the channel

and R is the channel radius.

It was found that spins of 11/2 and more gave alpha-particle reduced widths exceeding the Wigner sum rule limit, which suggested that the values for the cross sections were too large.

However, the figure for the total width of the level seemed reliable, $\Gamma = 400$ keV. But $\Gamma = \Gamma_p + \Gamma\alpha_o + \Gamma\alpha_1$ and, at $E_p = 4.4$ MeV, $\Gamma\alpha_1/\Gamma\alpha_o = \sigma(p,\alpha_1)/\sigma(p,\alpha_o) = 0.37$. Maximum (p,α_o) cross section was obtained if $\Gamma_p = 1.37\ \Gamma\alpha_o$. So $\Gamma\alpha_o = 0.15$ MeV and $\Gamma\alpha_1 = 0.05$ MeV. The corresponding reduced widths were less than the Wigner limits only for $\ell\alpha_o \leqslant 3$ and $\ell\alpha_1 \leqslant 4$, giving $J^\pi \leqslant 7/2^{\pm}$. The maximum cross sections obtained for J = 7/2 were then 36% less than the measured values.

The vanishing at $E_p = 4.4$ MeV of all A_L with L even and non-zero in the polynomial expansions, suggested that the resonance contributions to both the α_o and α_1 angular distributions there were isotropic. $J^\pi = 7/2^+$ yielded isotropic distributions for α_o and α_1 if it was assumed that only s-wave protons contributed; $J^{\pi} = 7/2^-$ could not give isotropic distributions. The existence of the large, resonant A_3 term in the α_o distribution could be explained as interference between the $7/2^+$ state and a neighbouring state of $\frac{1}{2}^-$, since such an interference would contribute an L = 3 term only, as required.

A tentative assignment of $J^{\pi} = 7/2^+$ was therefore adopted, and using it, partial widths Γ_p, Γ_{α_o} and Γ_{α_1} were calculated from the measured (p,α_o) and (p,α_1) total cross sections reduced by 36% and a total width of 400 keV. The dimensionless reduced widths for this state, $\theta^2 = \gamma^2 \left[2\mu R^2/(3\hbar^2) \right]$, did not exceed the Wigner sum rule limit. The effect of level shifts (Lane and Thomas, 1958) was neglected. Table 3 gives the properties of the 12.65 MeV state of C^{11} derived from the present experiment.

Table 3

Properties of the 12.65 MeV C^{11} level, from the $B^{10}(p,\alpha)Be^7$ reaction

J	Laboratory energies (MeV)				θ_p^2	$\theta_{\alpha_o}^2$	$\theta_{\alpha_1}^2$
	E_p	Γ_p	Γ_{α_o}	Γ_{α_1}			
$7/2^+$	4.36	0.20	0.15	0.05	0.02	0.29	0.08

4.3.4 Other levels

The α_1 yield was peaked strongly at forward angles at $E_p = 3.0$ MeV (see fig. 17), which could have been due to the state at 11.45 MeV excitation in C^{11}. The α_o yield was only weakly resonant. The anomaly at a proton energy of (5.10 ± 0.05) MeV depicted by Ophel et al., corresponding to an excitation energy of 13.33 MeV in C^{11}, was confirmed. The broad peak at $E_p = 6.3$ MeV covered the region where several resonances had been observed previously. The analysis of section 4.3.3 suggests that one of these states could be the $J^{\pi} = \frac{1}{2}^{-}$ state interfering with that at 4.4 MeV.

CHAPTER 5

THE $F^{19}(p,n)Ne^{19}$ REACTION BETWEEN 5 AND 11 MEV

5.1 Introduction

As outlined in Chapter 1, another reaction well suited to investigation by an activation technique was $F^{19}(p,n)Ne^{19}$ $(\beta^+)F^{19}$. Having developed the apparatus described in chapter 3 to the point where it was operating very reliably it was decided to investigate the value of a study of the $F^{19}(p,n)Ne^{19}$ reaction in the tandem energy range.

A number of groups had examined the higher excitation energy region in Ne^{20}, and Warsh et al. (1962) were known to be conducting a detailed study of the $F^{19}(p,\alpha)O^{16}$ reaction at Florida State University. The present state of our knowledge of the relevant energy region in Ne^{20} is shown in table 4 of section 5.4. Willard et al. (1952), using a single NaI crystal and a long counter, had examined the $F^{19}(p,\alpha\gamma)O^{16}$ and $F^{19}(p,n)Ne^{19}$ reactions in close detail from 2 to 5.4 MeV proton energy, and had discovered a number of resonances, which were verified by several workers including Blasser et al. (1951) and Marion et al. (1955) who also studied the $F^{19}(p,n)Ne^{19}$ reaction. In view of this agreement and the thoroughness of Willard's studies, in which excitation functions were taken in 7 keV steps, no attempt to repeat this work was expected to be useful.

The agreement between the positions of levels seen in different reactions leading to a Ne^{20} compound nucleus also strongly suggested that, below about 18 MeV excitation energy, compound nucleus effects predominated. However, the reaction mechanisms operating at the higher energies which the tandem could attain were not known. Some preliminary data had been obtained by Broude and Gove (1960) on the yields of the $F^{19}(p,\alpha_o)O^{16}$ and $F^{19}(p,\gamma)Ne^{20}$ reactions from 4 to 10 MeV proton energy, and Warsh had kindly sent details of his $F^{19}(p,\alpha)O^{16}$ work, including an excitation function from 3 to 12 MeV bombarding energy and a number of angular distribution measurements. Their hopes of making a direct reaction analysis of the results were largely unfulfilled by the presence of several features which strongly indicated that a sizeable proportion of compound nucleus formation was taking place. For example, the excitation function for the reaction was not a smoothly varying one, there were correlations between resonances in the excitation curves for the ground, first and second excited state groups, and direct interaction fits were found at minima in the cross sections. It was concluded by the Florida group that "... a direct reaction - compound nucleus interference calculation should be made when the state of the reaction theory permits it." Broude and Gove had remarked : "The α yield shows a large number of narrow resonances in contrast to the gamma excitation function. This in itself suggests that the broad peaks in the gamma yield may be envelopes of unresolved resonances. Further, there appear to be some correlations between the two modes of decay ... " "which suggests that some further measurements could be made to establish whether this correspondence is genuine." Teplov et al. (1960) had earlier remarked that in the proton energy region from 5 to 6.5 MeV, there were sizeable contributions from both direct and compound nucleus interactions.

All of this work had concerned primarily the $F^{19}(p,\alpha)O^{16}$ reaction. It was clear that extension of the earlier $F^{19}(p,n)Ne^{19}$ yield function up into the 20 MeV excitation energy range in Ne^{20} would help to clarify these reaction-mechanism discussions by bringing the results of a study of a different reaction to bear on the subject.

5.2 Experimental Details

In the reaction $F^{19}(p,n)Ne^{19}(\beta^+)F^{19}$ the positron decay of Ne^{19} proceeded 100 percent to the ground state of F^{19}, and so no

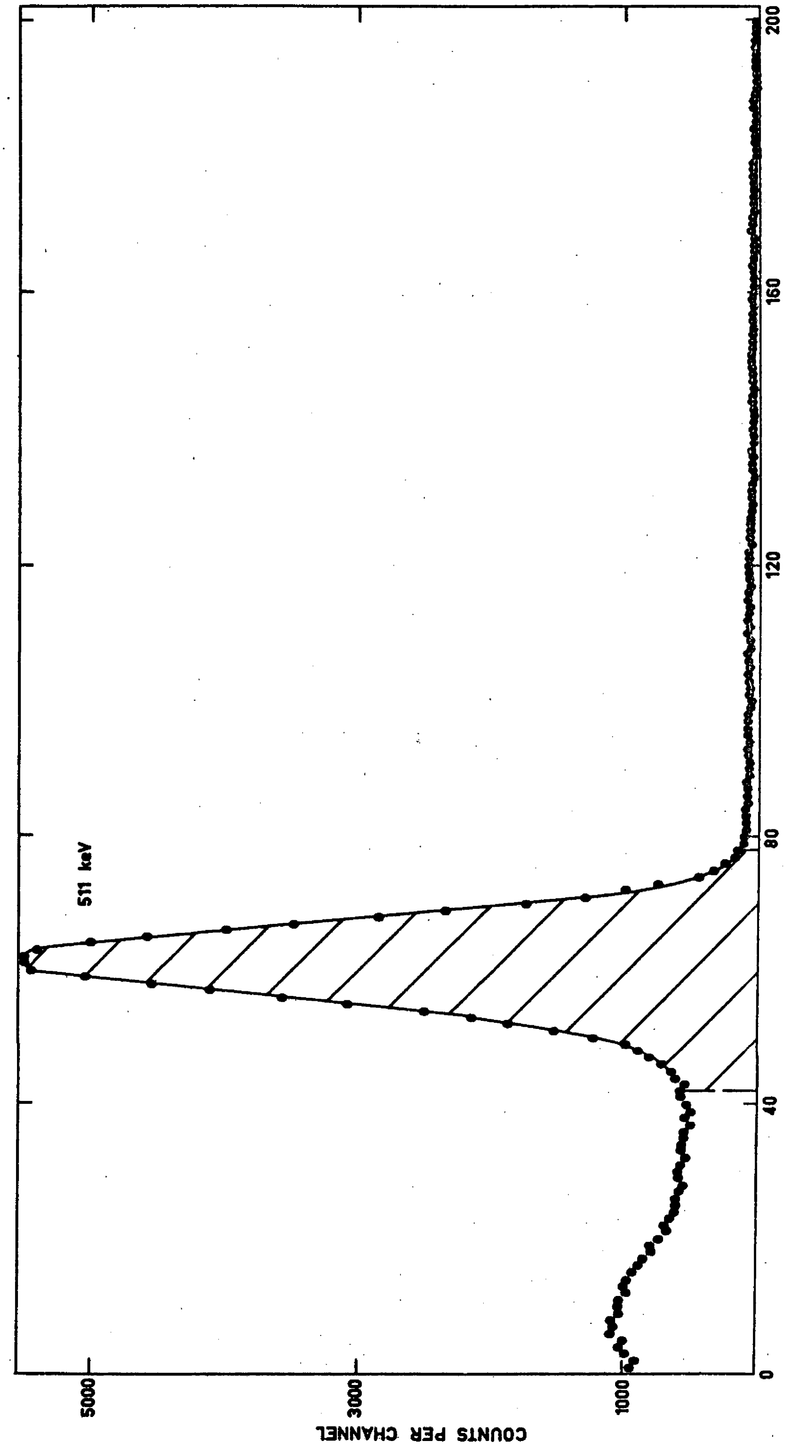

Fig. 22 A gamma-ray spectrum taken with one of the crystal spectrometers after a bombardment of F^{19} with 8.3 MeV protons. The hatched area indicates the energy interval selected for the coincidence measurements.

unique γ-ray existed as in the $B^{10}(p,n)C^{10}(\beta^+)B^{10}$ case. However, due to the care taken to eliminate all sources of background positron activity, the contribution from other such activities present on or near the target had been shown to be negligible (chapter 2). Apart from the half-life measurements at 4.8 MeV proton energy, others were subsequently taken at E_p = 10.8 MeV to verify that the earlier conclusion was valid over the whole of the energy range of interest. As a result, a measure of the neutron yield was obtained by recording coincidences between the two 0.511 MeV annihilation quanta (fig. 22).

The apparatus used was the same as that described in chapter 3, except that the triple (fast-slow) coincidence technique was used. Here a fast (time) coincidence was required directly after amplification of the pulses from the detectors, and also a triple coincidence demanded between the positive output of the fast coincidence unit and the outputs of the two single channel analysers, each of whose window was set over a 0.511 MeV γ-ray photopeak. This technique increased the experimental resolution and eliminated the necessity for a second coincidence unit to record accidental coincidences.

The fluorine target was obtained by vacuum evaporation of MnF_2 onto a 3 mgm/cm^2 gold foil, the thickness of gold being chosen to prevent the radioactive Ne^{19} nuclei formed in

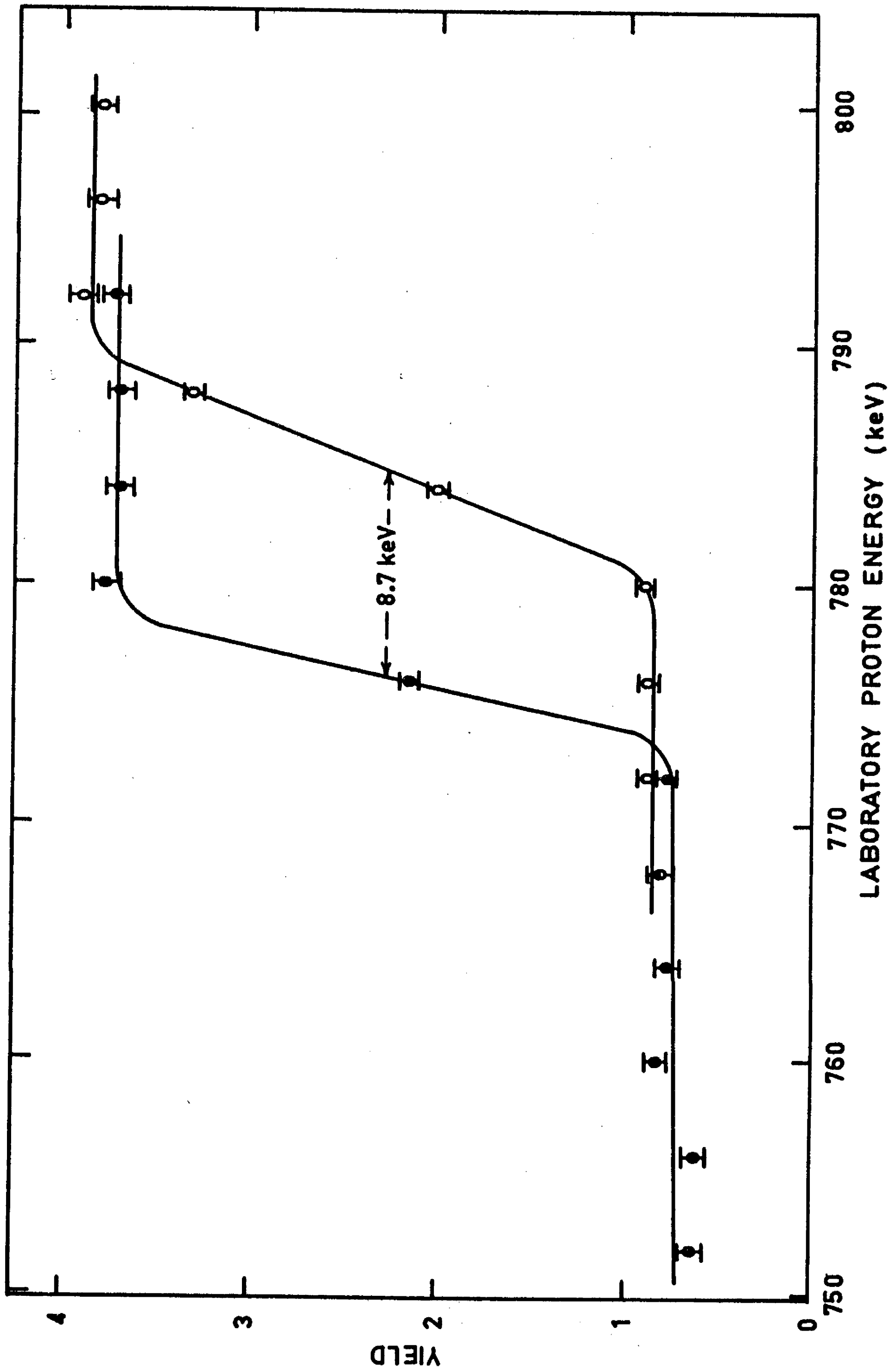

Fig. 23 The measurement of the thickness of the MnF_2 target. The closed circles represent the yield of 12.3 MeV gamma rays from the thick aluminium target around the 773 keV $Al^{27}(p,\gamma)Si^{28}$ resonance. The open circles show the apparent energy shift of this resonance when the MnF_2 coated side of the Al target was presented to the proton beam.

the reaction from recoiling out of the target and being lost from the counting region.

The target thickness was determined as follows. A piece of thick aluminium foil was placed alongside the gold backing during the evaporation of the MnF_2 target, and the thickness of MnF_2 deposited was determined by observing the apparent energy shift of the 773 keV $Al^{27}(p,\gamma)Si^{28}$ resonance when the proton beam, obtained from the Canberra 1.2 MeV Cockcroft-Walton accelerator, passed through the MnF_2 layer. A 12.6 cm. diameter x 10.2 cm. thick sodium iodide crystal was used to detect the 12.3 MeV gamma radiation proceeding to the ground state of Si^{28}. As fig. 23 shows, the result, typical of several determinations, was a proton energy loss of 8.7 keV at Ep(lab) = 780 keV.

During a run over a selected energy range three determinations of the neutron yield were made, and averaged, every 20 keV. All sections of the curve were repeated once, and some energy intervals as many as three times. The statistical errors on the final curve were less than one percent.

This method of measuring the total reaction cross section assumed that the final nucleus was formed in its ground state, or decayed to it if it was formed in an excited state. Any mode of decay of the final nucleus other than positron decay prevented the desired (p,n) event from being detected. This difficulty

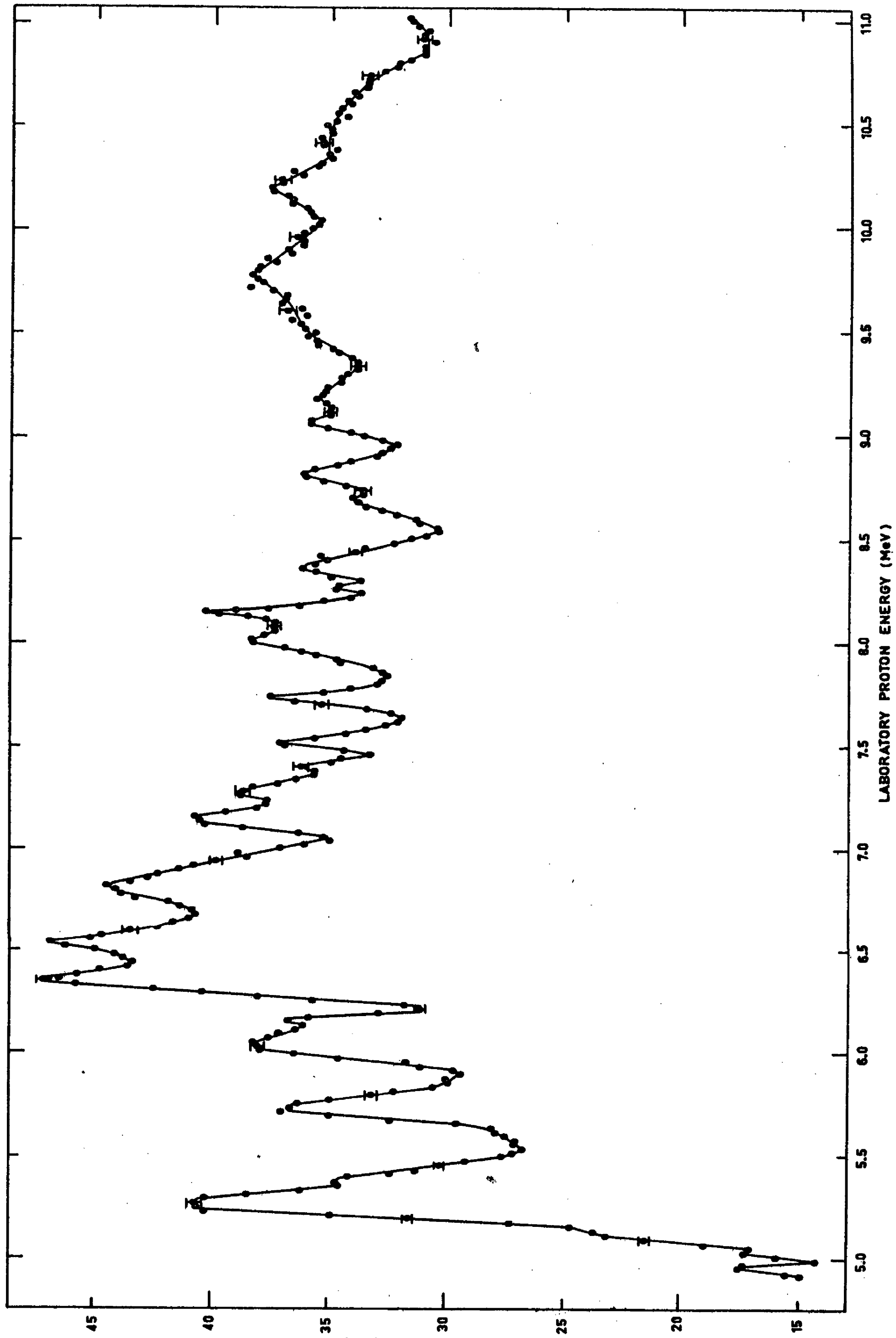

Fig. 24 The total $F^{19}(p,n)Ne^{19}$ cross section as a function of proton energy.

arose in only one case in the activation work reported in this thesis, namely in the availability of the $F^{19}(p,n)Ne^{19}(\alpha)O^{15}$ channel above 7.95 MeV laboratory proton energy. Hence, above this energy the results were incomplete to the extent that they did not contain events which produced Ne^{19} in a state which decayed by this means.

5.3 Results

The results are displayed in figure 24. Maxima in the excitation function occur at proton bombarding energies of 4.96, 5.03, 5.11, 5.26, 5.37, 5.73, 6.03, 6.15, 6.35, 6.53, 6.81, 7.14, 7.27, 7.41, 7.52, 7.74, 8.02, 8.15, 8.28, 8.37, 8.70, 8.82, 9.08 MeV (all $\pm$ 0.02 MeV), 9.2, 9.5, 9.8 and 10.2 MeV, corresponding to possible levels in the compound nucleus Ne^{20} at 17.55, 17.62, 17.69, 17.84, 17.94, 18.28, 18.57, 18.68, 18.87, 19.04, 19.31, 19.62, 19.75, 19.88, 19.98, 20.19, 20.46, 20.58, 20.71, 20.79, 21.11, 21.22, 21.47 MeV (all $\pm$ 0.02 MeV), 21.6, 21.9, 22.1 and 22.5 MeV.

The absolute $F^{19}(p,n)Ne^{19}$ cross section was determined as follows. The proton stopping cross section per molecule of MnF_2 at Ep = 780 keV was found from the relationship

$$\mathcal{E}(\text{molecule } X_nY_m) = n.\mathcal{E}(\text{atom } X) + m.\mathcal{E}(\text{atom } Y)$$

or $$\mathcal{E}(MnF_2) = \mathcal{E}(Mn) + 2\,\mathcal{E}(F)$$

where $\mathcal{E}$ is the stopping cross section and $\mathcal{E}$ (Mn) and $\mathcal{E}$(F) were inferred from Whaling (1958), Demirlioglu and Whaling and Green et al. (1955).

It was found that $\mathcal{E}(MnF_2) = 28.0 \times 10^{-18}$ keV-cm^2/molecule, and consequently, using the measured proton energy loss in the target, that the content of fluorine was 19.5 ± 2.5 μgm/cm^2.

The detection efficiency of the positron counting system was determined using a Na^{22} source which was calibrated to $\pm$ 2.5 percent and which was mounted in the target chamber in an identical fashion to the target. A correction for the coincidences recorded due to the presence of the 1.28 MeV Na^{22} γ-ray Compton "tail" was made. The formulae developed in Chapter 2 were then used to determine the absolute $F^{19}(p,n)Ne^{19}$ cross section as 27 ± 4 mb. at a proton energy of 5.58 MeV.

The main sources of error were the uncertainties in the target thickness, and in the efficiency of the counting system due to the possible error in the source strength. Comparisons with the two previously reported measurements of this cross section (Blasser et al., 1951, and Gibbons and Macklin, 1959) were difficult because of the small energy region in common, the thick targets used previously and the lack of good error estimates. However, agreement between the three to better than a factor of two was present at 4.9 MeV proton energy.

5.4 Discussion

The results, not unlike the $F^{19}(p,\alpha)O^{16}$ yield curve in appearance, showed a large amount of structure in the excitation function, superimposed on a smoothly varying background. This presumably direct interaction and interference contribution led to considerable reduction in the "peak-to-valley" ratio, but was not thought likely to affect the structure of the excitation function markedly.

The structure, almost certainly due to some compound nucleus mechanism, was not easily explained at such high excitation energies. If the maxima were interpreted as individual compound nucleus levels, their density was some 30 times less than that predicted by level density formulae. For example, around 18 MeV excitation the experimental density was about one per 100 to 150 keV, whereas the work of Le Couteur et al. (1954 and 1959) predicted a density of states of about one level every 4 keV. The formula of Cameron (1958), derived from earlier work using the Fermi gas model, gave a similar value, although Cameron had not tested his formula in this energy region. It seemed clear that individual compound states were not being seen.

There was therefore a possibility that the peaks seen were due to statistical or random fluctuations in the sense described by Ericson (1960). His theory applied to the so-called continuum energy region in nuclei, where the number of available exit channels was so large that the lifetime of the compound nucleus was small and the average level width (or uncertainty in energy of the compound system) Γ was very much larger than the level spacing. Then there was a considerable amount of overlapping of the energy levels, and, particularly if there was a spread in the beam energy of the order of Γ or larger, all the many intermediate states excited contributed coherently though randomly to the reaction process. The result was statistical fluctuations in the cross section as a function of energy. However, the generalization that the levels of many nuclei with $A > 10$ and with anomalously small densities at high excitation energies were due to these sorts of fluctuations (for example, Austin, 1962) seemed far too wide. For the following reasons, the variations in the $F^{19}(p,n)Ne^{19}$ results were not thought to be explained by Ericson's theory :

(a) The energy spread in the beam from the tandem was ~ 2 keV as was the target thickness at this energy. Hence it seemed unlikely that the experimental energy spread could have led to averaging over a large number of compound nucleus states.

(b) The magnitude of the fluctuations predicted by Ericson was

$$\sigma = \bar{\sigma}\,(1 \pm 1/(nN)^{\frac{1}{2}})$$

RESONANCES IN THE COMPOUND SYSTEM Ne^{20}

PROTON ENERGIES (MEV)													
$F^{19}(p,n)$ Jenkin*	$F^{19}(p,n)$ Willard	$F^{19}(p,n)$ Blaser	$F^{19}(p,n)$ Marion	$F^{19}(p,\gamma)$ Broude	$F^{19}(p\alpha\gamma)$ Willard	$F^{19}(p,\gamma)$ Gemmell	$F^{19}(p,\alpha_0)$ Warsh	$F^{19}(p,\alpha_0)$ Ranken	$F^{19}(p,\alpha\pi)$ Ranken	$F^{19}(p,\alpha_0)$ Broude	$O^{16}(\alpha,\alpha)$ Hunt ***	$O^{16}(\alpha,\alpha)$ Jadogne ***	$Ex(Ne^{20})$ MeV
10.2							10.22						
9.8							9.82						22.1
							9.60						
9.5							9.50						
				9.30			9.32						
9.2													
9.08												9.1	
8.82							8.88			8.80			
8.70							8.70						21.1
8.37													
8.28				8.30			8.30			8.32		8.3	
8.15													
8.02													
							7.80			7.82			
7.74										7.70			
							(7.60)						
7.52				7.55			7.50			7.50			20.0
7.41						(7.65)**					7.37		
7.27										7.27			
7.14													
							7.03						
											6.91		
										6.87			
6.81													
											6.66		
6.53		6.5		6.50		(6.85)**	6.45			6.50			19.0

Table 4 Data on the positions of levels of the nucleus Ne^{20}.

6.35							6.35						
							(6.25)			6.25			
6.15		6.1									6.16		
6.03							6.00				5.96	6.0	
							(5.88)						
5.73		5.8	5.75				5.80			5.66	5.72		
											5.53		
5.37		5.4	5.4				5.38			5.37	5.38		18.0
5.26			5.3										
	5.20			5.20	5.20	(5.5)**			5.17	5.20	5.19		
5.11	5.07		5.1		5.07								
5.03							5.05						
4.96	4.99		5.0		4.99			4.97	5.00	4.95	4.95		
	(4.85)						4.85	4.90	4.90				
	4.78	4.8	4.8		4.78								
	4.71				4.71			4.68	4.71	4.70	4.71		
	4.62		4.61				4.65						
	4.57				4.57								
	4.49		4.49		4.49		4.50						
	4.46							4.46		4.47			
								4.36	4.37	4.35			17.0
	4.29				4.29		4.32				4.26		
								4.12					
					4.00		4.03				4.02		
					3.92		3.95	3.98	3.93				16.6

* The present experiment.

** It has been suggested by Broude that these figures are approximately 300 keV too large.

*** Resonances seen in $O^{16}(\alpha,\alpha)$ expressed in terms of the proton energy giving the same excitation to Ne^{20}.

X63-552

where N = number of compound nucleus states excited and n = number of final states to which the compound nucleus decayed.

This meant that the reaction cross section for which n was large should have had small fluctuations. The low energy level structure of Ne^{19} was not well known, but if it was assumed that it had a level density similar to F^{19}, then the variations predicted by the above expression were too small to explain the $F^{19}(p,n)Ne^{19}$ structure, particularly below about 20.5 MeV excitation.

(c) A comparison of the positions of the maxima in the (p,n) excitation function with the work of others on resonances in Ne^{20} above 16.6 MeV excitation is shown in Table 4. The agreement between the four sets of (p,n) data where they overlap was quite good, and that between the (p,α_o) results reasonable. The two sets of (p,γ) results covered different energy regions except for agreement on the E_p = 5.20 MeV level.

It was not to be expected that all reactions would show every resonance in Ne^{20}, as selection rules applied which were especially strong in the (p,α_o) case. However, the agreement evident between the levels seen in the different reactions leading to a Ne^{20} compound nucleus strongly suggested an interpretation of the maxima in the results in terms other than those of Ericson, since, from his model in which averaging effects were inherent, he logically predicted that there was no correlation between statistical fluctuations in the cross section functions of different reactions leading to and from the same compound nucleus.

If there was, in fact, a level spacing of only a few keV, then it was possible that the levels were sufficiently close to cause overlapping in such a way that they fell into groups. In 1955 Lane et al. had provided a "giant resonance" model which was intermediate between the independent particle model and the uniform model. According to their interpretation, the average widths of levels of the compound nucleus were larger close to states of the independent-particle model than those situated further away. As a consequence, the nuclear cross sections had a gross structure. But the conventional nuclear potential gave values for the widths of the "giant resonances" which were far too large.

Izumo (1961) attacked the problem differently. He noted that nuclear reactions at intermediate energies had previously been intepreted either by a direct interaction theory, in which the incident particle gave its energy to only one or two target nucleons, or by the statistical model, in which a compound nucleus was formed when the incident particle shared its energy with all of the target nucleons. Izumo suggested that the real situation lay somewhere between these two; that is, that the bombarding particle interacted strongly with a few target nucleons (via two body forces) and that the remainder of the target nucleons acted like an inert core which always remained in its ground state and affected the incident particle and outer nucleons only through an average potential acting on them. In this way only a partial equilibrium was reached in the compound state. Since only a few nucleons were involved the model predicted "intermediate resonances" in the excitation function, about 70 keV wide, which, because of the compound state assumption, were correlated with "intermediate resonances" in other reactions producing the same intermediate nucleus.

Izumo used his model (1962, 1963) to predict the angular distributions, nuclear temperatures, total and partial widths and excitation functions for many nuclei at intermediate excitation energies. He found moderate agreement with experimental results if he assumed that the number of outer nucleons reacting strongly with the bombarding particle was about 6. This number six was, he suggested, almost independent of mass number and excitation energy within the ranges $20 < A < 180$ and $5 < E_x < 25$ MeV. His nuclear core, then, had little in common with the shell model. Finally Izumo claimed that, in a large number of reactions in which different compound nuclei were formed, the positions of almost all of the "intermediate resonances" coincided; and he divided nuclei into three groups at these energies, with 5, 6 and 7 outer nucleons respectively taking part in the reactions.

Some objections can be raised to this model, such as the meaning of the "magic" number six, and the almost complete absence of any participation of the nuclear core in the reactions at these energies. One wondered, too, if Izumo's very sweeping conclusions would be born out when more data was obtained in these wide mass and energy ranges. The "coincidences" of the "intermediate resonances" in different nuclei as shown in fig. 6 of his 1963 article seemed suspect. However, data such as our $F^{19}(p,n)Ne^{19}$ cross section function below 8 MeV proton energy required some sort of compound state interpretation. Izumo was one of the first to appreciate the need for such a model. With an ever increasing amount of high resolution data now becoming available in this energy range, it is to be hoped that his work will inspire others to further studies.

Above 20 MeV excitation in Ne^{20} it appeared that the levels were becoming so broad and closely spaced that statistical effects were becoming important, for only a suggestion of structure was present.

SECTION TWO

CHAPTER SIX

NEUTRON-ALPHA SCATTERING FROM 16 TO 24 MEV

6.1 Introduction

Experimental neutron-He^4 studies have two main objectives. Firstly, accurate total cross section, differential cross section and relative polarization data can be interpreted in terms of the relevant scattering phase shifts. Since the polarizing power of helium can be calculated from these phase shifts, helium can then be used confidently as a polarizer or polarization analyser.

Secondly, He^4 is the simplest spin zero nucleus, and it is of considerable theoretical interest to see how well the experimental results can be understood in terms of what is known of the nucleon-nucleon interaction. Reviews on the subject of nucleon-alpha-particle scattering have been published by Hodgson (1958) and Burke (1960).

Most n-He^4 measurements below 10 MeV have been fitted well with the phase shifts of Dodder, Gammel (1952) and Seagrave (1953). However, during recent years many experiments in the 20 MeV neutron energy range have been carried out which required a knowledge of the analysing power of helium (Benenson et al., 1962; Perkins and Simmons, 1963; Bertozzi et al., 1963), even though, above 10 MeV, the phase shifts were not well known. For example, Benenson et al. had to calculate the n-He^4 analysing power at 23.7 MeV neutron energy from phase shifts obtained by extrapolating up the phase shifts given by Seagrave.

Recent measurements of the asymmetry in the elastic scattering of polarized neutrons by helium at energies near 20 MeV (May et al., 1963; Trostin et al., 1961) have further emphasized the lack of knowledge of the n-α phase shifts in this energy range.

Phase shifts which have been used at these higher energies are those extracted by Perkins (1963) from the p-He^4 phase shifts of Gammel and Thaler (1958), who used an optical model potential to extend the p-He^4 phase shifts up to 40 MeV. Perkins derived his n-He^4 phase shifts (GTP) by calculating the logarithmic derivatives of the wave functions at a radius of 2.9f, and by assuming that these described the n-He^4 system at a CM energy reduced by 0.8 MeV, the coulomb energy difference between the mirror nuclei He^5 and Li^5. In addition to the GTP phases, there were the n-α phase shifts proposed by May et al. (MWB2), who also found that the p-α phase shifts suggested by Brockman (B) fitted their asymmetry data well at 16.4 MeV neutron energy. The GTP phase shifts appeared to fit asymmetry measurements at 16.4 MeV and 20.7 MeV, but not those at 23.7 MeV (May et al., Trostin et al.). The MWB2 phase shifts were consistent with the total elastic scattering cross section and asymmetry measurements at 23.7 MeV neutron energy.

The variation with energy of the n-α phase shifts must, of course, be consistent with parameters of the resonance levels of the compound nucleus. A state of He^5 in the energy range of present interest is the $3/2^+$ level at 16.70 MeV excitation energy. In the past, a number of attempts have been made to fit the pronounced maximum in the T(d,n)He^4 cross section at 110 keV deuteron energy (16.70 MeV excitation in He^5). Single-level formulae were used, but fits were found for a variety of channel radii and penetration factors. It has been remarked by Bransden (1960) that "it is just possible, although unlikely, that the fits arise out of the freedom allowed by the formulae, rather than from the existence of a genuine level". "An attempt by Flowers to explain the reaction purely by barrier penetration effects ...... was unfortunately rendered inconclusive by fitting the theory to data that is in conflict with that now generally accepted". Hence there was some uncertainty as to the nature of this anomaly.

Determinations of phase shifts in the 20 MeV energy range may also have to take into account the inelastic process $He^4(n,d)T$, the threshold of which occurs at a neutron energy of 22.07 MeV. The conditions that this threshold should cause an observable anomaly (cusp or rounded step) in the cross section of another channel were that there were only two outgoing particles (Delves, 1958) and that there was no coulomb interaction between them (Breit, 1957). The second of these conditions was not fulfilled in the present experiment.

This chapter describes the performance and interpretation of an experiment to measure angular distributions of neutrons scattered by alpha-particles, at neutron energies of 16.4, 20.0, 21.0, 21.85, 22.6 and 23.7 MeV. This was done by observing the energy spectra of the recoiling alpha-particles in a high-pressure gas scintillator.

The principal purpose of the experiment was to provide some of the data necessary for determining n-He^4 phase shifts in the neutron energy range from 16 to 24 MeV. In this chapter the data obtained are compared with angular distributions computed from the sets of phase shifts which have been suggested by the various authors. However, the data may be good enough to extract S-, P- and D-wave n-α phase shifts directly, and this will be tried later.

Additional data were taken in 25 keV steps over the 16.70 MeV resonance of He^5 (E_N = 22.15 MeV), and through the $He^4(n,d)T$ threshold. It was hoped that these studies would clarify the situation regarding the He^5 state at 16.70 MeV excitation.

Two notable investigations of the n-He^4 elastic scattering process had been made previously. Bonner et al. (1959) found only a slowly decreasing cross section for the neutron energy range 16 to 21.9 MeV, but observed a pronounced resonance at 22.15 MeV. Austin et al. (1962) measured neutron angular distributions in the range 2 to 23 MeV neutron energy.

6.2 Method

The neutron angular distributions were measured by observing the energy spectrum of the recoiling alpha-particles in a high-pressure gas scintillator. It has been shown by Barschall and Kanner (1940) that the energy distribution of the recoiling alpha-particles in the laboratory system is proportional to the angular distribution of the scattered neutrons in the centre-of-mass system, provided that this distribution is expressed as a function of the cosine of the centre-of-mass scattering angle. This proportionality also holds relativistically (Barschall and Powell, 1954). Throughout the discussions that follow the neutron energies quoted are measured in the laboratory system, and the scattering angle, θ, is expressed in centre-of-mass coordinates.

6.3 Detector

Most of the earlier measurements based on the above

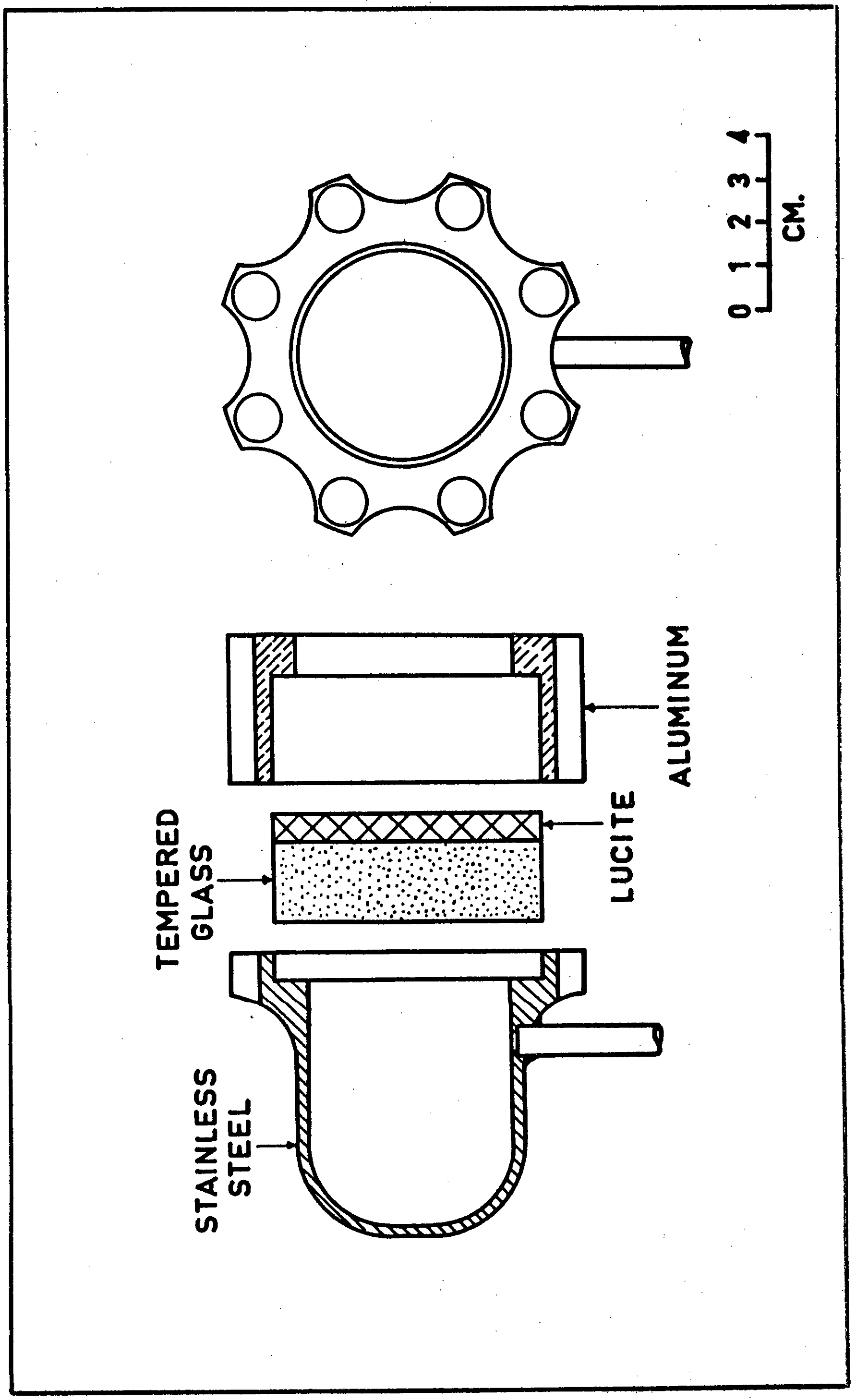

Fig. 25 The cell of the high-pressure gas scintillation counter, showing a cross section on the left, and a view looking into the cell on the right.

principle used ionization chambers or proportional counters. Since the range of the recoiling alpha-particles must be small compared to the dimensions of the counter, a high gas pressure had to be used at higher neutron energies. Consequently the complete collection of ions produced was difficult, and so recently a high-pressure gas scintillator has been employed (Shamu, 1962; Austin et al., 1962).

In the present experiment a counter very similar to the second of the two described by Shamu was used. The gas scintillator was a mixture of helium and xenon at a total pressure of about 140 atm. The helium served both as a target for the incident neutrons and as part of the detection system. The xenon was necessary to increase the light output and to decrease the range of charged particles in the gas. The percentage of xenon and the total gas pressure were chosen to yield the highest stopping power consistent with a minimum contribution from xenon disintegration particles. In all cases the maximum range of the recoiling alpha-particles was less than 4 mm. As a result, the pressures of xenon which were used ranged from 24.5 atm for data at 16.4 MeV neutron energy to 38 atm for data at 23.7 MeV.

The gas scintillator was contained in a thin-walled, stainless-steel cell, with a tempered-glass window. The glass was backed with a perspex disc in order to apply a more uniform retaining pressure. The counter is shown in figure 25, with a cross-section view on the left and a view looking into the counter on the right. The seal between the cell and the window was a teflon ring. An Australian-made viton-A O-ring was originally used, but it outgassed, contaminated the gases used, and thereby severely impaired the light output and resolution of the detector. The scintillations were viewed through the glass window with a photomultiplier tube.

A source of alpha-particles, consisting of a deposit of polonium on the end of a silver wire,which was fastened to a 1.5 mm diameter steel rod, could be moved in and out of the counter through the gas filling tube. The steel rod passed out of the tube through a teflon gasket at an elbow in the tube.

In order to reduce the spread in the pulse height of the scintillation pulses, the inside of the steel cell was coated with a high reflectance surface of magnesium oxide over a thin film of aluminium. In addition, the MgO and the inside of the glass window were coated with a wavelength shifter, diphenyl stilbene, because most of the scintillation light was in the ultra-violet region of the spectrum. Good resolution was difficult to obtain because absorption of the light on the reflecting surfaces meant that tracks of equal energy, occurring in different parts of the gas volume, did not produce pulses of the same height. Further investigations on the roles of the different components of the present counter showed that a clear, even aluminium layer was a

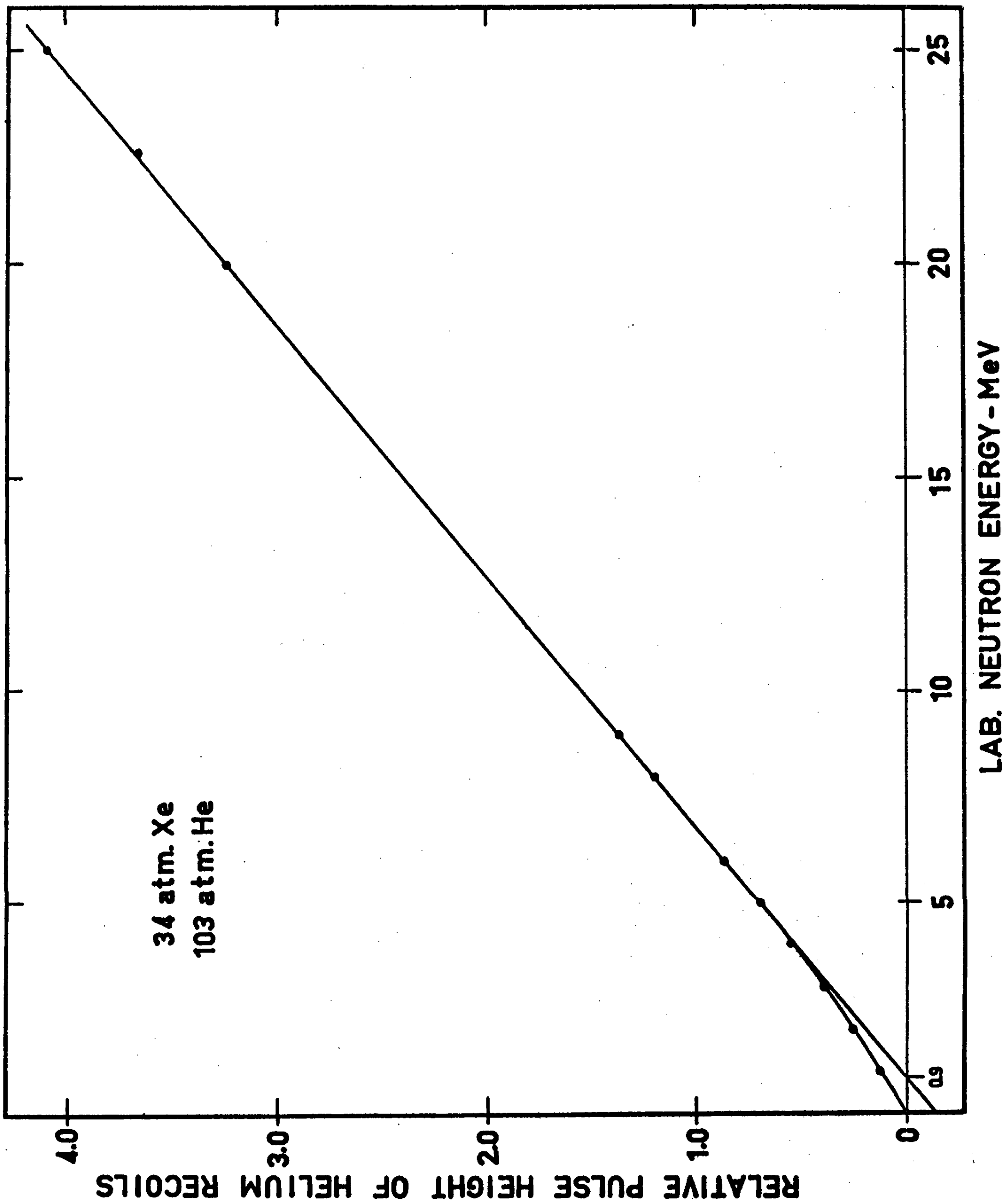

Fig. 26 Linearity curve for the gas scintillation counter filled with a mixture of helium and xenon. The ordinate refers to the pulse height for the maximum-energy helium recoils relative to that for alpha-particles from the Po source.

significant factor, but more important, that the relative amounts of wave-length shifter on the walls and window of the cell had to be adjusted accurately to obtain uniform efficiency throughout the gas volume. A resolution of 5% was obtained for 15 MeV alpha-particles.

Shamu (1962) found that, for a mixture of 42 atm of helium and 8 atm of xenon, the counter gave a response which was linear to better than 3% over the alpha-particle energy range from 0.4 to 14 MeV. This was not found to be the case for the higher gas pressures used in this experiment. A curve taken at pressures of 34 atm of xenon and 103 atm of helium is shown in figure 26. These pressures are typical of those used in the experiment. The $T(d,n)He^4$ and $T(p,n)He^3$ reactions were used as neutron sources. The determination of the maximum recoil energy is discussed later. The counter was non-linear for alpha-particles of energy less than about 2.5 MeV, and linear from 2.5 to 16 MeV, with an intercept of about $E_\alpha = 0.6$ MeV on the energy axis. When the helium pressure was reduced to 7 atm, while retaining an xenon pressure of 34 atm, the curve was more nearly linear, and the straight line drawn through the higher energy points intersected the energy axis at 0.25 MeV alpha-particle energy. Further, when the conditions used by Shamu were duplicated, the response curve for alpha-particles was again found to be linear. In 1956 Nobles had obtained a positive intercept of 0.5 MeV for an xenon-filled scintillation counter.

These effects were investigated further by observing the variation in pulse height of groups of electrons, alpha-particles and protons as a function of helium pressure, for a constant xenon pressure of 34 atm and a neutron energy of 22.6 MeV. The results obtained indicated that, for the alpha-particles, "quenching" of the light took place even when only a small amount of helium (e.g. 6 atm) was added. The quenching effect was observed to increase with addition of helium up to a total pressure of about 145 atm, the highest used.

6.4 Other Apparatus

Monoenergetic neutrons were produced by bombarding tritium, in a gas target, with deuterons. The method was similar to that developed by Johnson and Banta (1956), in which a uranium tritide furnace was used as the tritium store. The deuterons were provided by the A.N.U. tandem, and, after passing through a 3 mm diameter collimator, entered the tritium target through a 1.2 μ thick nickel foil. The neutron flux was monitored by integrating the deuteron beam current.

The energy spread in the neutron beam produced was due to straggling of the incident deuterons in the nickel foil and the tritium gas, and the variation of the neutron energy over the angle subtended by the counter at the source. The tritium gas pressure was adjusted so that the total energy spread of the neutrons was about 70 keV for the measurements around the 16.7 MeV level of He^5, and a little greater elsewhere.

A continuum of neutrons from the breakup of incident deuterons was present in addition to the monoenergetic neutrons. Since it was difficult to take into account the effect of these breakup neutrons, the low energy part of the pulse-height distribution which could be affected by them was omitted. Other factors which determined the minimum angle at which data were reliable were the non-linearity of the counter, the maximum electron pulse height and the magnitude of the counter backgrounds.

The scintillation counter was placed at 0^o with respect to the deuteron beam for all measurements except those at 16.4 MeV neutron energy, when it was at 73^o. The axis of the cylindrical counting volume pointed at the tritium target. The distance from the centre of the 5 cm long tritium cell to the centre of the counter was 22.8 cm, except for the 16.4 MeV measurements, for which it was 30.5 cm.

The gas scintillations were recorded with an EMI 5 cm. diameter photomultiplier. The voltage pulses from the photomultiplier were amplified by a Tennelec preamplifier and a Franklin double-delay-line amplifier, and stored in an RIDL pulse-height analyser. The linearity of the amplifier and analyser system was checked periodically with the aid of a Franklin precision pulse generator. The system was found to be consistently linear to less than one percent for the range of pulse heights of interest. The gain stability of the electronics was checked frequently with the aid of the polonium alpha source.

6.5 Experimental Procedure

The procedure generally used for taking data was as follows :

First, the scintillation counter, filled with the helium-xenon mixture, was bombarded with neutrons for a measured integrated beam current. The beam currents used were chosen so as not to endanger the nickel foil of the tritium target, and, for the same reason, the beam was focussed so that about 10% of it fell onto the collimator.

Secondly, the effect of background neutrons, produced in the nickel foil and the tantalum backing of the target, was subtracted by taking a run at the same neutron energy with the tritium target evacuated. This background was only present at small pulse heights.

Thirdly, after the above data had been taken at several energies, the counter background was measured at these energies by bombarding the counter with neutrons when it was filled only with xenon (at the same pressure as before). This counter background was caused primarily by disintegrations of xenon nuclei, but also by recoil and disintegration particles from the counter wall.

The output of light produced by the disintegration and recoil particles was different in pure xenon than for the helium-xenon mixture for the same neutron energy. Also, the variation in light output as a function of gas composition was not the same for different kinds of particles. Hence, accurate normalization of the counter-background data to that for the gas mixture was difficult. However, for the helium-xenon filling, an appreciable number of pulses caused by counter background were observed just above the alpha-particle recoil spectrum. Therefore the amplifier gain was adjusted so that these particles had the same pulse height for both the xenon and helium-xenon fillings. The magnitude of the gain change required was supported by the investigations of the way in which the pulse height of these particles varied as a function of helium pressure. A procedure used previously (Austin et al., (1962)), of adjusting the gain until the pulse height of the Po alpha-particles for the two counter fillings was the same, was found to be grossly in error at the pressures used here, due to saturation or "quenching" effects.

Because of the fact that the light output as a function of gas composition was not the same for different kinds of particles, this gain adjustment would have been in error for some portion of the background unless it was all caused by one kind of particle. Therefore two auxiliary experiments were carried out to study the nature of this background. In one experiment the contribution of the counter walls was reduced by covering the inside of the steel cell with 0.2 mm of lead, and by decreasing by more than a factor of two the amount of reflecting material and wavelength shifter inside the cell. No significant decrease in the number of background pulses was observed, which implied that most of these pulses corresponded to xenon disintegrations. In the other experiment the size of the background was measured as a function of xenon pressure. This experiment also indicated that the background was caused mostly by xenon disintegrations. Of the several kinds of charged disintegration particles which could be emitted with energies in the range of interest, protons had the highest probability of penetrating the coulomb barrier of the xenon nucleus. Consequently it is believed that most of the observed disintegration pulses corresponded to protons.

For the experimental procedure outlined above, an error in the counter background was introduced if the xenon or tritium pressures were not the same for steps one and three (that is, for counter fillings of the mixture and pure xenon, respectively). Therefore, at several energies, data were also taken in the sequence three-one-two, a procedure which eliminated these possible sources of error. Very good agreement was found between the two sets of data.

In addition to the neutron and counter backgrounds, another correction which had to be applied to the data was that for the wall effect. Some of the recoiling alpha-particles hit the window, end wall and cylindrical wall of the counter. For each recoil energy, the number of recoils hitting the walls was calculated from the geometry of the counter (end wall assumed plane), and added to the measured number at that energy. These recoils produced smaller pulses than they would have without wall effect, and the resulting events had to be subtracted from the number of pulses observed at lower energies. This subtraction was done under the assumption that all residual ranges of the recoils hitting the walls were equally probable.

Several other corrections to the data had to be considered. However, since they proved to have a negligible effect on the data, and because they are described in detail elsewhere (Austin et al., 1962), they are discussed only briefly here. The background caused by room-scattered neutrons was estimated by placing a shaddow cone between the neutron source and the detector; and the effect of neutrons scattered by the steel body of the scintillation counter was assessed by slipping over the counter a slightly enlarged copy of the steel cell. These effects were negligible, as were those due to the finite resolution of the counting system and to multiple neutron scattering in the gas scintillator. An estimate of the number of neutrons scattered backward into the counter by the

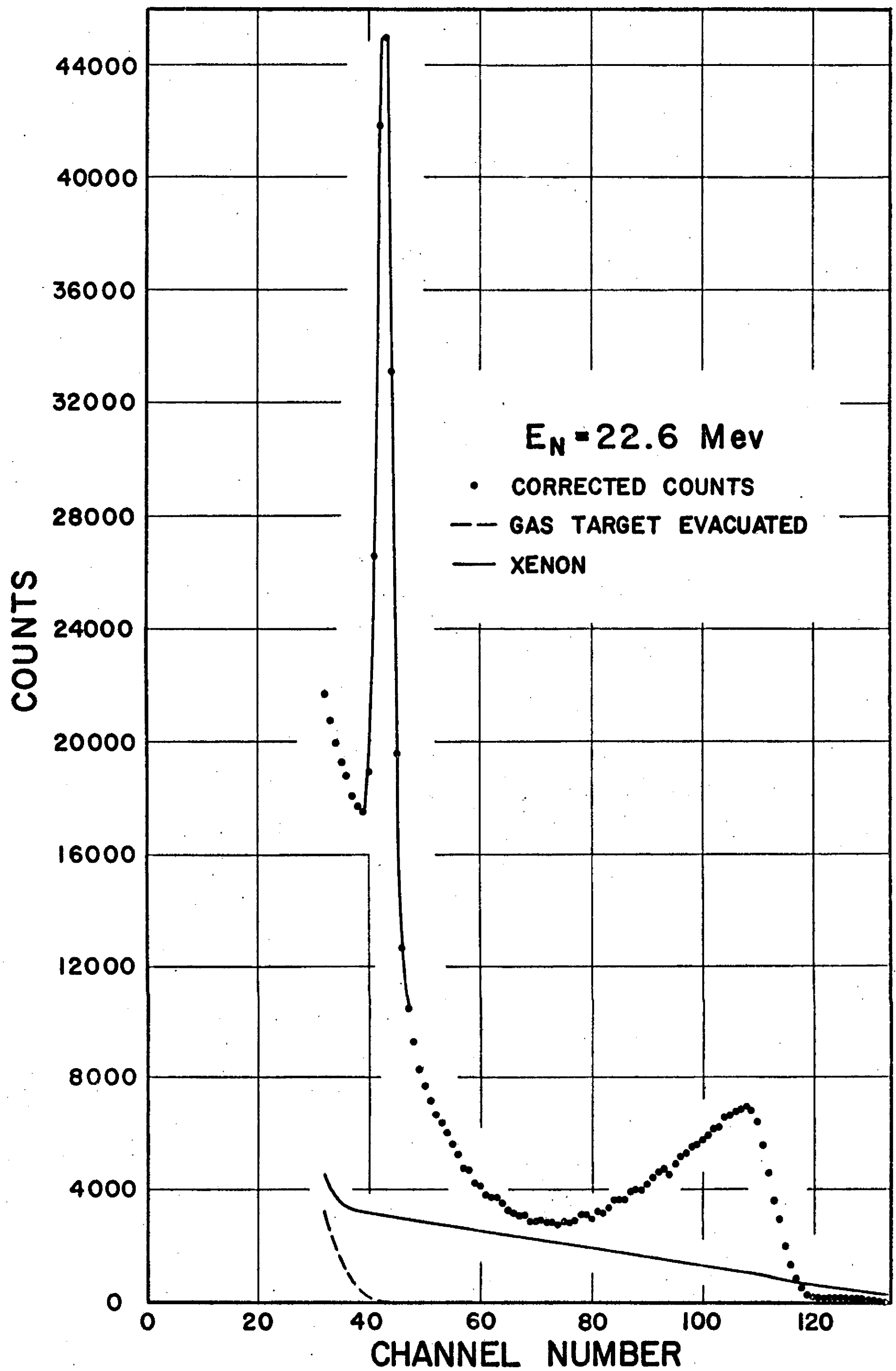

Fig. 27 Background corrections and corrected pulse-height distribution for 22.6 MeV neutrons. The broken and solid curves represent the neutron and counter backgrounds, respectively. The peak is due to the $He^4(n,d)T$ reaction.

window indicated that this background was unimportant.

Figure 27 shows the background corrections and the corrected pulse-height distribution for 22.6 MeV neutrons. The broken curve and the solid curve represent the neutron background and the counter background, respectively. For the smallest recoil energies, where it is seen to be largest, the former background varied from 3% for 16.4 MeV neutrons to 5% for 24 MeV neutrons. The counter background is seen to be relatively largest near the minimum in the corrected distribution, that is, near channel 70 in the figure. Near this minimum the counter or "xenon" background ranged from 20% of the total number of counts at 16.4 MeV to 56% at 24 MeV. The correction for the wall effect, which is not shown in the figure, was less than 5% of the corrected counts for all of the data of this experiment.

The pulse-height distribution obtained after all corrections were applied is shown by the closed circles. Of the several factors mentioned earlier which had bearing on the determination of the minimum channel at which the corrected data was reliable, the magnitude of the backgrounds at low pulse heights imposed the most severe restriction. The peak in this distribution at channel 43 was caused by disintegration particles from the $He^4(n,d)T$ reaction, since both the deuteron and triton were detected by the gas scintillator. The threshold for this reaction is 22.07 MeV neutron energy. The tail above channel 108 is a result of the resolution of the counter. To decide which channel corresponded to the maximum helium-recoil pulse height which would have been observed if the counter had not had finite resolution, the pulse-height distribution was extrapolated smoothly beyond the point where it began to drop off. A vertical line was then drawn at such a position that the number of pulses larger than this pulse height was equal to that below this pulse height and between the extrapolated and observed distributions. The channel corresponding to this line was taken as equivalent to a neutron CM scattering angle of 180°.

6.6 Analysis of the Data

The pulse height distributions of the recoil alpha-particles which were obtained corresponded only to relative angular distributions. A cross section scale was determined by fitting each distribution with a series expansion of Legendre polynomials, as described in chapter 4 of this thesis. It was found that an expansion containing polynomials of orders zero to four was sufficient to fit all the angular distributions satisfactorily, including those over the 16.70 MeV resonance of He^5. A differential elastic scattering cross section scale was then found by normalizing the value of the zero-order coefficient to the total elastic scattering cross section, which was extracted from the n-He^4 total cross section measurements of Shamu et al.

(1963). The contribution to n-He^4 total cross section of the $He^4(n,d)T$ reaction was found from the inverse reaction $T(d,n)He^4$, whose cross section is well known. In this way a cross section scale was established for the measured angular distributions. The method was subject to some uncertainty since the data extended over only a limited angular range, and did not cover the small-angle region where the differential cross section was largest.

In the next section the angular distribution results are compared with angular distributions computed from sets of phase shifts which have been published by various authors. These calculations were carried out on an IBM 1620 computer, using the following formula

$$\sigma(\theta) = A^* A + B^* B$$

where

$$A(\theta) = 1/2ik \sum_{L=0}^{\infty} \sum_{J} (J+\tfrac{1}{2}) \left[\exp(2i\,\delta_{LJ}) - 1\right] P_L(\cos\theta)$$

$$B(\theta) = 1/2ik \sum_{L=1}^{\infty} \sum_{J} 2i(J-L) \left[\exp(2i\,\delta_{LJ}) - 1\right] P_L(\cos\theta)$$

and in which $J = L \pm \frac{1}{2}$

δ_{LJ} are the phase shifts

and $P_L(\cos\theta)$ are the Legendre polynomials.

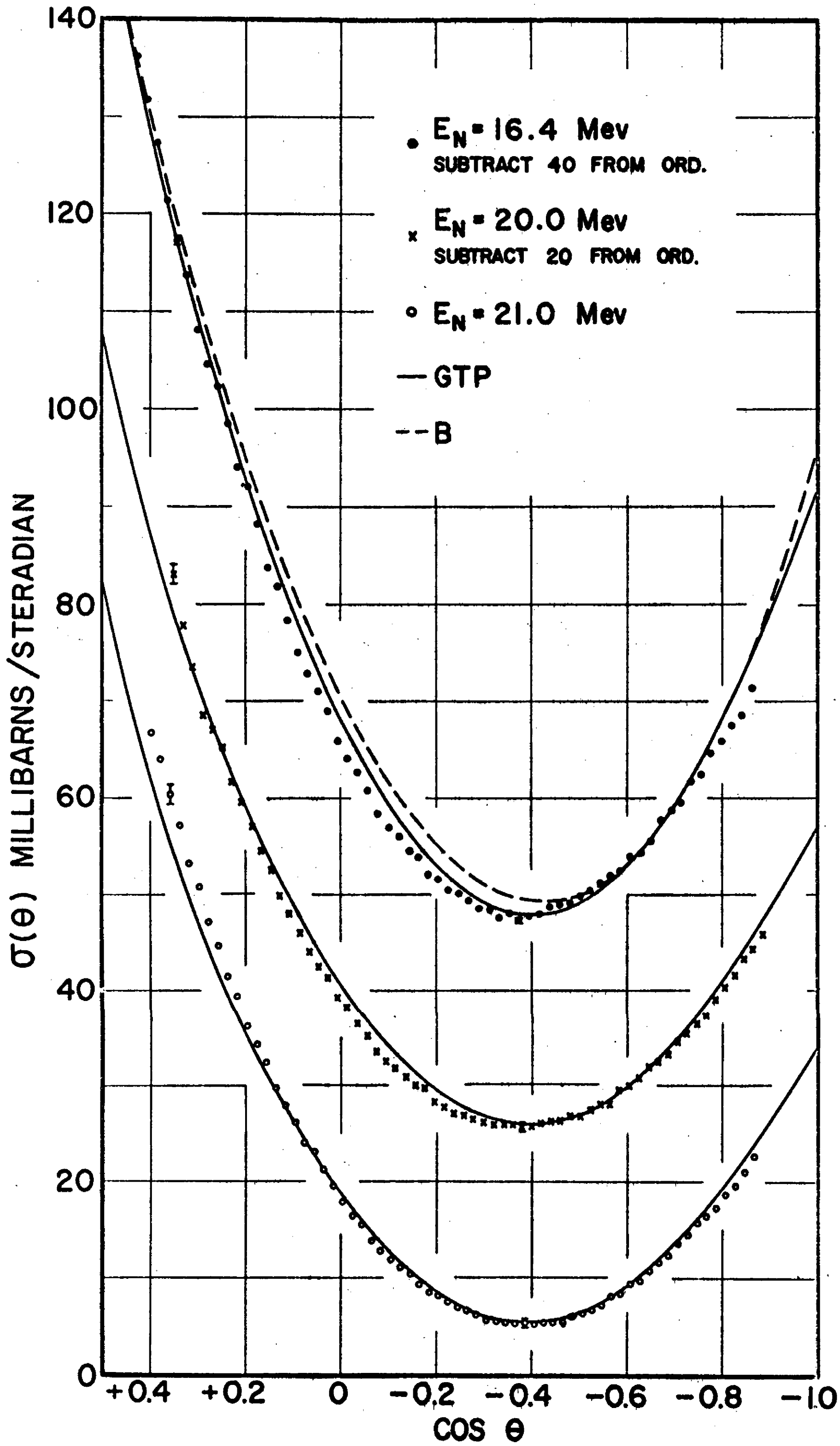

Fig. 28 Differential cross sections in the C.M. system for the scattering of 16.4, 20.0, and 21.0 MeV neutrons by α-particles. The ordinate scales are to be adjusted as shown. The solid curves were calculated using the GTP phase shifts, and the dotted curve using Brockman's phase shifts.

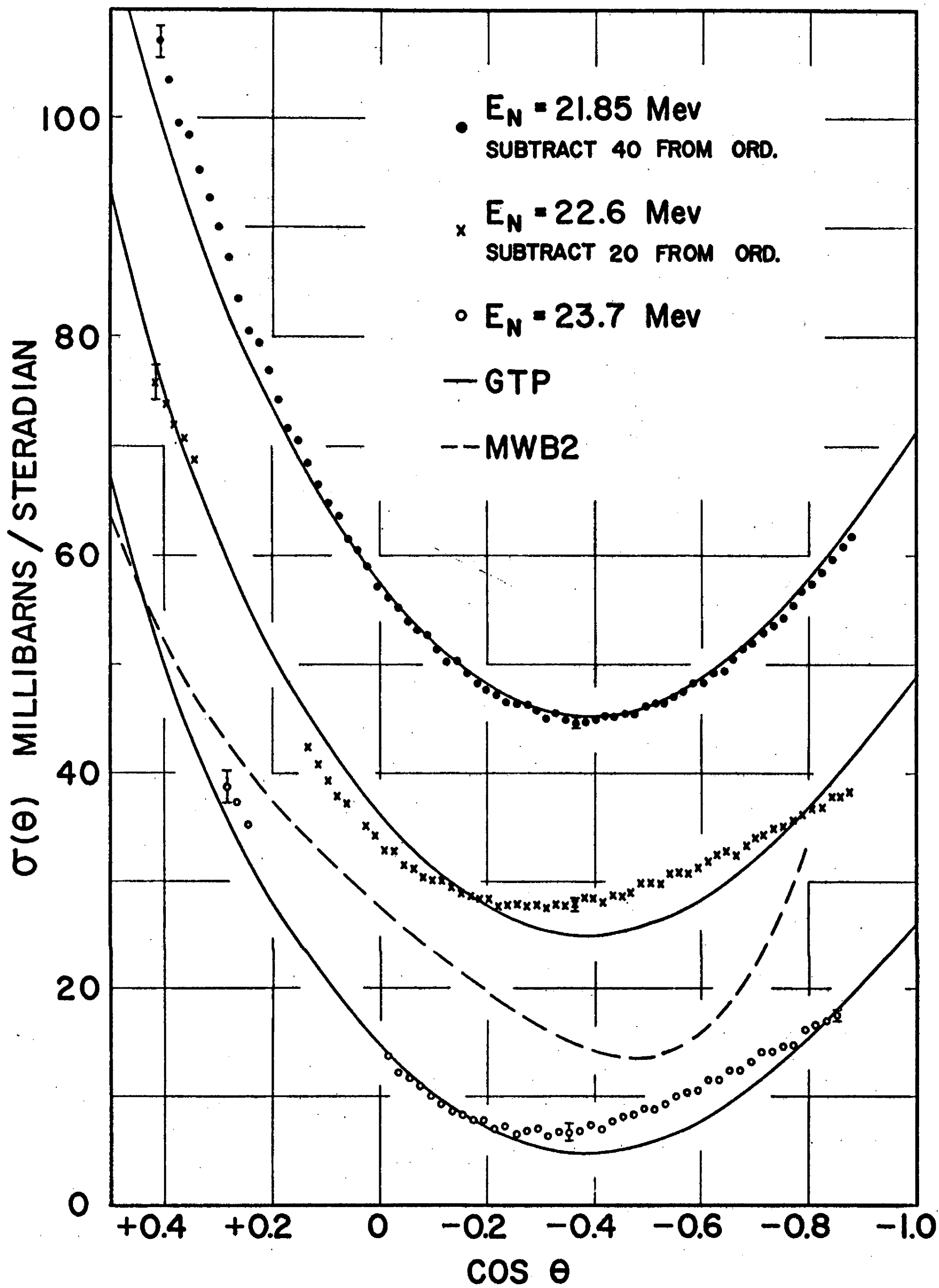

Fig. 29 Differential cross sections in the C.M. system for the scattering of 21.85, 22.6 and 23.7 MeV neutrons by α-particles. The ordinate scales are to be adjusted as shown. The solid curves were calculated using the GTP phase shifts. The dotted curve was calculated using the phase shifts suggested by May et al. for 23.7 MeV neutrons.

6.7 Results

The angular distributions which were obtained below and above the E_N = 22.15 MeV resonance are shown in figures 28 and 29. The differential elastic scattering cross sections are plotted as a function of the cosine of the CM scattering angle, θ. The statistical uncertainties were greatest for the 16.4 MeV data, where they ranged from 1% at the smallest angle to 3.5% at the minimum of the distribution. For the measurements at 22.6 and 23.7 MeV, no angular distribution data were obtained near cosθ = +0.2 because of the presence of disintegration particles from the $He^4(n,d)T$ reaction. The neutron energy spread was less than 170 keV for each of these measurements, except at 16.4 MeV, where the spread was about 700 keV.

Systematic errors may be present in the angular distributions because of experimental uncertainties in the background corrections. For each of these distributions an indication of the magnitude of this error at a small angle and at the minimum in the distribution is given by an error bar. At the largest angle this error was about equal to, or less than, the size of the data point (except at 23.7 MeV). The size of each of these error bars corresponds to an estimated uncertainty of $\pm$ 10% in the background corrections. There were two possible sources of error in the abscissa scale. Firstly, the estimation of the channel for which cos θ = −1.0 was

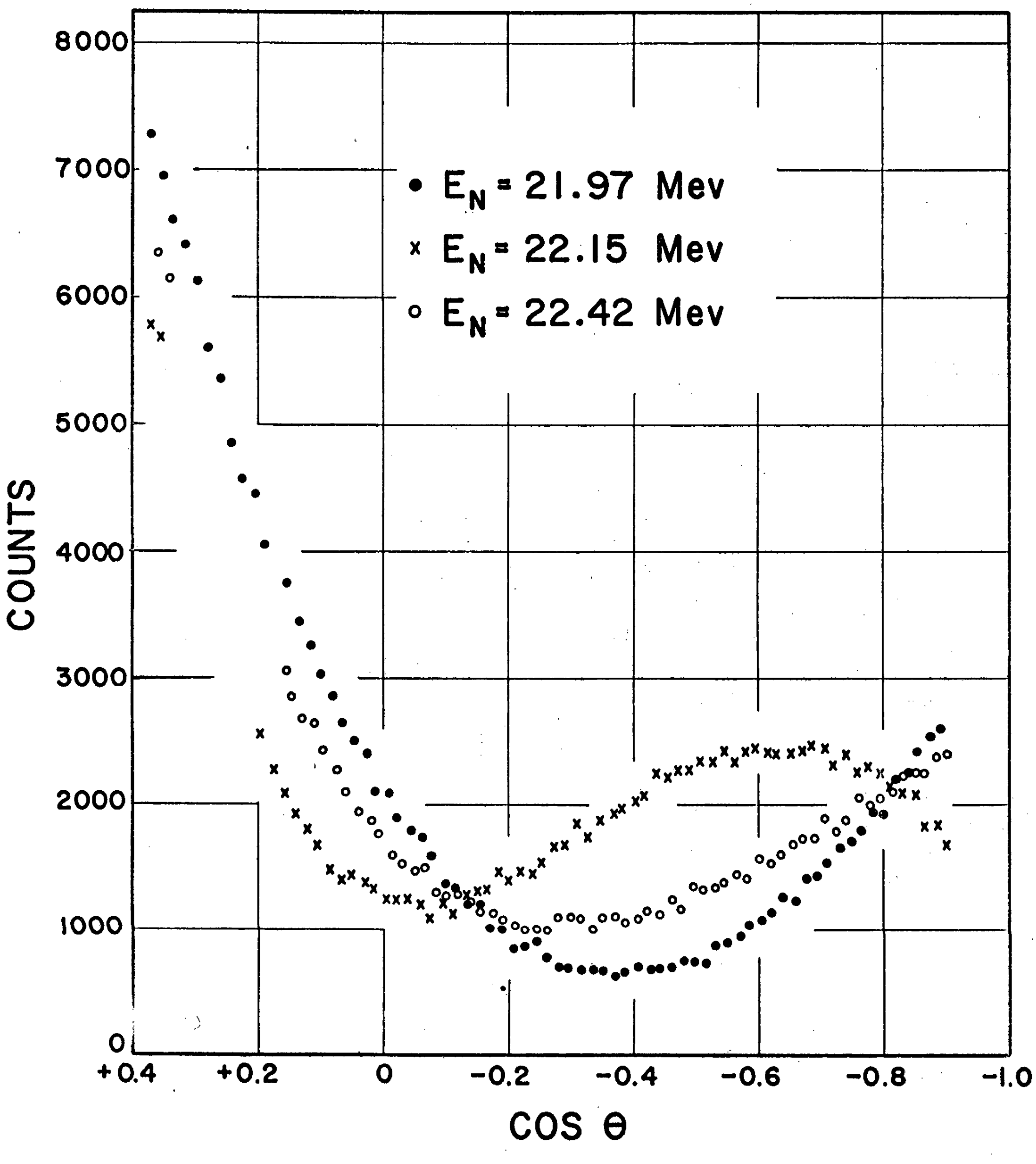

Fig. 30 Relative angular distributions of neutrons scattered by α-particles, for neutron energies just below, on, and just above the 22.15 MeV resonance.

subject to a maximum uncertainty of one channel, or about 1%. Secondly, the extrapolation of the linear portion of the linearity curve (figure 26) back to zero pulse height to determine "zero" channel, or cos θ = +1.0, may also have been in error, but by less than 1%.

In figures 28 and 29 the solid curves are differential elastic scattering cross sections computed from the GTP phase shifts, and the broken curves at 16.4 and 23.7 MeV are cross sections computed from the Brockman (B) and May, Walter and Barschall (MWB 2) phase shifts, respectively.

Relative angular distributions which were measured just below, on, and just above the 22.15 MeV resonance are shown in figure 30. These distributions have been corrected for backgrounds and wall effect. The neutron energy spread for the data in figures 30 and 31 was about 70 keV.

In figure 31 a part of the angular distribution data taken over the resonance is presented as excitation functions. Each of these data points is the sum of two channels of a pulse-height distribution. The smooth curves through these data points are fits by eye to the data.

The observed yield from the $He^4(n,d)T$ reaction is shown at the top of figure 31 by the closed circles. The broken curve represents the $He^4(n,d)T$ cross section computed from the cross section for the inverse reaction by using the principle of

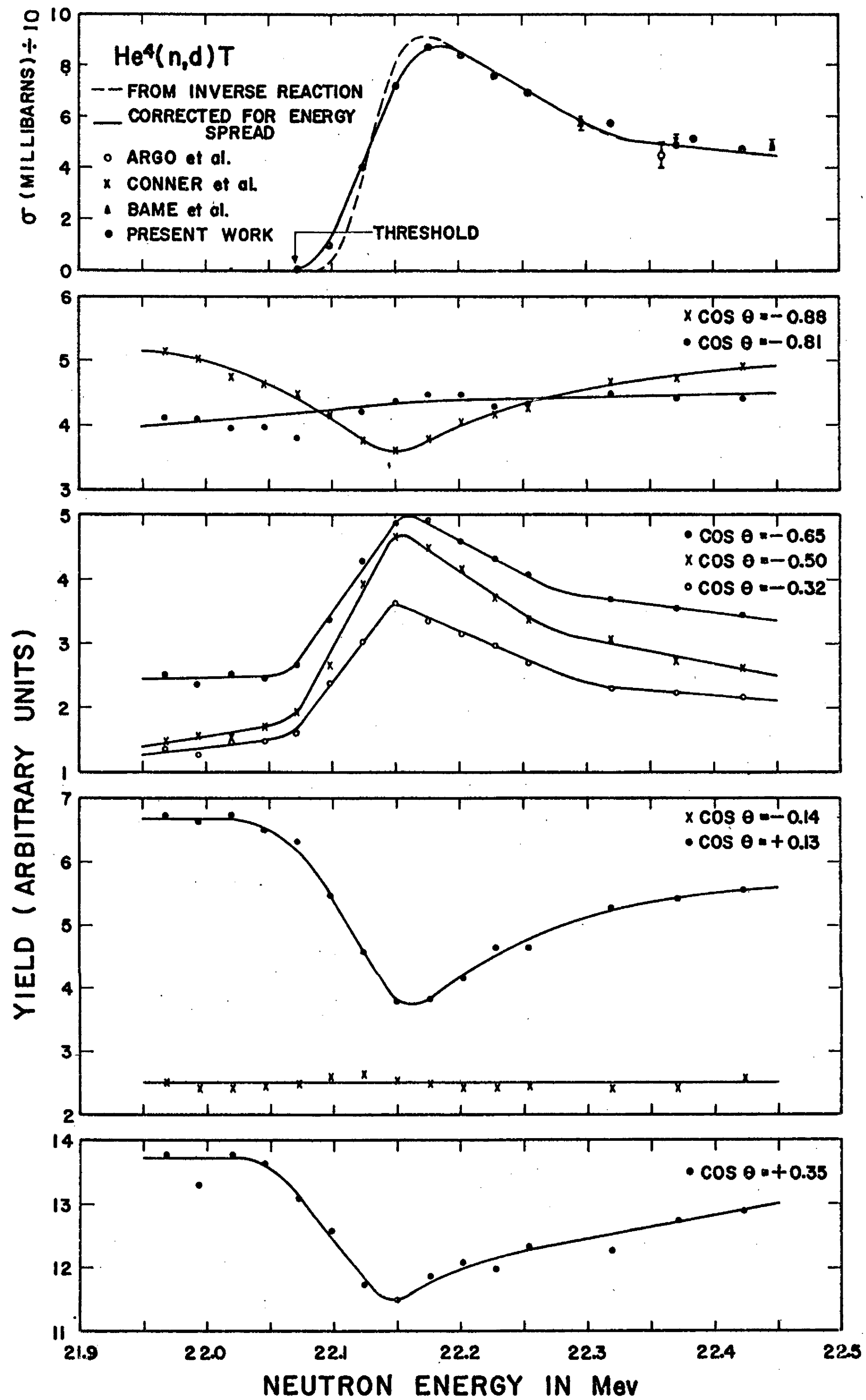

Fig. 31 The observed yield from the He^4(n,d)T reaction compared with that calculated from the inverse reaction; and, below, part of the angular distribution data taken over the resonance presented as excitation functions.

reciprocity. This curve corresponds to a smooth curve drawn through a plot of published measurements for the inverse reaction. For the open circle, crosses and closed triangle, the individual published cross sections were used for the computation. The solid curve was obtained by adjusting the broken curve for the neutron energy spread. For this adjustment, the energy spread was approximated by a rectangular function with a width of 70 keV. The relative cross section data of the present experiment was assigned a cross section scale by normalizing the data to the solid curve near its peak. The present data were corrected for backgrounds, wall effect, and a variation in neutron flux with energy of about 2%. This variation was caused by the change in the cross section of the neutron producing reaction, and by the loss of tritium through the nickel foil. The data clearly supports the higher values for the inverse cross section in the region of $E_N = 22.35$ MeV.

The angular distributions were fitted with Legendre polynomial expansions. The ratio of each of the coefficients to the zero-order coefficient is shown in figure 32 and listed in Table 5. The coefficients represented by the solid symbols in figure 32 were obtained from the data displayed in figures 28, 29 and 31. Coefficients for two sets of data are shown at 21.0 and 21.85 MeV. The open symbols at these energies correspond to data taken with the same xenon pressure in the counter as at 23.7 MeV.

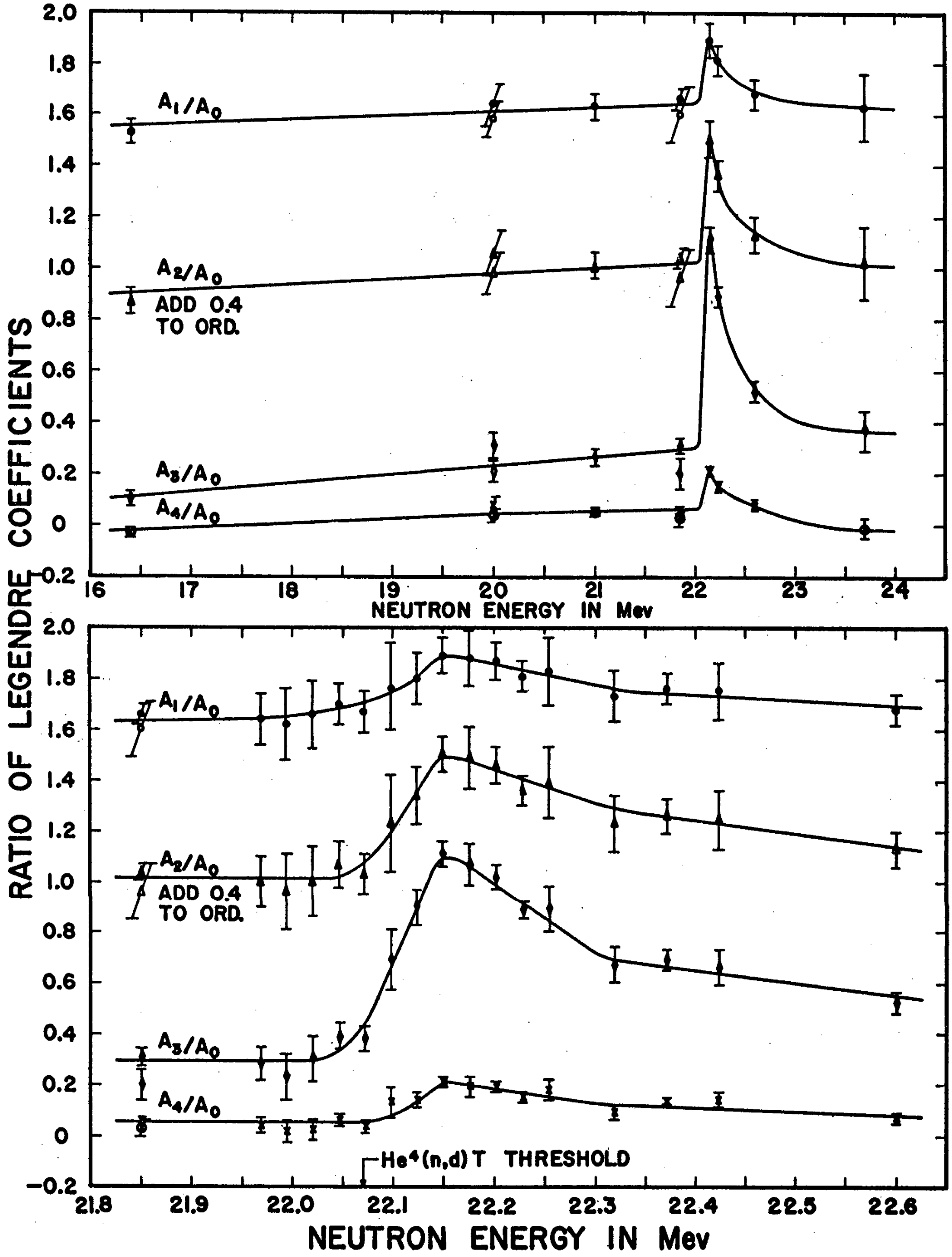

Fig. 32 The energy dependence of the ratios of the coefficients obtained from a Legendre-polynomial-expansion fit to the neutron angular distributions.

TABLE 5

RATIOS OF COEFFICIENTS OBTAINED FROM LEGENDRE-POLYNOMIAL-EXPANSION FITS TO THE ELASTIC SCATTERING ANGULAR DISTRIBUTIONS

E_N (MeV)	σ_{TOT} (mb)	σ_{d+T} (mb)	A_o (mb/sr)	A_1/A_o	A_2/A_o	A_3/A_o	A_4/A_o
16.4	908	0	72.2	1.53±0.05	1.27±0.05	0.10±0.03	-0.03±0.02
20.0	755	0	60.1	1.64±0.08	1.46±0.09	0.31±0.05	0.08±0.03
20.0	755	0	60.1	1.58±0.07	1.38±0.08	0.21±0.04	0.04±0.02
21.0	729	0	58.0	1.63±0.05	1.41±0.05	0.26±0.03	0.05±0.02
21.85	719	0	57.2	1.66±0.04	1.44±0.04	0.30±0.03	0.06±0.01
21.85	719	0	57.2	1.60±0.11	1.36±0.11	0.20±0.06	0.03±0.03
21.97	720	0	57.3	1.64±0.10	1.40±0.10	0.28±0.06	0.04±0.03
21.99	722	0	57.5	1.62±0.14	1.36±0.15	0.23±0.09	0.01±0.04
22.02	728	0	57.9	1.66±0.13	1.40±0.14	0.30±0.09	0.02±0.04
22.05	741	0	58.9	1.70±0.08	1.47±0.09	0.39±0.05	0.06±0.02
22.07	770	0	61.3	1.67±0.08	1.43±0.08	0.38±0.05	0.03±0.02
22.10	810	3	64.2	1.76±0.18	1.63±0.19	0.69±0.12	0.13±0.06
22.12	863	35	65.9	1.80±0.10	1.74±0.11	0.90±0.07	0.14±0.03
22.15	905	81	65.6	1.89±0.07	1.90±0.07	1.11±0.05	0.21±0.02
22.18	863	91	61.4	1.88±0.11	1.89±0.12	1.07±0.08	0.19±0.04
22.20	804	86	57.1	1.87±0.07	1.86±0.07	1.02±0.05	0.19±0.02
22.23	783	77	56.2	1.80±0.06	1.76±0.06	0.89±0.04	0.15±0.02
22.25	769	69	55.7	1.83±0.13	1.79±0.14	0.89±0.09	0.18±0.04

(continued next page)

TABLE 5 (cont'd)

RATIOS OF COEFFICIENTS OBTAINED FROM LEGENDRE-POLYNOMIAL-EXPANSION FITS TO THE ELASTIC SCATTERING ANGULAR DISTRIBUTIONS

E_N (MeV)	σ_{TOT} (mb)	σ_{d+T} (mb)	A_o (mb/sr)	A_1/A_o	A_2/A_o	A_3/A_o	A_4/A_o
22.32	748	54	55.2	1.73 ± 0.10	1.63 ± 0.11	0.67 ± 0.07	0.09 ± 0.03
22.37	736	49	54.7	1.76 ± 0.06	1.66 ± 0.07	0.69 ± 0.04	0.13 ± 0.02
22.42	728	46	54.3	1.75 ± 0.11	1.65 ± 0.12	0.66 ± 0.07	0.14 ± 0.03
22.6	711	40	53.4	1.68 ± 0.06	1.53 ± 0.07	0.52 ± 0.04	0.07 ± 0.02
23.7	665	35	50.1	1.63 ± 0.13	1.42 ± 0.14	0.37 ± 0.08	-0.01 ± 0.04

The means square errors which are given for each of the ratios are related to the mean square errors defined by Rose (Lawrence). The method used to obtain the values of A_o given in the table has been discussed in the previous section of the chapter. The angular distribution coefficients are given in detail because Pisent (1963) and Pisent and Saruis (1963) have recently developed a method for extracting phase shifts from such coefficients. Also, the smooth variation of the coefficients with energy was a useful preliminary indication of the reliability of the data.

6.8 Discussion

As can be seen from figures 28 and 29 discussed above, the agreement between the data and angular distributions calculated from the GTP phase shifts at neutron energies from 16 to 21 MeV was very good. It supported the validity of the GTP phase shifts in this energy range. Austin et al. (1962) had earlier suggested that this might not be so.

Figures 30 and 31 show how markedly the elastic scattering cross section changed near $E_N = 22.15$ MeV. As outlined in the introduction to this chapter, several authors had suggested that the maximum in the $T(d,n)He^4$ cross section, generally interpreted as a $3/2^+$ level in He^5 at 16.70 MeV excitation, might have been associated only with the proximity of its own neutron threshold. However, in the present experiment the elastic scattering channel was investigated; a channel other than the one in which the threshold occurred. As mentioned in the introduction, it has been pointed out (Wigner, 1948) that a threshold in one channel can cause an observable anomaly in another channel under certain conditions. However, the $He^4(n,d)T$ threshold cannot have caused the anomaly in the elastic scattering channel in the present experiment because of the coulomb interaction between the two outgoing particles. Furthermore, the changes in the differential cross section away from a parabolic shape, even below the $He^4(n,d)T$ threshold, suggested that neutrons with ℓ -values greater than one were participating in the elastic scattering process (Wheeler and Barschall, 1940). The presence of D-wave neutrons would agree with the $J^{\pi} = 3/2^+$ assignment made to the He^5 excited state; and, indeed, preliminary calculations have shown that a good fit to the angular distribution data taken at 22.15 MeV neutron energy can be obtained with a $D_{3/2}$ phase shift of 90^o and a transmission coefficient less than one. These facts were further evidence for an interpretation of the anomaly in terms of a level in the compound nucleus, He^5, at an excitation energy of 16.70 MeV.

At neutron energies above 22 MeV the agreement between the data and the angular distributions predicted by the GTP phase shifts was not as good. This was not altogether surprising, since Gammel and Thaler took no account in their calculations either of the opening up of the inelastic channel or of the presence of the resonance. They derived only real phase shifts. At 22.6 MeV either or both of these factors may have influenced the angular distribution. However, at 23.7 MeV, the $3/2^+$ level, which is about 105 keV wide, would only have contributed a few degrees to the $D_{3/2}$ phase shift. The fact that the data differed from the GTP predictions in essentially the same way at both 22.6 and 23.7 MeV suggested that it is not reasonable to ignore the inelastic channel when determining phase shifts in this energy range.

APPENDIX A

The purpose of this appendix is to calculate the difference between the activities induced in a target by a constant beam current and by one with a periodic variation of the type seen during the activation experiments.

Let $N(t)$ = number of radioactive nuclei present at time t

k = rate of production of such nuclei for a constant bombarding current

λ = decay constant (probability that any particular nucleus will disintegrate in unit time).

Then $N(t).\lambda$ = rate of decay

and $$dN(t)/dt = k - N(t).\lambda \qquad \ldots\ldots\ \ldots\ldots\ \ldots\ldots\ (1)$$

for a constant beam current.

Using an integrating factor $e^{\lambda t}$, integration of this equation yields

$$N(t)e^{\lambda t} = (k/\lambda)(e^{\lambda t} - 1)$$

or $$N(t) = (k/\lambda)(1 - e^{-\lambda t}) \qquad \ldots\ldots\ \ldots\ldots\ (2)$$

At time $t = \infty$, $k/\lambda = N(\infty)$,

giving $N(t) = N(\infty)(1 - e^{-\lambda t})$, the well-known form.

In the case of C^{10}, $\lambda = 0.036\ sec^{-1}$

$t = 60$ sec,

so $N(60) = 25\ k.$

In practice there were two approximately sinusoidal variations in the beam current about its mean. The first was a very small fluctuation with a frequency of 2 cycles/sec., which was caused by the periodic motion of the Van de Graaff accelerator charging belt. The second was a larger fluctuation, of $\pm$ 3% maximum amplitude and 0.2 cycle/sec. frequency, which was apparent in the pen records taken of the beam current.

For such variations, a sin ωt, equation (1) becomes

$$dN(t)/dt = k(1 + a \sin \omega t) - N(t).\lambda$$

This equation can be integrated using the integrating factor $e^{\lambda t}$, giving

$$N(t) = (k/\lambda)(1 - e^{-\lambda t}) + (ka/\lambda^2 + \omega^2) \times (\lambda \sin \omega t - \omega \cos \omega t + \omega/e^{\lambda t}) \quad \ldots. (3)$$

Equations (2) and (3) differ by the factor

$$(ka/\lambda^2 + \omega^2)(\lambda \sin \omega t - \omega \cos \omega t + \omega/e^{\lambda t}) \quad \ldots (4)$$

For the larger fluctuation, and using the C^{10} half-life,

$$\lambda = 0.036 \text{ sec}^{-1}$$

$$t = 60 \text{ sec}$$

$$a = \pm 0.03$$

and $\omega = 2\pi f = 1.3$ radians/sec,

and so the difference (4) has a maximum absolute value of

$$\simeq (ka/\omega)(1 - e^{-\lambda t})$$

$$= 0.02k.$$

This is only 0.1 percent of the activity induced by a constant beam current. Hence, a maximum error of 0.1 percent will result in the cross section calculations if it is assumed that a constant beam current gave the measured integrated charge.

A very similar result pertains to the $F^{19}(p,n)Ne^{19}$ measurements reported in chapter 5, in which the decay of Ne^{19} was followed.

APPENDIX B

The subject of this appendix is the determination of the γ-ray photopeak, total detection efficiencies of the two crystal spectrometers for the 0.511 and 0.717 MeV γ-rays. These have been denoted $\mathcal{E}_1$ and $\mathcal{E}_2$ respectively. They are related to the total detection efficiencies $\mathcal{E}_1^T$ and $\mathcal{E}_2^T$ by the relationship $\mathcal{E}_i = r_i \mathcal{E}_i^T$, i = 1,2, where r_i = peak-to-total detection efficiency ratios. Graphs of r versus γ-ray energy for NaI crystals have been given by Marion (1960).

B.1 The measurement of $\mathcal{E}_1$ (0.511 MeV γ-ray)

A calculation of $\mathcal{E}_1^T$ could not be made because a large number of the positrons produced were energetic enough to escape from the B^{10} target and move a substantial distance before annihilating. A Na^{22} source, calibrated to ± 2.5 percent in a 4π β-γ coincidence counter, was therefore used to determine $\mathcal{E}_1^T$ experimentally. The source was mounted in the target chamber in an identical fashion to the B^{10} targets. The number of counts appearing in the 0.511 MeV single channel analyser window was corrected for the contribution of the Compton-scattering "tail" of the 1.28 MeV γ-ray associated with the decay of Na^{22} nuclei.

B.2 The determination of $\mathcal{E}_2^T$ (0.717 MeV γ-ray)

The total efficiency, that is the probability of detecting a γ-ray emitted into 4π steradians from a point source S, is given by

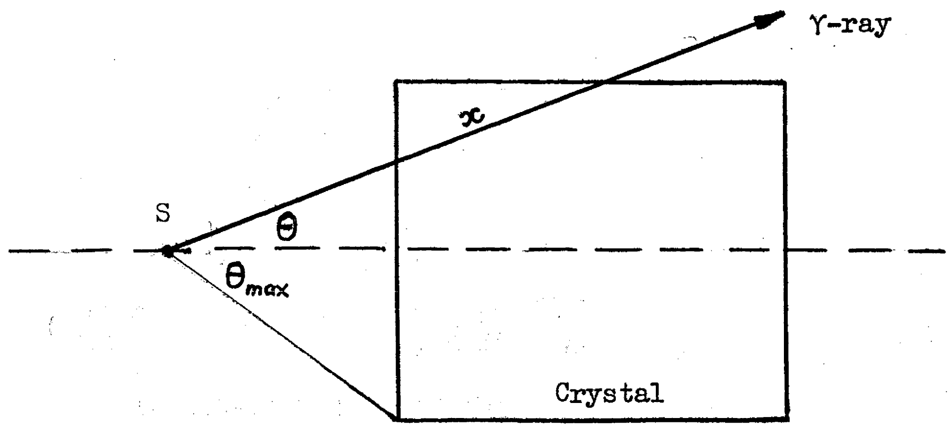

fig. B1

$$\mathcal{E}_2^T = \tfrac{1}{2}\int_0^{\theta_{max}} (1 - e^{-\tau x}) \sin\theta \, d\theta$$

where τ = absorption coefficient in the crystal.

This integral has been plotted for NaI crystals as a function of γ-ray energy by Marion (1960).

However, when there is absorption in media between the γ-ray source and the detector, as in the present case, the efficiency is given by

$$\mathcal{E}_2^T = \frac{1}{2} \int_0^{\theta_{max}} e^{-\sum \tau_i x_i} (1 - e^{-\tau x}) \sin\theta \, d\theta$$

where τ_i are the absorption coefficients for the different media - the brass walls of the target chamber, the tantalum cylinder and lining, the 0.32 cm lead sheet and the aluminium casing of the crystal. This integral was performed numerically using Simpson's Rule, yielding $\mathcal{E}_2^T = 0.066$, a value which indicated that there was 48 percent absorption in the media listed. The error involved in such a calculation may be large. For example, the calculation assumes that the photopeak of the full energy γ-ray is infinitely narrow, that is, that any scattering whatever prevents the detection of the γ-ray. In fact, finite resolution and a quite broad single channel analyser window were used.

It was decided to check the calculation by measuring experimentally the absorption for the Cs^{137}, 0.66 MeV γ-ray. This was done by simulating as nearly as possible the actual experimental conditions on a bench, but in a manner that enabled the absorbers to be removed. Under a wide range of experimental conditions (SCA window width, source position, etc.) the absorption was consistently 10 percent greater than the calculated value. This was considered reasonable agreement, the experimental value being used in the calculations of the reaction cross section because of its consistency.

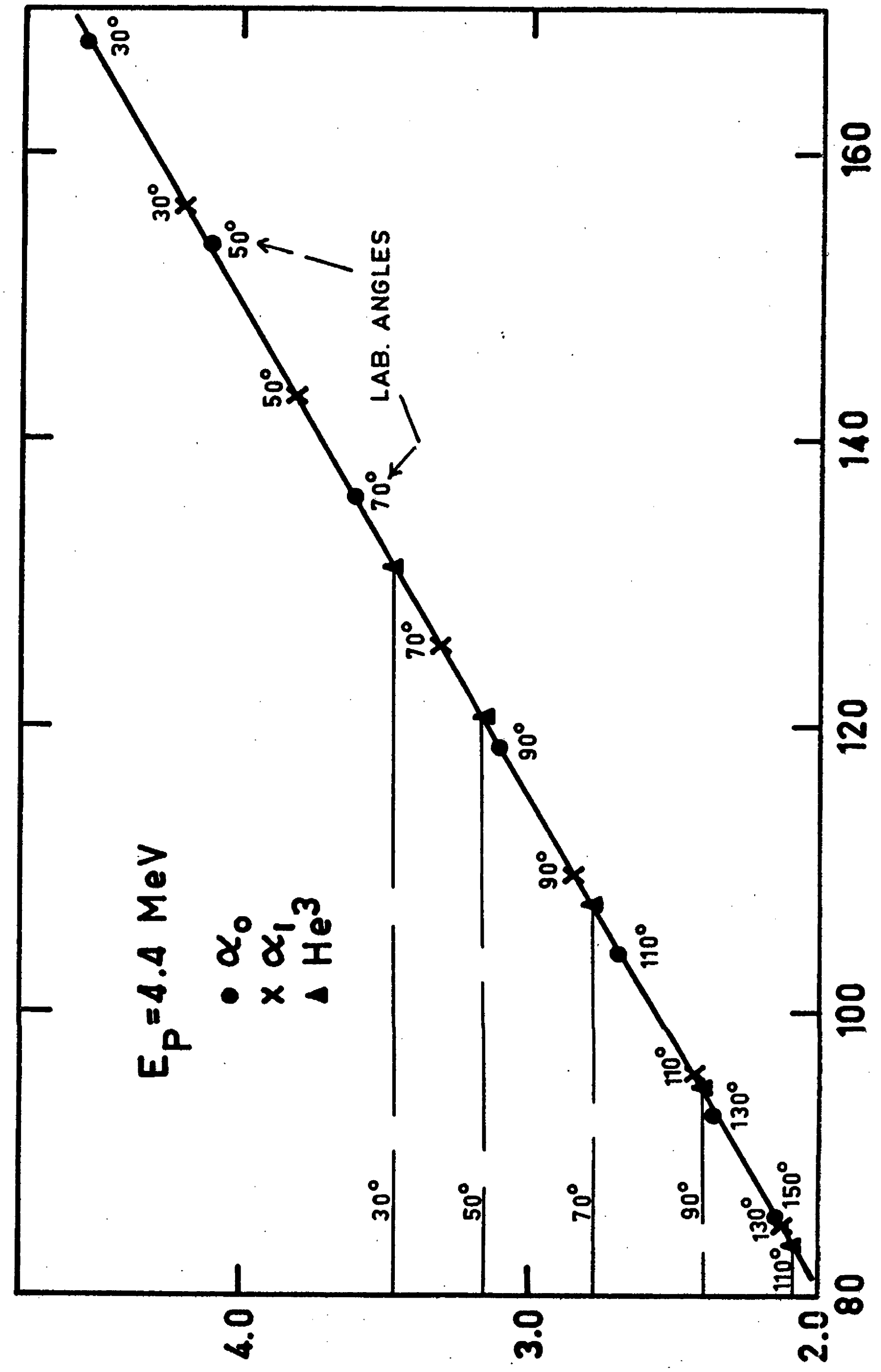

Fig. C1 This figure is explained in the text.

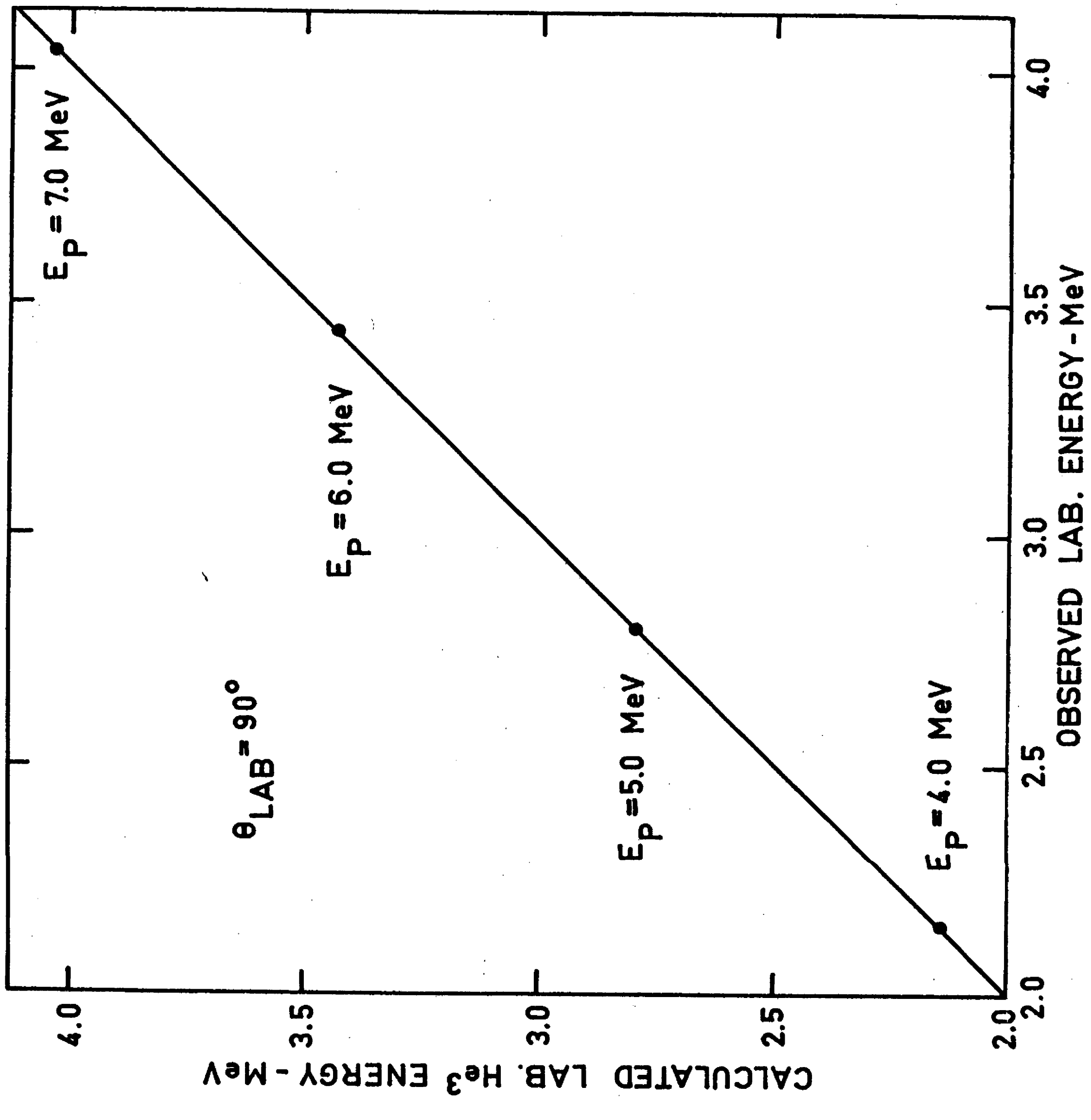

Fig. C2 This figure is explained in the text.

K63-544

APPENDIX C

The identification of the He^3 group from the proton bombardment of B^{10}, proceeding to the groundstate of Be^8, is the subject of this appendix.

Firstly, at a proton energy of 4.4 MeV, charged-particle spectra were taken at laboratory angles of 30°, 50°, 70°, 90°, 110°, 130° and 150°. The multichannel analyser used was calibrated for channel number versus particle energy using the positions and calculated energies of the α_0 and α_1 groups from the $B^{10}(p,\alpha)Be^7$ reaction. The position of the "unknown" peak at each angle was plotted on the resulting curve, and the energies of the groups so obtained was found to be consistent with those energies calculated from the kinematics of the $B^{10}(p,He^3_0)Be^8$ reaction (see figure C1).

Secondly, spectra were taken at laboratory proton energies of 4.0, 5.0, 6.0 and 7.0 MeV, and a plot made of the calculated He^3 energy versus the observed energy of the "unknown" peak. A straight line of unit slope resulted, as figure C2 shows.

The "unknown" peak was therefore unambiguously identified as the He^3 group from the reaction $B^{10}(p,He^3_0)Be^8$.

REFERENCES

F. Ajzenberg and W. Franzen, Phys. Rev. 95 (1954) 1531.

F. Ajzenberg-Selove and T. Lauritsen (A-S and L), Nucl. Phys. 11 (1959) 1.

F. Ajzenberg-Selove and T. Lauritsen (A-S and L), Nuclear Data Sheets, Sets 5 and 6 (1962).

Andreev, Deineko and Malakhov, Izv. Akad. Nauk. SSSR 26 (1962) 1134.

S.M. Austin, Bull. Am. Phys. Soc. 7 (1962) 605.

Austin, Barschall and Shamu, Phys. Rev. 126 (1962) 1532.

Bair, Kington and Willard, Phys. Rev. 100 (1955) 21.

H.H. Barschall and M.H. Kanner, Phys. Rev. 58 (1940) 590.

H.H. Barschall and J.L. Powell, Phys. Rev. 96 (1954) 713.

F.J. Bartis et al., University of Washington Cyclotron Research, Annual Progress Report (1962).

S. Bashkin and T.R. Ophel, Nucl. Instr. and Methods 15 (1962) 112.

Bertozzi, Demos, Kowalski, Sargent, Turchinetz, Fullwood and Russell, Phys. Rev. Lett. 10 (1963) 106.

Biedenharn, Blatt and Rose, Rev. Mod. Phys. 24 (1952) 249.

Blaser, Boehm, Marmier and Scherrer, Helv. Phys. Acta 24 (1951) 465.

J.M. Blatt and L.C. Biedenharn, Rev. Mod. Phys. 24 (1952) 258.

J.M. Blatt and V.F. Weisskopf, "Theoretical Nuclear Physics" (Wiley and Sons, New York, 1952) p. 394.

N. Bohr, Nature 137 (1936) 344.

Bonner, Prosser and Slattery, Phys. Rev. 110 (1958) 163.

B.H. Bransden, in "Nuclear Forces and the Few-Nucleon Problem" (Pergamon, New York, 1960) Vol. 2, p. 547.

G. Breit, Phys. Rev. 107 (1957) 1612.

K.W. Brockman, Phys. Rev. 110 (1958) 163.

C. Broude and H.E. Gove, Proc. Inst. Conf. on Nuclear Structure, Kingston (U. of Toronto Press, 1960) p. 754; and private communication from Broude.

P.G. Burke, in "Nuclear Forces and the Few-Nucleon Problem" (Pergamon, New York, 1960) Vol. 2, p. 413.

A.G.W. Cameron, Can. J. Phys. 36 (1958) 1040.

M. Cerino, Nucl. Phys. 2 (1956/57) 113.

Craig, Donahue and Jones, Phys. Rev. 88 (1952) 808.

J.W. Cronin, Phys. Rev. 101 (1956) 298.

R.B. Day and T. Huus, Phys. Rev. 95 (1954) 1003.

Delsasso, White, Barkas and Creutz, Phys. Rev. 58 (1940) 586.

L.M. Delves, Nucl. Phys. 9 (1958/59) 391.

D. Demirlioglu and W. Whaling (to be published)

D.C. Dodder and J.L. Gammel, Phys. Rev. 88 (1952) 520.

T. Ericson, Advances in Physics 9 (1960) 425.

J.R. Erskine and D.S. Gemmell, Nucl. Instr. and Methods (to be published).

R.D. Evans, "The Atomic Nucleus" (McGraw-Hill, New York, 1955).

U. Farinelli and R. Malvano, Rev. Sci. Instr. 29 (1958) 699.

E. Fermi, Z. Physik 88 (1934) 161.

E. Fermi et al., Ric. Sci. 5 (1934) 282.

J.M. Freeman et al., AERE (Harwell, England) Research Report R-4131 (1962).

J.L. Gammel and R.M. Thaler, Phys. Rev. 109 (1958) 2041.

G. Gamow and E. Teller, Phys. Rev. 49 (1936) 895.

Gemmell, Morton and Smith, Nucl. Phys. 10 (1959) 45.

J.H. Gibbons and R.L. Macklin, Phys. Rev. 114 (1959) 571.

A. Graue and B. Trumpy, Phil. Mag. 2 (1957) 138.

Green, Cooper and Harris, Phys. Rev. 98 (1955) 466.

Hansen, Jopson, Mark and Swift, Nucl. Phys. 30 (1962) 389.

Herrmannsfeldt, Burman, Stahelin, Allen and Braid, Bull. Am. Phys. Soc. 4 (1959) 77.

P.E. Hodgson, Phil. Mag. Suppl. 7 (1958) 1.

Hunt, Mehta and Davis, from Ph.D. thesis of K.L. Warsh, Florida State University (unpublished).

K. Izumo, Prog. Theor. Phys. 26 (1961) 807.

K. Izumo, Tokyo Institute of Nuclear Study, Report INSJ-51 (1962)

K. Izumo, Tokyo Institute of Nuclear Study, Report INSJ-59 (1963).

Jadogne, Macq and Steyaert, Phys. Lett. 2 (1962) 325.

C.H. Johnson and H.E. Banta, Rev. Sci. Instr. 27 (1956) 132.

Kalinin, Oglobin and Petrov, Soviet J. of Atomic Energy 2 (1957) 193.

I. Kaplan, "Nuclear Physics" (Addison-Wesley, Mass., 1956) chapter 10.

E.J. Konopinski and G.E. Uhlenbeck, Phys. Rev. 60 (1941) 308.

Lane, Thomas and Wigner, Phys. Rev. 98 (1955) 693.

A.M. Lane and R.G. Thomas, Rev. Mod. Phys. 30 (1958) 257.

L.G. Lawrence, Australian National University Report ANU-P/287.

K.J. Le Couteur and J.M.B. Lang, Proc. Phys. Soc. A67 (1954) 586.

K.J. Le Couteur and D.W. Lang, Nucl. Phys. 13 (1959) 32.

J.B. Marion, 1960 Nuclear Data Tables (National Academy of Sciences, Washington, 1960) part 3.

Marion, Bonner and Cook, Phys. Rev. 100 (1955) 91.

May, Walter and Barschall, Nucl. Phys. 45 (1963) 17.

Miller, Gibson and Donovan, Ann. Review of Nucl. Science 12 (1962) 189.

A.H.F. Muggleton and F.A. Howe, Nucl. Instr. and Methods 13 (1961) 211.

R.A. Nobles, Rev. Sci. Instr. 27 (1956) 280.

Ophel, Glover and Titterton, Nucl. Phys. 33 (1962) 198.

J.C. Overley and W. Whaling, Phys. Rev. 128 (1962) 315.

R.B. Perkins and J.E. Simmons, Phys. Rev. 130 (1963) 272.

R.B. Perkins, private communication, 1963.

G. Pisent, Helv. Phys. Acta 36 (1963) 248.

G. Pisent and A.M. Saruis, Il Nuovo Cimento, Series X, 28 (1963) 600.

Ranken, Bonner and McCrary, Phys. Rev. 109 (1958) 1646.

J.B. Reynolds, Phys. Rev. 98 (1955) 1289.

M.E. Rose, Phys. Rev. 91 (1953) 610.

J.D. Seagrave, Phys. Rev. 92 (1953) 1222.

R.E. Shamu, Nucl. Instr. and Methods 14 (1962) 297.

Shamu, Ohlsen and Young, Phys. Lett. 4 (1963) 286.

Sharp, Gove and Paul, Atomic Energy of Canada Ltd., Report AECL-268 (Second edition, 1955).

Sharp, Kennedy, Sears and Hoyle, Atomic Energy of Canada Ltd., Report AECL-97 (revised edition, 1954).

R. Sherr and J.B. Gerhart, Phys. Rev. 91 (1953) 909.

Sherr, Meuther and White, Phys. Rev. 75 (1949) 282.

Takayanagi, Gale, Garg and Calvert, Nucl. Phys. 28 (1961) 494.

T. Teichmann and E.P. Wigner, Phys. Rev. 87 (1952) 123.

Teplov, Shevchenko and Ruuge, JETP (USSR) 39 (1960) 923,
JETP (Soviet Physics) 12 (1961) 640.

Trostin, Smotryaev and Levintov, JETP (USSR) 41 (1961) 725,
JETP (Soviet Physics) 14 (1962) 524.

Warsh, Blieden and Temmer, Bull. Am. Phys. Soc. 7 (1962) 300.

Warsh, Temmer and Blieden, Phys. Rev. 131 (1963) 1690.

V.F. Weisskopf, Phys. Rev. 52 (1937) 295.

W. Whaling, "Handbuch der Physik" (Springer-Verlag, Berlin, 1958) Vol. 34.

J.A. Wheeler and H.H. Barschall, Phys. Rev. 58 (1940) 682.

E.P. Wigner, Phys. Rev. 73 (1948) 1002.

Willard, Bair, Kington, Hahan, Snyder and Green, Phys. Rev. 85 (1952) 849.